Robust-Optimal Control of a Servo Motor.

Doctor of Philosophy in Electronic Engineering.

By Paul J. Kettle.

Dublin City University
School of Electronic Engineering
Supervised By Dr. Aengus Murray.

12/1994

I hereby certify that this material, which I now submit for assessment on the programme of study leading to the award of Doctor of Philosophy in Electronic Engineering is entirely my own work and has not been takes from the work of others save and to the extent that such work has been cited and acknowledged within the text of my work.

Signed:_____ ID No.: 90700261

Date: 24/02/95

Acknowledgements.

The author would like to acknowledge the financial support of Power Electronics Ireland at Dublin City University who funded this research.

I would also especially like to acknowledge the contributions of my supervisor Dr. Aengus Murray and my surrogate supervisor Dr. Anthony Holohan for their support and guidance during the course of this research.

I would further like to acknowledge the support of my family and friends with a particular mention for Emer, Dave, John, Peter and my mother.

And finally I would like to acknowledge Aphra for her support and understanding during the past years.

Many thanks to you all P...

Abstract.

This work develops a frequency domain loop shaping design strategy based on linear quadratic gaussian controllers with loop transfer recovery (LQG/LTR). The design strategy presented is an integrated design synthesis procedure which is conducive to educated trade-off management. The controller design specification are expressed in terms of loop shaping bounds for load dynamic and model uncertainties, command response times and disturbance response times. The design philosophy is to first and foremost satisfy the stability constraints subject to the model variation specification and then to satisfy the time domain design specifications. The LQG/LTR controller is synthesised in discrete time, the resulting design is a Robust-Optimal design. Asymptotic disturbance rejection is achieved by using a disturbance estimate feedforward technique.

Within the servo control industry two position feedback sensors are commonly used, namely the resolver and the optical encoder. In this work the controllers designed are applicable to both types of feedback sensors. Particular attention is given to the resolver sensor and corresponding estimator design. Often the resolver sensor is favoured because of its robust construction which is particularly suited for industrial environments. In this work a modified Extended Kalman estimator is developed which eliminates the need for a resolver to digital converter. A steady state solution for the Extended Kalman estimator is developed which provides a numerically robust and efficient estimator design. Finite manufacturing process and demodulation circuitry can often distort the resolver's outputs, these distortions introduce amplitude, bias and phase discrepancies onto the resolver channels which subsequently introduce velocity ripple into the closed loop system. In this work a parameter estimation scheme is developed which estimates and corrects the imperfections of the sensor interface.

Keywords:

Optimality, Optimal, Robustness, Robust, LQG, Linear Quadratic Gaussian, LTR, Loop Transfer Recovery, Robustness Recovery, Resolver, Optical Encoder, Kalman Filter, Extended Kalman Estimator, Extended Kalman Filter, Motor Control, Servo, Frequency Shaping, Loop Shaping, Sensitivity, Return Difference, Feedforward.

Table of Content:

List of Acronyms:

LQ	Linear Quadratic controller
LQG	Linear Quadratic Gaussian controller
FS-LQG	Frequency Shaped Linear Quadratic Gaussian controller
PI-LQG	Proportional and Integral Linear Quadratic Gaussian controller
DE-LQG	Disturbance Estimate Linear Quadratic Gaussian controller
LTR	Loop Transfer Recovery
FS-LTR	Frequency shaped Loop Transfer Recovery
LQG/LTR	Linear Quadratic Gaussian controller with Loop Transfer Recovery
DSP	Digital Signal Processor
KE	Kalman Estimator
KF	Kalman Filter
DKF	Discrete-time Kalman filter
DTIK	Discrete Time Invariant Kalman
DLTV	Discrete Linear Time Varying
RDC	Resolver to Digital Converter
DK-Smoother	Discrete Kalman Smoother implementation
DK-Predictive	Discrete Kalman Predictive implementation
DK-Current	Discrete Kalman Current implementation
MIPS	Million Instruction cycles Per Second
SISO	Single Input Single Output
MIMO	Multiple Input Multiple Output

1. Introduction.

Within the servo control and industrial control industry there is an increasing trend to move towards using digital control techniques. This trend reflects the reducing costs and hence increasing availability of fast microprocessor technology. The availability of fast Digital Signal Processors (DSPs) at competitive prices has increased the choice and complexity of control algorithms that can be used for fast control applications. Conventionally these algorithms, because of their numerical complexity, were only used in high budget applications such as military or aerospace applications. However with an increasing number of MIPS/pound more elaborate control algorithms are finding their way into the commercial control sector.

In this work one such controller, the linear quadratic gaussian controller, with loop transfer recovery (LQG/LTR) is developed for applications in servo motor control. "Very few published papers deal with either the method itself or with the applications orientated studies that have exploited the LQG/LTR methodology. As a consequence, this powerful method is not readily accessible to the practising engineer " [Athans 86]. To this day there is still a void of published literature regarding practical design / implementation issues on the LQG/LTR methodology. Very few published works deal with discrete time issues regarding LQG/LTR design. This work is a contribution in this direction. It presents a systematic design methodology for synthesis of a discrete time LQG/LTR controller.

No matter how powerful the design methodology, a typical application requires several iterations. Hence it is important that the design procedures are transparent, are conducive to educated trial and error design iterations, and that the number of design parameters be kept at an absolute minimum. The design methodology developed in this work presents graphically each stage of the design, from which informed design decisions can be made.

The LQG/LTR design is usually graphically presented in the frequency domain, consequently most of the associated literature deals with a continuous time synthesis of the controller. Conventionally LQG/LTR synthesis is performed in continuous time, the final design is then mapped into discrete time using the bilinear transformation or an similar transformation. Surprisingly few published papers deal with the development of discrete time LQG/LTR controllers. In this work issues regarding the discrete time design and implementation of the controller are studied, it will become apparent that the continuous time design holds important consequences

in a discrete time implementation. In the present work the LQG/LTR design synthesis is performed in discrete time, in total three discrete LQG controller structures will be evaluated.

By using an estimation technique the number of required feedback sensors can be reduced. In this work the resolver[1] is used for position feedback information. Conventionally this resolver signal is converted into digital position and analogue velocity information using a resolver to digital converter (RDC). The RDC is susceptible to quantization noise and providing poor velocity information at low speeds [Murray 91]. Chapter 2 deals with the development of a novel estimation scheme which eliminates the need for the RDC, enhances the quality of the feedback information and provides significant cost savings. This chapter also presents a parameter estimation technique for estimating and tracking imperfections in the resolver interface. The resulting sensor interface provides significant cost savings while retaining the performance properties of the conventional interface.

In conventional control design the design specifications are often specified in terms of time response characteristics, disturbance and noise suppression properties and gain and phase margins. Often the design procedure satisfies one of the above specifications and is then iterated to optimise for the others. In this work these design specifications are integrated in a single design procedures.

In general a model of a physical system is an approximation of that physical system. In practice high frequency components are often approximated to gains, to reduce the complexity of the design / implementation. Furthermore in servo applications the load characteristics can also change depending on the nature of the application, such parameter changes can be characterised as model uncertainty or model error. However high frequency model errors impose a limit upon the control system bandwidth and thereby limit the performance of the feedback system. Furthermore parameter variation can effect the stability of the feedback system. In this work these model uncertainties are used to loop shape the controller design in a similar manner to the H^{∞} design procedure.

The emphasis of this design methodology is a controller design that is first and foremost robust to such parameter variations and secondly optimal from a time

---

[1]The controllers designed in this work are not restricted to the Resolver class of sensor. It shall be shown that the solution for the Optical Encoder sensor is a subset of the Resolver solution.

response point of view. Chapter 3 deals with the development of such a robust controller. The design is specified in terms of bounds on the variation of the load dynamics. Subject to these bounds, the performance and response of the system is optimised via a Linear Quadratic (LQ) constraint. The controller design in chapter 3 incorporates the state estimator developed in chapter 2. During the design, trade-offs can be made between command response and disturbance response times depending on the applications requirements.

For most servo control applications performance of the controller is reflected in the cost of the overall system. In this work the performance of the controller is improved while reducing the cost and complexity of the overall system. This is achieved by using a high performance DSP with ample computational resources for the control application, surplus resources are subsequently used to eliminate some of the conventional hardware and complexity. The increased cost of the DSP is partly justified by the savings made by eliminating some of the conventional circuits and the increased performance of the design. The cost of performance is thus linked to the cost of the processors. As the costs of these devices further reduces the corresponding cost of performance will also reduce.

From an optimality and efficiency point of view the motor mechanical constants and its load mechanical constants[2] should be matched. In this work further insight into the choice of a motor for a particular application is given in terms of the constraints of the robustness bounds. In an application where the motor is undersized, the robustness bound design will produce a controller design with a damped response or alternatively a design with a narrow bandwidth resulting in a design with a degraded response time. By increasing the size of the motor the robustness bounds are subsequently relaxed and the response times can thus be improved. In general, robustness bounds will place constraints on the response of a system. Indeed the relative size of the motor and load constants can be used as a tuning parameter at design time.

In conventional position servos proportional controllers are often used. These controllers are however susceptible to tracking or steady state errors due to external forces [Ohishi 87]. These external forces generally comprise of load torque and frictional torques such as static friction, Coulomb friction and viscosity friction.

---

[2]Namely load Inertia and viscosity. Note that these constants are really time varying parameters. For the purpose of this controller design they are assumed to be constant. A robust controller design is one which remains stable even in the presence of such an assumption.

Conventionally the effects of these disturbances are minimised by designing a controller with a high loop gain. However a finite error will persist for a finite loop gain. An alternative approach is to use integral action, this however introduces additional dynamics into the closed loop system and hence affects the transient response to command changes [Kettle 93]. In this work the state estimator is used to provide estimates of the sum of the external disturbance torques entering the plant. This torque figure is then fed forward and used to quickly suppress the affects of the disturbances. This technique overcomes the steady state and transient errors due to external disturbances without the degradation in command response [Franklin 80]. This work can be distinguished from other disturbance feedforward techniques [Ohishi 87 89a 89b], [Hoir 88 89] and [Rognon 88] by the manner in which the disturbance torque / acceleration information is evaluated. In this work disturbance torque is estimated using an integral error technique which is inherent in the framework of the Kalman estimator. This technique produces an estimate of torque which is less susceptible to measurement noise and hence superior to derivative based observers [Schmidt 92], [Lorenz 88].

The controller design strategy put forward is this work can be described as a simplified H^{∞} controller for single input single output systems. Every solution of a H^{∞} problem has an equivalent LQG solution. In this work the design problem is posed in terms of bounds on the uncertainties associated with the plant under control. These bounds loop shape the controller design and ultimately set the bandwidth of the controller. The performance and response times of the controller are then subsequently optimised using LQ constraints subject to these uncertainty bounds. In this work this procedure is presented graphically. At each stage in the design the designer can make informed decisions regarding the available trade-offs.

A continuous LQ controller is inherently robust offering a 60° phase margin, an infinite gain margin and a downside gain margin of 0.5. The LQG controller design does not inherit these robustness properties of the LQ design. During a LQG design it is necessary to recover these robustness properties. This is accomplished using a loop transfer recovery (LTR) procedure.

The computational overhead of a particular design is a fundamental consideration when choosing a particular controller implementation. Throughout this work trade-offs are highlighted between performance and computational overhead. In this work a novel approach is introduced regarding sample frequency selection. Three Kalman filter structures are presented, the choice of a particular structure depends on the

available computational resources, the robustness requirements and the chosen sample frequency.

Chapter 4 deals with the design and implementation of the LQG/LTR loop shaped controller for a DC servo motor. During the course of the chapter three controller implementations are developed, each subsequent development improves the performance of the controller.

All in all LQG/LTR augmented with loop shaping is a very powerful design synthesis procedure. The procedure is conducive to educated trial and error design iterations, and offers a well defined trade-off management perspective on controller synthesis.

2. The Estimator Design.

This section deals with the design of the state estimator which is used in subsequent sections to close a feedback control loop. The objective here is to minimise the number of feedback sensors thus reducing the cost and complexity of the implementation. Two sensors will be used, one for position information and one for current information. The current feedback information is used in the position / velocity servo to enhance the disturbance rejection properties of the design. As will be apparent in later chapters the current feedback measurement could be eliminated at the expense of the disturbance response performance.

Within the servo industry two position sensors dominate the market, namely the resolvers and the optical encoders. The resolver is in effect a rotating transformer, this sensor technology has been in use for the past 50 years and is often favoured because of robustness and reliability in an industrial environment. The resolver also provides absolute position information which is necessary in AC motor control applications. This technology is however analogue based and hence prone to environment noise. The optical encoder is a digital based technology and hence can often provide superior signal to noise ratios. Optical encoders are however more expensive than their analogue counterparts. In this research a feedback estimator based on the resolver is developed. It shall be shown that an equivalent optical encoder based feedback estimator is a subset of this resolver feedback estimator.

Conventional resolver interfaces require the use of a resolver to digital converter (RDC). This is usually a hybrid converter which is comprised of analogue multipliers and a digital tracking loop [Boyes 80]. Figure **[2-1]** described the internals of a RDC. An RDC tracking converter is a type 2 servo loop.

The resolver outputs described by equation **[2-2]** are multiplied by the sine and cosine of the digital position, this results in an error signal described by equation **[2-1]**. The carrier is demodulated from the error signal to produce an error proportional to the sine of the position error. The tracking loop increments / decrements the digital position counter until the error is driven to zero at which point the resolver position is the measured position. The outputs from the RDC are digital position and analogue velocity information. The RDC converter is an expensive component in a conventional resolver interfaces. The research here shows how this component can be eliminated and hence further reduce the cost and complexity of this sensor interface.

$$\varepsilon = A\cos(2\pi f_c t)(\sin\theta\cos\varphi - \cos\theta\sin\varphi)$$
$$= A\cos(2\pi f_c t)\sin(\theta - \varphi) \qquad \textbf{[2-1]}$$

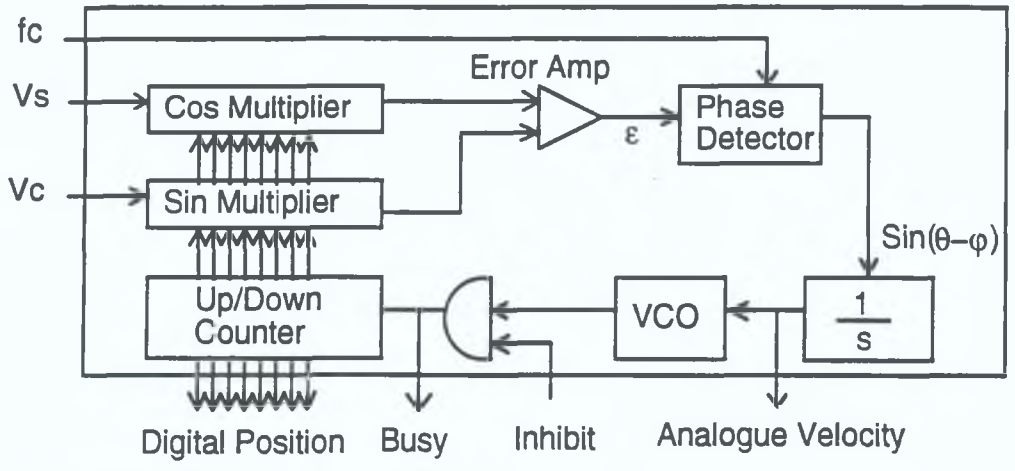

Fig. [2-1] Resolver to digital converter.

The sensor interface used in this research comprises of a steady state extended Kalman estimator. In the case of the resolver the inputs to the estimator are the sine and cosine channels of the resolver and the armature current feedback information. In the case of the optical encoder the problem reduces to the use of a Linear Kalman estimator with encoder position and armature current inputs. The outputs from both the Kalman Estimators in the final design are position, velocity, armature current and disturbance torque information. The following subsections deal with the development of a state estimator particular to the resolver.

2.1 The Resolver.

The resolver can be described as a rotating transformer excited by a carrier signal. The outputs from the resolver are the carrier signal amplitude modulated with the cartesian position information as described by equation **[2-2]**. This cartesian position information is then extracted using an envelope detection technique. Figure **[2-2]** depicts a modulated resolver channel and the output of the envelope detection stage. Appendix A describes the circuit used for this demodulation stage. The resulting demodulated signals describe the sensor's position in cartesian co-ordinates, equation **[2-3]**.

$$V_s' = A\sin(\theta) * \cos(2\pi f_c t)$$
$$V_c' = A\cos(\theta) * \cos(2\pi f_c t) \qquad \textbf{[2-2]}$$

$$V_s = \sin(\theta)$$
$$V_c = \cos(\theta) \qquad \textbf{[2-3]}$$

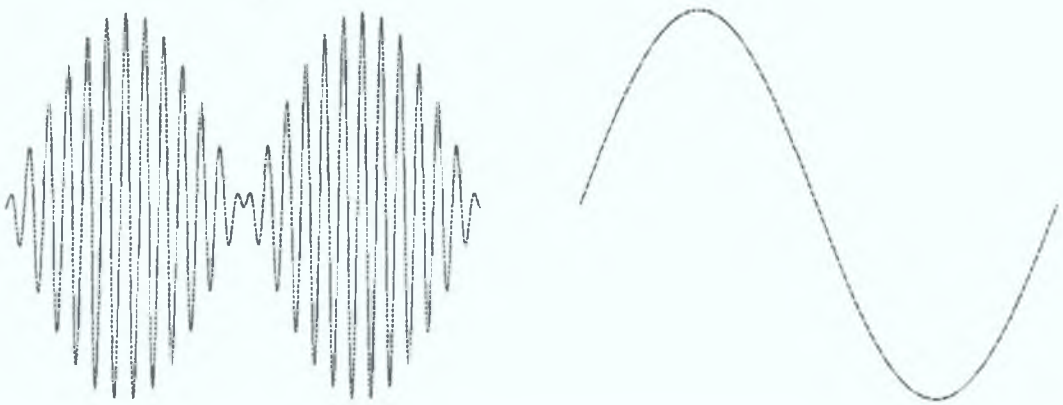

Fig. [2-2] Modulated resolver channel and demodulated channel.

These cartesian outputs are non-linear functions of resolver position. The Kalman filter cannot accommodate such measurements. By using simple trigonometric algebra θ can be described using equation **[2-4]**. This technique is however susceptible to amplitude and bias mismatch in the resolver channels as well as masking the well defined stochastic properties of the measurements. Equation **[2-3]** is very much an ideal representation of the demodulated resolver outputs [Hanselman 90]. In general the resolver channels can be better described by equation **[2-5]**, where ϕ describes a quadrature error between the two signals, *A* describes the amplitude of the resolver channels, *b* describes the bias on each channel and υ describes a Gaussian noise component with an variance *g*. These distortions are a consequence of the finite manufacturing processes used in the resolver construction and additional errors introduced during demodulation and filtering of the resolver channels.

$$\theta = \arctan\left(\frac{\sin(\theta)}{\cos(\theta)}\right) = \arctan\left(\frac{V_s}{V_c}\right) \qquad \textbf{[2-4]}$$

$$V_1 = A_1\sin(\theta+\phi) + b_1 + g_1\upsilon$$
$$V_2 = A_2\cos(\theta) + b_2 + g_2\upsilon \qquad \textbf{[2-5]}$$

In the following sections the Kalman filter is used to filter out the measurement noise and provide estimates for the states of the plant under investigation. In subsequent

sections an adaptive scheme will be used to compensate for the effects of amplitude and bias mismatches on each resolver channel. This scheme will serve as a self-tuning mechanism further reducing the cost of the design.

2.2 The Kalman Filter (KF) / Estimator.

Section 3.4 defines the discrete Kalman filter and its constituent components. In this section we will use the classical form of the Kalman filter. The filter problem can be described as follows.

Given a discrete time stochastic state space description of a system **[2-6]** and an observation model **[2-7]**, where Φ, Γ and H in equations **[2-6]** and **[2-7]** have their usual state space interpretation and where ω_k and υ_k denote process noise and measurement noise sequences respectively, then an estimate of the states of the plant is given by equation **[2-9]** where K_k is the Kalman gain described by equations **[2-10]**, **[2-11]** and **[2-12]**. These equations combine to form the algebraic Riccati equation. These process and measurement noise sequences are assumed to be uncorrelated, with zero mean and normal distributions. Formally these noises can be mathematically described using equations **[3-97]**, **[3-98]** and **[3-99]** in section 3.4. The matrices Q_k and R_k are defined as positive definite symmetric matrices [Kalman 60],[Gelb 74],[Grimble 88],[Haykin 89].

The Kalman filter is by definition a time varying filter hence the subscript notation on the transition matrix Φ_k, input coupling matrix Γ_k and observation matrix H_k. In this section the plant and observation models are assumed to be time invariant, hence the time varying properties of the filter will not be exploited. The subscript notation on the plant, coupling and observation matrices are consequently dropped.

Plant model:	$x_{k+1} = \Phi_k x_k + \Gamma_k u_k + G_k \omega_k$	**[2-6]**
Observation model:	$z_k = H_k x_k + \upsilon_k$	**[2-7]**
Predictive Est.:	$\hat{x}_{k+1\|k} = \Phi_k \hat{x}_{k\|k} + \Gamma_k u_k + G_k \varpi_k$	**[2-8]**
Current Est.:	$\hat{x}_{k\|k} = \hat{x}_{k\|k-1} + K_k\left(z_k - H_k \hat{x}_{k\|k-1}\right) - \overline{\upsilon}_k$	**[2-9]**
Gain:	$K_k = P_{k\|k-1} H_k^T \left\{ H_k P_{k\|k-1} H_k^T + R_k \right\}^{-1}$	**[2-10]**
A priori cov.:	$P_{k+1\|k} = \Phi_k P_{k\|k} \Phi_k^T + G_k Q_k G_k^T$	**[2-11]**

A posteriori cov.: $P_{k|k} = P_{k|k-1} - K_k H_k P_{k|k-1}$ **[2-12]**

For the linear time invariant system the Kalman gain will converge to steady state values. Indeed for a linear system the Kalman gains are independent of measurement information and consequently can be calculated off-line prior to implementation. For the infinite horizon linear time invariant problem the steady state Kalman filter is the optimum filter, in which case the initial transience of the Kalman gain can be replaced by the steady state gain. The steady state Kalman implementation greatly reduces the on-line computational overhead required by the full time varying Kalman implementation [Mendel 71]. The algebraic Riccati equation can be solved recursively until a steady state solution is reached. However, a preferred numerically robust solution is available by solving for the stable eigenvalues of the Hamiltonian matrix for the estimator problem, see equation **[3-15]** [Vaughan 70].

In the case of the optical encoder interface the observation and system models are both linear and time invariant, consequently the steady state Kalman filter implementation can be used for the construction of a state estimator. In the case of the resolver interface, however, the observation model is a non-linear function of position. Therefore an Extended Kalman filter construction is required.

2.3 The Extended Kalman Filter (EKF) / Estimator.

For the Extended Kalman filter the gaussian signal model equations **[2-6]** and **[2-7]** are replaced with nonlinear signal models described by equation **[2-13]** and **[2-14]**, where $\Phi(\cdot)$ and $\Gamma(\cdot)$ are nonlinear functions and $G(\cdot)$ is nonconstant in general. In this particular application only the observation signal model is nonlinear, consequently for this problem only equation **[2-14]** is required.

$$x_{k+1} = \Phi_k(x_k) + \Gamma_k(u_k) + G_k(x_k)\omega_k \qquad \textbf{[2-13]}$$

$$z_k = H_k(x_k) + \upsilon_k \qquad \textbf{[2-14]}$$

In the Extended Kalman filter design the nonlinear gaussian signal model is linearised about the most recent state estimate. This Extended Kalman filter is a suboptimal filter design because the linearised signal model is an approximation of the real signal model. In this case the suboptimality of the Extended Kalman filter exists only with the choice of a reference trajectory for the innovation sequence. For a concise

definition of the Extended Kalman see [Jazwinski 70, Theorem 8.1], [Anderson 79], [Mendel 87] and [Lewis 92].

In the Extended Kalman construction the nonlinear function if sufficiently smooth is expanded in a Taylor series expansion about the most recent estimate. This ensures that the available linear approximation of the observation model is the best available approximation and hence the reference trajectory is the best available trajectory. Equation **[2-15]** describes the first two terms of a Taylor series expansion for the nonlinear function, where H in equation **[2-15]** is a Jacobian matrix defined by equation **[2-16]**.

$$h_k(x_k) = h_k\left(\hat{x}_{k|k-1}\right) + H\left(x_k - \hat{x}_{k|k-1}\right) + \ldots. \qquad \textbf{[2-15]}$$

$$H = \left.\frac{\partial h(x)}{\partial x}\right|_{x=\hat{x}_{k|k-1}} \qquad \textbf{[2-16]}$$

By redefining the *a priori* and *a posteriori* error covariances the estimator problem can be redefined in terms of the linearised observation model. Equation **[2-17]** to **[2-23]** define the Extended Kalman filter for a gaussian signal model with a nonlinear observation model [Lewis 92].

Plant model: $$x_{k+1} = \Phi_k x_k + \Gamma_k u_k + G_k \omega_k \qquad \textbf{[2-17]}$$

Observation model: $$z_k = h_k(x_k) + \upsilon_k \qquad \textbf{[2-18]}$$

Predictive Est.: $$\hat{x}_{k+1|k} = \Phi_k \hat{x}_{k|k} + \Gamma_k u_k + G_k \varpi_k \qquad \textbf{[2-19]}$$

Current Est.: $$\hat{x}_{k|k} = \hat{x}_{k|k-1} + K_k\left(z_k - h_k\left(\hat{x}_{k|k-1}\right)\right) - \overline{\upsilon}_k \qquad \textbf{[2-20]}$$

Gain: $$K_k = P_{k|k-1} H_k^T\left(\hat{x}_{k|k-1}\right)\left\{H_k\left(\hat{x}_{k|k-1}\right) P_{k|k-1} H_k^T\left(\hat{x}_{k|k-1}\right) + R_k\right\}^{-1} \qquad \textbf{[2-21]}$$

A priori cov.: $$P_{k+1|k} = \Phi_k P_{k|k} \Phi_k^T + G_k Q_k G_k^T \qquad \textbf{[2-22]}$$

A posteriori cov.: $$P_{k|k} = P_{k|k-1} - K_k H_k\left(\hat{x}_{k|k-1}\right) P_{k|k-1} \qquad \textbf{[2-23]}$$

The overall structure of the Extended Kalman filter remains the same as that of the Linear Kalman filter. However from equation **[2-21]** it is immediately apparent that the EKF gains are a function of the most recent estimate. Thus the reduced computational overhead of the steady state Kalman implementation is not available with this design. This is a significant disadvantage when the gain calculation dominates the computational overhead of the Kalman implementation. In the

following section the structure of the EKF will be altered, in particular the manner in which the innovation sequence is evaluated. As a result of this a steady state solution for the EKF will be obtained.

2.4 The Steady State Extended Kalman Filter (SSEKF).

In this section a steady state implementation of the Extended Kalman estimator will be derived. This particular solution is unique to the nonlinear resolver problem. The observation model for the resolver problem is described by equation **[2-24]**. For this development it shall be assumed that the resolver channels have an amplitude of one and a mean of zero. It shall also be assumed that the measurement noises υ on each channel are uncorrelated and have gaussian distributions.

To simplify this derivation only a solution for a scalar plant model will be derived. The output of the resulting filter will be simply resolver position. Indeed for the scalar case the Extended Kalman estimator is really an Extended Recursive Least Squares estimator.

$$z_k = \begin{bmatrix} \sin\theta_k \\ \cos\theta_k \end{bmatrix} + \begin{bmatrix} \upsilon \\ \upsilon \end{bmatrix} \qquad \textbf{[2-24]}$$

From the observation model two matrices are defined namely equation **[2-25]** and **[2-26]**. Equation **[2-25]** is simply a matrix of the nonlinear functions of the observation model and **[2-26]** is the Jacobian matrix of equation **[2-25]** with respect to θ.

$$h\left(\hat{\theta}_{k|k-1}\right) = \begin{bmatrix} \sin\hat{\theta}_{k|k-1} \\ \cos\hat{\theta}_{k|k-1} \end{bmatrix} \qquad \textbf{[2-25]}$$

$$H\left(\hat{\theta}_{k|k-1}\right) = \begin{bmatrix} \cos\hat{\theta}_{k|k-1} \\ -\sin\hat{\theta}_{k|k-1} \end{bmatrix} \qquad \textbf{[2-26]}$$

Substituting these definitions into equation **[2-21]** gives equation **[2-27]**. For the scalar problem the error covariance is scalar and hence is represented in lowercase. Note that this solution is not unique to the scalar problem, the scalar problem is chosen here to simplify the development of a solution.

$$K_k = p_{k|k-1}\begin{bmatrix}\cos\hat{\theta}_{k|k-1} & -\sin\hat{\theta}_{k|k-1}\end{bmatrix}\left\{\begin{bmatrix}\cos\hat{\theta}_{k|k-1}\\ -\sin\hat{\theta}_{k|k-1}\end{bmatrix}p_{k|k-1}\begin{bmatrix}\cos\hat{\theta}_{k|k-1} & -\sin\hat{\theta}_{k|k-1}\end{bmatrix}+R_k\right\}^{-1} \qquad \textbf{[2-27]}$$

The R_k matrix is defined as the measurement covariance matrix. In the case of the resolver problem the measurement covariance matrix is defined by equation **[2-28]**, where σ in this equation is the variance of the measurement noise υ. Without loss of generality it shall be assumed that the stochastic properties of the measurement noise is the same for each channel. Furthermore it shall be assumed that these noises are uncorrelated with each other.

$$R_k = \begin{bmatrix}\sigma_\upsilon^2 & 0\\ 0 & \sigma_\upsilon^2\end{bmatrix} \qquad \textbf{[2-28]}$$

Substituting for R_k in equation **[2-27]** and expanding out the resulting expression yields a compact solution given in equation **[2-29]**.

$$K_k = \frac{p_{k|k-1}}{p_{k|k-1}+\sigma_\upsilon^2}\begin{bmatrix}\cos\hat{\theta}_{k|k-1} & -\sin\hat{\theta}_{k|k-1}\end{bmatrix} \qquad \textbf{[2-29]}$$

By substituting this latter expression for K_k into the scalar form of equation **[2-23]** the *a posteriori* error covariance update, independent of the most recent estimate, can be obtained **[2-30]**.

$$\begin{aligned} p_{k|k} &= p_{k|k-1} - \frac{p_{k|k-1}}{p_{k|k-1}+\sigma_\upsilon^2}\left[\sin^2\hat{\theta}_{k|k-1}+\cos^2\hat{\theta}_{k|k-1}\right]p_{k|k-1} \\ &= p_{k|k-1} - \frac{p_{k|k-1}}{p_{k|k-1}+\sigma_\upsilon^2}p_{k|k-1} \end{aligned} \qquad \textbf{[2-30]}$$

Equation **[2-30]** and the scalar version of equation **[2-22]** now describe an algebraic Riccati equation which is independent of the measurements and estimates. Consequently an off-line solution to these equations exists and hence a steady state solution.

The Kalman gain described by equation **[2-29]** can be partitioned into a linear portion and a nonlinear portion. The linear portion is a function of the *a priori* error covariance which is independent of measurement and state estimate information. The nonlinear portion is a function of the most recent position estimate. A steady state solution for the linear portion exists given a steady state solution to Riccati's equation. Indeed as will be established the linear portion of equation **[2-29]** is the Kalman gain for the linear problem.

For the linear scalar optical encoder problem the observation model is described by equation **[2-31]**, where υ is a gaussian noise source with a zero mean and a variance of σ. Substituting this description into equation **[2-10]** yields the Kalman gain as a function of the *a posteriori* error covariance **[2-32]**. This equation is the same as the linear portion of the Kalman filter gain for the resolver problem **[2-29]**.

$$z_k = \theta_k + \upsilon_k \qquad \textbf{[2-31]}$$

$$K'_k = \frac{p_{k|k-1}}{p_{k|k-1} + \sigma_k^2} \qquad \textbf{[2-32]}$$

This relationship between the Extended Kalman gain and the linear Kalman gain is not unique to the scalar problem. Similar results can be established for the non-scalar problem.

By substituting the gain equation **[2-29]** into equation **[2-20]** a current state estimate update equation can be established based on the non-linear gain matrix. Equation **[2-35]** describes this current estimate update.

$$\hat{x}_{k|k} = \hat{x}_{k|k-1} + \frac{p_{k|k-1}}{p_{k|k-1} + \sigma_\upsilon^2}\left[\cos\hat{\theta}_{k|k-1} - \sin\hat{\theta}_{k|k-1}\right]\begin{pmatrix}\sin\theta_k & -\sin\hat{\theta}_{k|k-1}\\ \cos\theta_k & -\cos\hat{\theta}_{k|k-1}\end{pmatrix} - \overline{\upsilon}_k \qquad \textbf{[2-33]}$$

$$\hat{x}_{k|k} = \hat{x}_{k|k-1} + \frac{p_{k|k-1}}{p_{k|k-1} + \sigma_\upsilon^2}\left[\sin\left(\theta_k - \hat{\theta}_{k|k-1}\right)\right] - \overline{\upsilon}_k \qquad \textbf{[2-34]}$$

$$\hat{x}_{k|k} = \hat{x}_{k|k-1} + K'_k \sin\left(\theta_k - \hat{\theta}_{k|k-1}\right) - \overline{\upsilon}_k \qquad \textbf{[2-35]}$$

The non-linear resolver problem has thus reduced to a linear optical encoder problem with a modified innovation sequence. In the case of the resolver problem the innovation sequence is simply the sine of the innovation sequence for the encoder

problem. The attractive numerically robust solutions to Riccati's equation are thus available in the resolver problem (see Section 3.1.2). The two problems are thus equivalent except for the manner in which the innovation sequence is evaluated.

Equation **[2-35]** is not a convenient form for implementation purposes because the quantity θ_k is not directly available. A better innovation sequence is given by equation **[2-36]**.

$$\sin\left(\theta_k - \hat{\theta}_{k|k-1}\right) = \sin\theta_k \cos\hat{\theta}_{k|k-1} - \cos\theta_k \sin\hat{\theta}_{k|k-1} \qquad \textbf{[2-36]}$$

For the remainder of this work the resolver problem will be solved as an encoder problem with the modified innovation sequence described by equation **[2-36]**. This procedure will be subsequently referred to as the SSEKF design.

2.5 The Estimator Design / Problem Formulation.

This section deals with the particulars regarding the design and implementation of a SSEKF based estimator[3]. The estimator designed in this section will form the basis for the estimator used in subsequent sections to construct the feedback loop in a Linear Quadratic Gaussian controller. The estimator has two functions in this design the first of which is to estimate the states of the plant under control using the available sensor information. In this particular case a position and a current sensor are used, from which position, velocity, armature current and disturbance torque states are estimated.

The second function performed by the estimator is the filtering of measurement and process noise. The position and current sensor information is analogue in origin and as a consequence is often corrupted with noise. In addition the sampling of these analogue signals introduces quantization noise onto the sensed information. In the case of the optical encoder the position information is digital in origin, hence the noise component of this measurement is comprised primarily of quantization noise.

---

[3] The terms Filter and Estimator are used interchangeably in this thesis. The internal structure of the Kalman Filter and the Kalman Estimator are identical. The difference lies in the interpretation of the output of the filter/estimator. In the case of the Kalman Estimator the outputs are the internal states of the Estimator, whereas in the case of the Kalman Filter the outputs are a linear combination of these internal states.

Quantization noise, to be denoted ε, can be described stochastically as a uniform distribution between $-\Delta/2$ and $\Delta/2$, where Δ is the quantization interval. Figure **[2-3]** shows the density function for this uniform distribution. The stochastic properties for this distribution namely its mean and variance are derived in equations **[2-37]** and **[2-38]** respectively [Swaszek 85], [Franklin 80].

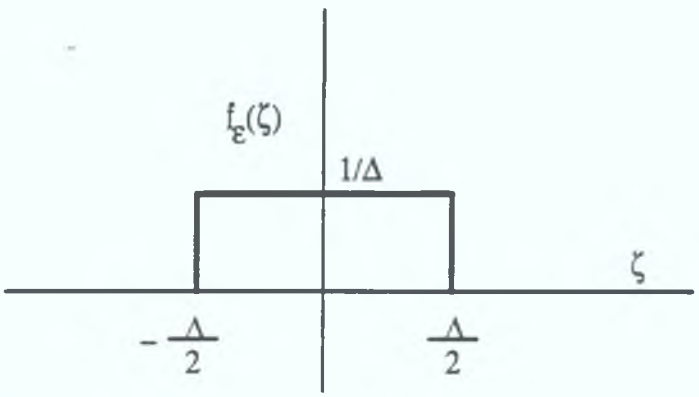

Fig. [2-3] Uniform Distribution

$$\mu_\varepsilon = E\{\varepsilon\} = \int_{-\infty}^{\infty} f_\varepsilon(\zeta)\zeta d\zeta = \int_{-\Delta/2}^{\Delta/2} \zeta \frac{1}{\Delta} d\zeta = \frac{1}{\Delta}\frac{\zeta^2}{2}\Big|_{-\Delta/2}^{\Delta/2} = 0 \qquad \textbf{[2-37]}$$

$$\sigma_\varepsilon^2 = E\{(\varepsilon - \mu_\varepsilon)^2\} = \int_{-\infty}^{\infty} (\zeta - 0)^2 f_\varepsilon(\zeta) d\zeta = \int_{-\Delta/2}^{\Delta/2} \frac{\zeta^2}{\Delta} d\zeta$$

$$\sigma_\varepsilon^2 = \frac{\zeta^3}{3\Delta}\Big|_{-\Delta/2}^{\Delta/2} = \frac{1}{3\Delta}\left[(\Delta/2)^3 - (-\Delta/2)^3\right] \qquad \textbf{[2-38]}$$

$$= \frac{\Delta^2}{12}$$

The quantization interval, Δ is a function of the scale and range of the parameter being measured. In the case of a resolver with a signal range from -1 to 1 the corresponding Δ for a 16 bit ADC is described by equation **[2-39]**. In the case of a current measurement in the signal ranges from -50 to 50, the corresponding Δ for a 12 bit ADC is described by equation **[2-40]**

$$\Delta = (u\_range - l\_range)/2^{BITS} \qquad \textbf{[2-39]}$$

$$\Delta = 2/2^{16}$$

$$\Delta = 100/2^{12} \qquad \textbf{[2-40]}$$

The noise variances due to quantization noise for position and current measurements are thus described by equations **[2-41]** and **[2-42]** respectively.

In the Kalman construction it is assumed that the noise sources have gaussian distributions. Quantization noise does not inherently satisfy this constraint. However in a configuration where the noise contribution due to quantization noise is equal in magnitude to the noise contribution due to other sources, the distribution of the quantization noise is masked by the white distribution of the other noise sources. Note that although a white noise source does not exist in nature, the distribution of an infinite sum of uncorrelated noise sources will approximate to a white distribution. In this situation it is assumed that the other noise sources have a white distribution and that the variance of these sources can be described by equations **[2-41]** and **[2-42]**. Hence the accumulative distributions of the measurement noise will approximate to a gaussian distribution, [Sripad 77] [Schucham 64].

$$\sigma_\theta^2 = \frac{\left(\frac{2}{2^{16}}\right)^2}{12} \qquad \textbf{[2-41]}$$

$$\sigma_I^2 = \frac{\left(\frac{100}{2^{12}}\right)^2}{12} \qquad \textbf{[2-42]}$$

The next stage in the construction of a Kalman estimator is to define the plant model for the system under investigation. The particulars of this model are presented in more detail in section 4.1. Here however it will suffice to say that the Kalman estimator's model will be an approximation to the physical system. The process covariance matrix Q defines the extent to which this model is an approximation. In a practical situation the extent to which these models are approximations is often not known. Thus a first attempt is to model the process noise of a noise source entering at the input to the plant. The relative variance of this noise source with respect to the variance of the measurement noise will define the relative weighting of the plant model and measurement information. If this process noise is high relative to the measurement noise the Kalman estimator will weight the *a posteriori* information. If the process noise is high relative to the measurement noise the Kalman filter will favour the measurement information. The ratio of the process noise covariance and measurement noise covariance matrices will define the bandwidth of the Kalman filter in a classical sense. Hence an estimator with a relatively large process noise covariance will converge faster than an estimator with a relatively low process noise covariance.

Figure [2-4] depicts a block diagram of the plant under investigation. In some circumstances the level of uncertainty for the model associated with the mechanical motor and its load may be much higher than the uncertainty associated with the current amplifier. In such a situation modelling this uncertainty as a process noise at the input to the current amplifier would be an unfair reflection of the true modelling uncertainty. The true model uncertainty can be better described by introducing an additional process noise at the input to the motor model. These process noises are reflected in the state noise covariance matrix Q. Estimates for Q can often be obtained from the identification procedures.

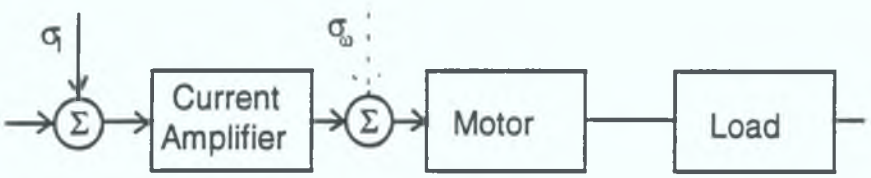

Fig. [2-4] Injection of process noise.

Note the above discussion regarding the choice of the process noise covariance may not seem very definitive. However in a practical application the derivation of a process noise model is often more complicated than the derivation of the approximated process model. Indeed this is one reason why the model is an approximation in the first place.

Later in section 3.3.3.1 it will become apparent that concise definitions for the noise covariance matrices are not necessary for the estimator design. The bandwidth of the estimator, as defined by the ratio of the process and measurement noise covariance matrices, is set by the Loop Transfer Recovery (LTR) procedure during the robust controller design. The noise covariance matrices developed in this section will form the basis of a nominal estimator used in the LTR design. The noise covariance matrices developed in this section suit a Kalman filter application more than an estimator application.

2.6 Amplitude, Phase and Bias Imbalance Estimation.

The estimator developed in the preceding sections for the resolver problem assume the availability of ideal resolver outputs as described by equation **[2-3]**. In reality the resolver signal is not ideal, it is often subject to amplitude imbalance, quadrature error, inductive harmonics, reference phase shifts, excitation signal distortion and disturbance signals [Hanselman 90]. These non-ideals are a consequence of the finite manufacturing process and mechanical constraints of the resolver unit. In addition to these inherent non-ideals the post resolver circuitry can introduce further amplitude, bias and phase imbalances onto the resolver signals.

In this section the accumulative effect of these imbalances will be estimated. These non-ideals contribute to a significant portion of the position distortion in the resolver transducer. Conventionally amplitude and bias imbalance are removed from the resolver signals prior to resolver to digital conversion (RDC). Post resolver phase and amplitude imbalance are minimised by using matched filters on each resolver channel. This calibration stage of the installation is labour intensive and hence expensive. In addition a high tolerance is required on the post resolver conditioning component. In this section an estimation scheme will be introduced which estimates these imbalances, hence reducing the cost and complexity of the design.

Equation **[2-43]** describes the resolver signal distorted with amplitude, bias and phase imbalances. This equation describes a non-linear problem with five unknown parameters and one unknown state. The framework of the Extended Kalman is well suited for such joint parameter and state estimation problems [Ljung 79]. By defining a state vector (**[2-44]**) with an element for each of the unknowns, a Kalman observation model can be defined by equations **[2-45]** and **[2-46]**. This observation model is a non-linear function of the states, hence an Extended Kalman filter construction is required. The appropriate Jacobian matrix for this observation model is described by equation **[2-47]**.

$$V_1 = A_1 \sin(\theta + \phi) + b_1 + g_1 \upsilon$$
$$V_2 = A_2 \cos(\theta) + b_2 + g_2 \upsilon \qquad \textbf{[2-43]}$$

$$x \equiv \{A_1 \quad A_2 \quad b_1 \quad b_2 \quad \phi \quad \theta\}^T \qquad \textbf{[2-44]}$$

$$z_k = h_k(x_k) + G\upsilon_k \qquad \textbf{[2-45]}$$

$$h_k(x_k) = \begin{bmatrix} x_k^{A_1} \sin\left(x_k^{\theta} + x_k^{\phi}\right) + x_k^{b_1} \\ x_k^{A_2} \cos\left(x_k^{\theta}\right) + x_k^{b_2} \end{bmatrix} \qquad \textbf{[2-46]}$$

$$H_k(x_k) = \begin{bmatrix} \sin\left(x_k^{\theta} + x_k^{\phi}\right) & 0 & 1 & 0 & -x_k^{A_1} \cos\left(x_k^{\theta} + x_k^{\phi}\right) & -x_k^{A_1} \cos\left(x_k^{\theta} + x_k^{\phi}\right) \\ 0 & \cos x_k^{\theta} & 0 & 1 & 0 & x_k^{A_2} \sin x_k^{\theta} \end{bmatrix} \qquad \textbf{[2-47]}$$

The measurement noise covariance matrix for this observation model can be derived as before. The process noise covariance matrix should convey the necessary adaptation rate for each of the states. In the case of the amplitude, bias and phase states, the adaptation rates should be relatively slow. These states are not expected to vary during operation but they may drift over the lifetime of the product. The initial error covariance matrix $P_{0|0}$ should be large enough to allow the states to converge to their nominal values. This matrix should reflect the uncertainty associated with the initial state estimate x_0.

The Extended Kalman estimator described above will accurately estimate position in the presence of amplitude, bias and phase imbalances. For the purpose of fullstate feedback control all the states of the plant are required, in this particular case position, velocity, current and disturbance torque. Thus the estimator described above must be augmented with the model for the plant under control. As will be seen in subsequent sections the plant can be described by a fifth order model. The resulting augmented system will be an eleventh order model.

In the context of this research a steady state solution for this augmented Extended Kalman estimator was not developed. Indeed it is quite likely that such a closed form solution does not exist because of the non-linearities associated with the coupling of the phase state ϕ. In the absence of a steady state solution the estimator must be implemented as a time varying Extended Kalman estimator. A time varying Extended Kalman implementation for an eleventh order system would occupy a significant portion of the computational resources.

The Extended Kalman filter is implemented using equations **[2-17]** to **[2-23]**. It is necessary to insure the numerical robustness of a particular implementation against the accumulative effects of roundoff error. In particular if the plant model is ill-

conditioned the system is extremely sensitive to roundoff error. The accumulative effects of this roundoff error is prone to causing the error covariance estimate to lose its positive semidefinite condition, in the event of which the estimator will diverge away from the true estimates, thus becoming unstable. In such a situation an alternative numerically robust implementation of the Riccati equation such as the Joseph Stabilised version is desirable. This however further increases the computational requirements of the estimator but ensures convergence even in the presence of roundoff error. Equation **[2-48]** described the *a posteriori* error covariance update for the Joseph Stabilised version of Riccati's equation [Lewis 86].

$$P_{k|k} = \left(I - K_k H(\hat{x}_{k-1})\right) P_{k|k-1} \left(I - K_k H(\hat{x}_{k-1})\right)^T + K_k R K_k^T \qquad \textbf{[2-48]}$$

Other Kalman implementations such as the square root filter (SRF) developed by Potter [Bierman 77] or Bierman UDU-factorisation modification of the SRF [Bierman 77], provide the same degree of numerical stability as the Joseph Stabilised filter. Each design introduces an additional degree of complexity as well as increasing the computational requirements of the implementation. For a comparison of the numerical efficiency and computational requirements of these filters see [Bierman 77],[Verhaegen 86]. The UDU implementation is the most efficient estimator design.

As stated the unknown parameters are time invariant. In the context of this work it is their initial set points which are unknown. Although these parameters can be expected to vary over the life span of the product, these variations can be assumed to be constant over the timeframe for control. Thus estimating these parameters at the frequency of the control loop is non-essential. To reduce the computational overhead of this implementation to a large degree, the parameter estimation and the state estimation functionality of this joint extended estimator are decoupled into separate modules.

The parameter estimation module will consist of the extended Kalman estimator presented in this section. The state estimator module will consist of the SSEKF developed in section 2.4. Although the parameter estimation module is numerically intensive it can be implemented at a frequency which reflects the rate at which the parameters are varying. Indeed with suitably selected transition matrices multiple sample rates can be catered for. This facilitates an initial power-up self-diagnostic mode with a reasonably fast sample rate and a run-time mode with a slow sample rate. This inevitably reduces the burden on the computational resources.

The output from the parameter estimator module is used to linearise and correct imbalances in the measurement information which is subsequently used in the state estimator module and control loop. Figure **[2-5]** shows a functional block diagram description of this system. Note that the phase imbalance can only be corrected given prior knowledge of the resolver position. This information is not available at the imbalance correction stage. The phase correction can take place internally in the Extended Kalman innovation sequence, but this is at the cost of the steady state solution. Thus phase correction is available but the cost is a significant increase in the computational overhead.

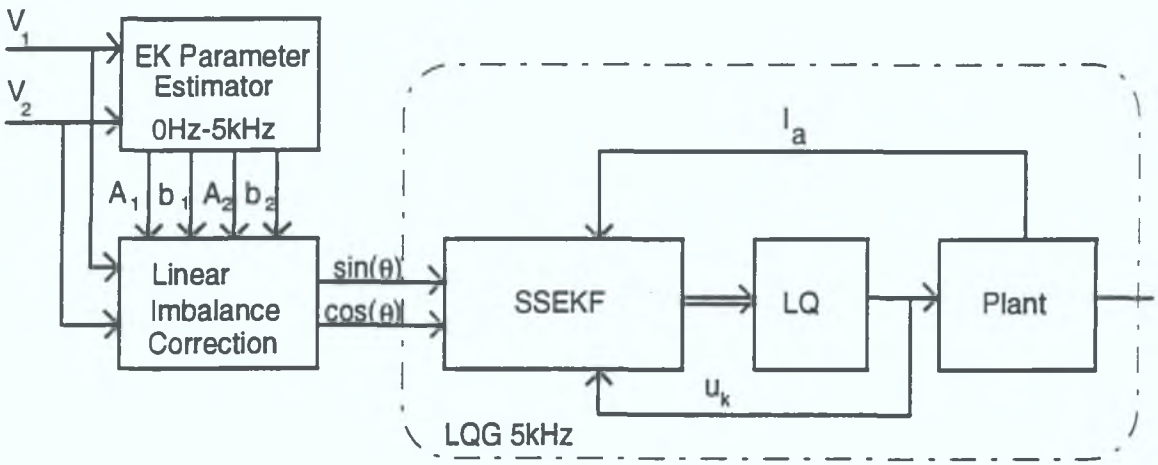

Fig. [2-5] Functional block diagram of controller.

3. The Controller Design.

This chapter deals with the development of a full state feedback controller. A full state feedback controller is used in this design because it is the optimal controller structure, with full control over the location of the roots of the closed loop system. The assignment of the root locations is at the discretion of the designer. Often, in the design of a control system, standard forms are used to assign the root locations, such forms comprise of sets of normalised polynomials such as the ITAE [Graham 53] and Butterworth polynomials. The resulting controller is a deterministic controller, an example of an ITAE controller can be found in [Kettle 93]. The roots of the polynomials are used in conjunction with Ackermann's formula to arrive at the desired full state feedback gain K [Franklin 80].

In this chapter a robust optimal Linear Quadratic Gaussian controller (LQG) is developed based on the Kalman estimator developed in the previous chapter and on a Linear Quadratic controller (LQ) presented in section 3.1. The root locations of the LQG design are selected optimally based on state weighting and stochastic process information. The course of this chapter examines the robustness, noise attenuation and disturbance suppression properties of the LQG design, modifications to the design are developed to overcome short falls in the design with regard to these properties.

3.1 The Linear Quadratic Controller (LQ)

A deterministic criterion for arriving at the desired optimal feedback gain, based on a linear quadratic (LQ) cost function is developed in this section. Equation **[3-1]** describes this cost function. The theory and use of the criterion ties in with the Kalman estimator theory. The final system will comprise of an integration of the two techniques to form a robust optimal controller structure (LQG).

$$J = \tfrac{1}{2}\sum_{k=0}^{N}\left[x_k^T Q_1 x_k + u_k^T Q_2 u_k\right] \qquad \textbf{[3-1]}$$

The LQ control criterion is based on the minimisation of the performance criterion given by equation **[3-1]**, where Q_1 is a positive semidefinite symmetric weight matrix

and Q_2 is a positive definite weight matrix which are selected by the designer to describe the relative importance of plant states and the cost of the resulting control. The LQ control problem can be stated as the minimisation of the cost function constrained by the dynamics of the plant **[3-2]**.

$$-x_{k+1} + \Phi x_k + \Gamma u_k = 0 \qquad \textbf{[3-2]}$$

This problem is a standard constrained-minimisation problem and can be solved by using the method of Lagrange multipliers. The solution involves reformulating the problem in terms of the Lagrange multiplier λ_{k+1}. The new cost function is described by equation **[3-3]**. Then minimising J with respect to u_k, x_k and λ_k produces three equations **[3-4]**, **[3-5]** and **[3-6]**. These equations describe a two point boundary value problem the solution of which can be found in [Bryson 75] and [Franklin 80].

$$J = \tfrac{1}{2}\sum_{k=0}^{N}\left[x_k^T Q_1 x_k + u_k^T Q_2 u_k + \lambda_{k+1}\left(-x_{k+1} + \Phi x_k + \Gamma u_k\right)\right] \qquad \textbf{[3-3]}$$

$$\frac{\partial J}{\partial u_k} = u_k^T Q_2 + \lambda_{k+1}^T \Gamma = 0 \qquad \textbf{[3-4]}$$

$$\frac{\partial J}{\partial \lambda_{k+1}} = -x_{k+1} + \Phi x_k + \Gamma u_k = 0 \qquad \textbf{[3-5]}$$

$$\frac{\partial J}{\partial x_k} = x^T Q_1 - \lambda_k^T + \lambda_{k+1}^T \Phi = 0 \qquad \textbf{[3-6]}$$

The solution of the boundary value problem yields the discrete *Riccati equation* **[3-7]** and **[3-8]**, this is a non-linear equation, the closed form solution of which is not readily obtainable. The optimal feedback gain K given by equation **[3-9]** is derived from equation **[3-4]**, **[3-7]** and the solution for λ_{k+1}.

$$S_k = \Phi^T M_{k+1} \Phi + Q_1 \qquad \textbf{[3-7]}$$

$$M_{k+1} = S_{k+1} - S_{k+1}\Gamma\left[Q_2 + \Gamma^T S_{k+1}\Gamma\right]^{-1}\Gamma^T S_{k+1} \qquad \textbf{[3-8]}$$

$$K_k = \left[Q_2 + \Gamma^T S_{k+1}\Gamma\right]^{-1}\Gamma^T S_{k+1}\Phi \qquad \textbf{[3-9]}$$

Here S_k is a positive definite matrix of the performance index under optimal control, M_{k+1} is an intermediate term in the calculation of the performance index and K_k is the weighting of states under optimal control [Kalman 60].

The recursive Riccati equation must be solved backwards because some of the boundary conditions to the boundary value problem are given at the endpoints. The result of this is a set of optimal feedback gains K_k for k=1 to N where N is the length of the iteration. For the infinite time linear problem, which is the most likely scenario for a servo system, the set of gains K will converge to a steady state gain, and for the infinite time problem the steady state solution is the optimum feedback solution. This iterative process is however numerically intensive and as a result can be inaccurate, consequently a nonrecursive solution to Riccati's equation is often preferred [Vaughan 70]. This nonrecursive solution involves rewriting the difference equations **[3-4]**, **[3-6]** in terms of x and λ, the resulting set of equations are then combined to form what is known as a Hamiltonian equation **[3-10]**.

$$\begin{bmatrix} x \\ \lambda \end{bmatrix}_{k+1} = \begin{bmatrix} \Phi + \Gamma Q_2^{-1}\Gamma^T\Phi^{-T}Q_1 & -\Gamma Q_2^{-1}\Gamma^T\Phi^{-T} \\ -\Phi^{-T}Q_1 & \Phi^{-T} \end{bmatrix} \begin{bmatrix} x \\ \lambda \end{bmatrix}_k \qquad \textbf{[3-10]}$$

$$\mathbf{H}_c = \begin{bmatrix} \Phi + \Gamma Q_2^{-1}\Gamma^T\Phi^{-T}Q_1 & -\Gamma Q_2^{-1}\Gamma^T\Phi^{-T} \\ -\Phi^{-T}Q_1 & \Phi^{-T} \end{bmatrix} \qquad \textbf{[3-11]}$$

The Hamiltonian matrix **[3-11]** is a square matrix of dimension $2n$, where n is the order of the plant. The n stable eigenvalues of the Hamiltonian matrix are the eigenvalues of the optimal constant gain closed loop system [Vaughan 70]. The infinite time problem performance index S_∞, can be evaluated using **[3-12]**, where X_I and Λ_I are the stable eigenvectors and eigenvalues of the Hamiltonian matrix. The optimal feedback gain for the infinite time problem is given by equation **[3-9]** where S_{k+1} is replaced by S_∞, and K_k is replaced by K_∞.

$$S_\infty = \Lambda_I X_I^{-1} \qquad \textbf{[3-12]}$$

This nonrecursive solution is the preferred solution of Riccati's equation and is the technique used in many simulation packages e.g. Matlab® Control toolbox "dlqr.m" [Little 92].

3.1.1 Heuristic Tuning

Using the results of the previous section, the solution of the linear quadratic controller problem has reduced to the choice of the performance weights Q_1 and Q_2, this often requires some trial and error with the aid of computer simulation.

A guideline for an 'acceptable' choice of the performance weights is to choose Q_1 and Q_2 as diagonal matrices, with diagonal elements given by **[3-13]**, **[3-14]**, where ρ in equation **[3-13]** is selected by trial and error [Bryson 75 Ch. 5]. This method is known as Bryson's inverse square method. Note that ρ is proportional to the bandwidth of the resulting controller and intuitively is proportional to the cost of control. The philosophy behind this criterion is that a fixed percentage change in each of the states makes an equal contribution to the overall cost. Alternative approaches based on nominal values instead of maximum values, or maximum deviations instead of maximum values are suggested by [Kwakernaak 72] and [Franklin 80] respectively. Further approaches can be found in [Grimble 88a].

A heuristic algorithm for tuning the LQ controller is of the form:

- Determine the maximal allowable deviations.
  $\max x_i, \quad i = 1,\ldots,n ; \max u_i, \quad i = 1,\ldots,m$

- Assign cost-index weight matrices **[3-13]** & **[3-14]**

$$Q_1 = \begin{cases} q_{i,j} = 0, i \neq j \\ q_{i,i} = \rho / (\max x_i)^2 \end{cases}, \text{for } i,j = 1..n \qquad \textbf{[3-13]}$$

$$Q_2 = \begin{cases} q_{i,j} = 0, i \neq j \\ q_{i,i} = 1 / (\max u_i)^2 \end{cases}, \text{for } i,j = 1..m \qquad \textbf{[3-14]}$$

- Solve for the optimal feedback gain using the LQ cost function equation **[3-1]**, using **[3-11]**, **[3-12]** and **[3-9]**.

- Alter ρ until a satisfactory response is found.

The choice of a particular approach will depend on the application. In this work a variation on maximum value approach is used, these values are readily available from plant and actuator models and are used as nominal maximum values for the controller design. The maximum values are adjusted depending on the requirement of the application. For example in a servo application the relative weighting of the current and position states could be relaxed, the control of the motor's position is more important than the amount of current used to control this position. Relaxing the current weighting reduces the cost of current during control. There is however a limit

on the extent to which current weighting can be relaxed. This limit is coupled to maximum current available from the amplifier. Note that these criteria are guidelines regarding the correct choice of Q_1 and Q_2, hence the heuristic nature of this section.

3.1.2 The Estimator and Controller Duality.

As mentioned in the outset of this chapter, there is an attractive cohesion between the LQ controller design and the steady state Kalman Estimator (KE). This cohesion is called the *duality principle,* which was first observed by R.E. Kalman in [Kalman 60]. Both the LQ controller and the KE use Riccati's equation in their construction. In the LQ controller Riccati's equation **[3-7], [3-8]** is a backward difference equation, in the KE it is a forward difference equation, these differences emanate from the different boundary conditions used in their respective constructions. By appropriately changing the variables (see Table **[3-1]**) the estimator Riccati's equation can be mapped to the LQ controller Riccati's equation. Thus the Hamiltonian solution for the controller problem can be applied to the estimator problem. Indeed a Hamiltonian matrix can be constructed for the estimator problem using Table **[3-1]**. This matrix is given in equation **[3-15]**. The use of equation **[3-15]** is often the preferred solution of Riccati's equation in the estimator problem, see Matlab® Control toolbox "dlqe.m" [Little 92].

Controller	*Description*	**Estimator**	*Description*
x_k	(Observable) State variable of plant to be regulated.	x_k	(Unobservable) State variable of random process.
u_k	Control variables.	y_k	Observed random variables.
Φ	Transition matrix.	Φ^T	Transition matrix
M_k	Matrix of quadratic performance under optimal regulation.	P_k	Covariance of optimised estimated error.
S_k		P_k^-	A prior covariance matrix.
Γ	Coupling of control states.	H^T	Coupling of measured states.
Q_1	Matrix of quadratic form defining performance criterion.	$\Gamma R_w \Gamma^T$	Covariance of random excitation.
Q_2	Matrix of quadratic form defining performance criterion.	R_v	Covariance of random measurements.

Table [3-1] Estimator controller duality.

$$\mathbf{H}_e = \begin{bmatrix} \Phi^T + H^T R_v^{-1} H \Phi^{-1} \Gamma R_w \Gamma^T & -H^T R_v^{-1} H \Phi^{-1} \\ -\Phi^{-1} \Gamma R_w \Gamma^T & \Phi^{-1} \end{bmatrix} \qquad \textbf{[3-15]}$$

3.2 Properties of the LQ Controller

3.2.1 Gain and Phase Margins

One of the most attractive features of the LQ controller is its robustness properties. It has long since been established [Safonov 77] that the LQ controller has an infinite gain margin (GM), a 50%-gain reduction tolerance in each feedback loop and a 60° phase margin (PM). Kalman in [Kalman 64] showed for a continuous time description of the system, that the condition for optimality (namely that the return difference matrix satisfies **[3-16]**) inscribed a circle of exclusion in the Nyquist plane about the -1+*j*0 point, of radius 1 see Figure **[3-1]**. Safonov and Athans [Safonov 77] showed that the exclusion of the Nyquist contour from this region guarantees the infinite gain and 60° phase margins. The 50%-gain reduction tolerance in each of the feedback loops was highlighted in a paper by Rosenbrock [Rosenbrock 71]. This paper showed by example, that with a greater than 50% reduction in feedback gains, the closed loop system could become unstable. The downside gain margin is a measure of how far the point of encirclement must be moved in order that the number of encirclements about this point fail to equal the number of poles in the right half plane. This means that failure of one of the feedback sensors could affect system stability. It must however be stressed, that these margins are guaranteed minimum robustness margins. In a given implementation the resulting margins could indeed be better. However an essential requirement of most industrial control systems is that a change in the loop gains between zero and their designed values should leave the system with an adequate stability margin[4]. The LQ controller doesn't inherently satisfy this constraint. Thus simulation of the sensor feedback failure should be carried out for each design. This shortfall of the LQ controller is only of significant importance in MIMO systems. In this particular work, the emphasis is on reduced sensor feedback using an estimator for state reconstruction, hence the number of physical sensors is very small thus the number of failure combinations is small. Moreover in the servo industry, if the tachogenerator feedback loop fails, the overspeed protection for the servo would simply trip. Other control applications could be less forgiving.

$$\left|S_k(i\omega)\right| = \left|1 + k\Phi(s)g\right| > 1 \qquad \textbf{[3-16]}$$

[4] The loop gain could change as a result of feedback sensor failure, or some other unpredicted event.

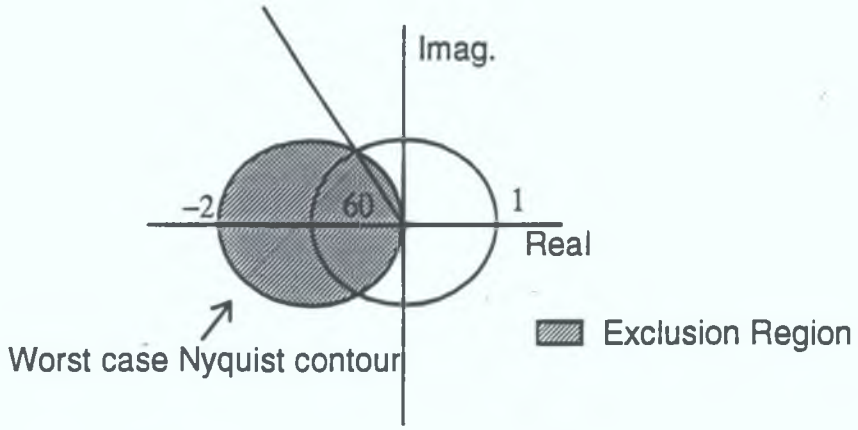

Fig [3-1] Nyquist contour

3.2.1.1 Gain and Phase Margins for Discrete Time Systems

The attractive gain and phase margins just described are valid for a continuous time system. There is an equivalent but less attractive discrete time interpretation of the return difference inequality. These discrete time robustness margins give further insight into the trade-off between robustness and sample frequency selection. Willems [Willems 78] derived the solution to the inverse problem and showed that the minimum gain, downside gain and phase margins can be described by equations **[3-17]**, **[3-18]** and **[3-19]**, where the parameter β is defined by **[3-20]** and where p_0 and r_0 in **[3-20]** are the coefficients of z^0 in the open loop and closed loop system respectively.

$$\text{Gain margin} = \left\{1 - \frac{1}{\beta}\right\}^{-1} \qquad \textbf{[3-17]}$$

$$\text{Down side gain margin} = \left\{1 + \frac{1}{\beta}\right\}^{-1} \qquad \textbf{[3-18]}$$

$$\text{Phase margin} = 2\sin^{-1}\left(\frac{1}{2\beta}\right) \qquad \textbf{[3-19]}$$

$$\beta = \sqrt{\frac{p_0}{r_0}} \qquad \textbf{[3-20]}$$

One drawback with the evaluation of these robustness bounds is that the parameter β is not directly accessible from the controller design procedures. Anderson [Anderson 89] extended these results into a generally, more readily accessible parameter γ, where γ is defined by equation **[3-21]**. U. Shaked in [Shaked 86] derived a similar set of results using a singular value constraint.

$$\gamma = \left(\Gamma^T S_\infty \Gamma + 1\right)^{-\frac{1}{2}} = \frac{1}{\beta} \qquad \textbf{[3-21]}$$

A graphical interpretation of these results can be obtained by looking at the discrete time Nyquist plot defined by equation **[3-22]**. This described a circle of exclusion, of radius γ depicted in Figure **[3-2]**.

$$\left|1 - K^T\left(e^{j\omega} I - \Phi\right)^{-1}\Gamma\right| \geq \gamma \qquad \textbf{[3-22]}$$

where $\gamma^{-1} > 1$

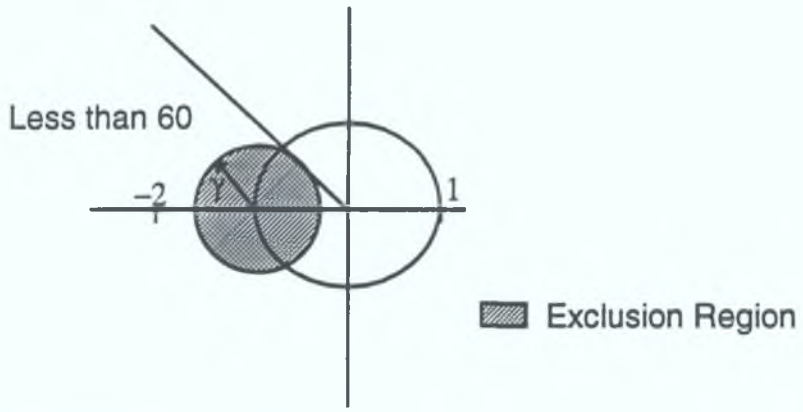

Fig [3-2] Nyquist contour for a discrete system

The design trade-off that can be made between sample frequency and robustness can be seen using a simple design example. Consider the scalar example of a plant and full state feedback controller **[3-23]**, the discrete time description is given by **[3-24]**. Choose for this example $a = -0.5, b = 100$ and k equal to the solution of the LQ problem for a $Q_1 = \rho, Q_2 = 1$.

$$\dot{x} = ax + bu \quad , u = -kx \qquad \textbf{[3-23]}$$

$$x_{k+1} = e^{-aT} x_k + bTu_k \quad , u_k = -kx_k \qquad \textbf{[3-24]}$$

Figure **[3-3]** shows a plot of the phase margin as a function of sample frequency and the LQ tuning parameter ρ. From the figure it can be seen that, as the sample frequency is increased, the minimum phase margin will converge towards 60°. This makes intuitive sense because as the sample frequency is increased the system will converge towards a better approximation of the continuous time system. As the

bandwidth of the controller is increased with increasing ρ the rate at which the minimum gain margin converged towards the 60° margin decreased. Thus, in order to maintain the same minimum phase margin the sample frequency must be increased. A contour drawn across the surface from point A to point B, would represent a good design trade-off, this would correspond to a minimum phase margin of approximately 55°. The 60° minimum phase margin can only be realised through an excessive increase in sample frequency or an equivalent reduction in controller bandwidth.

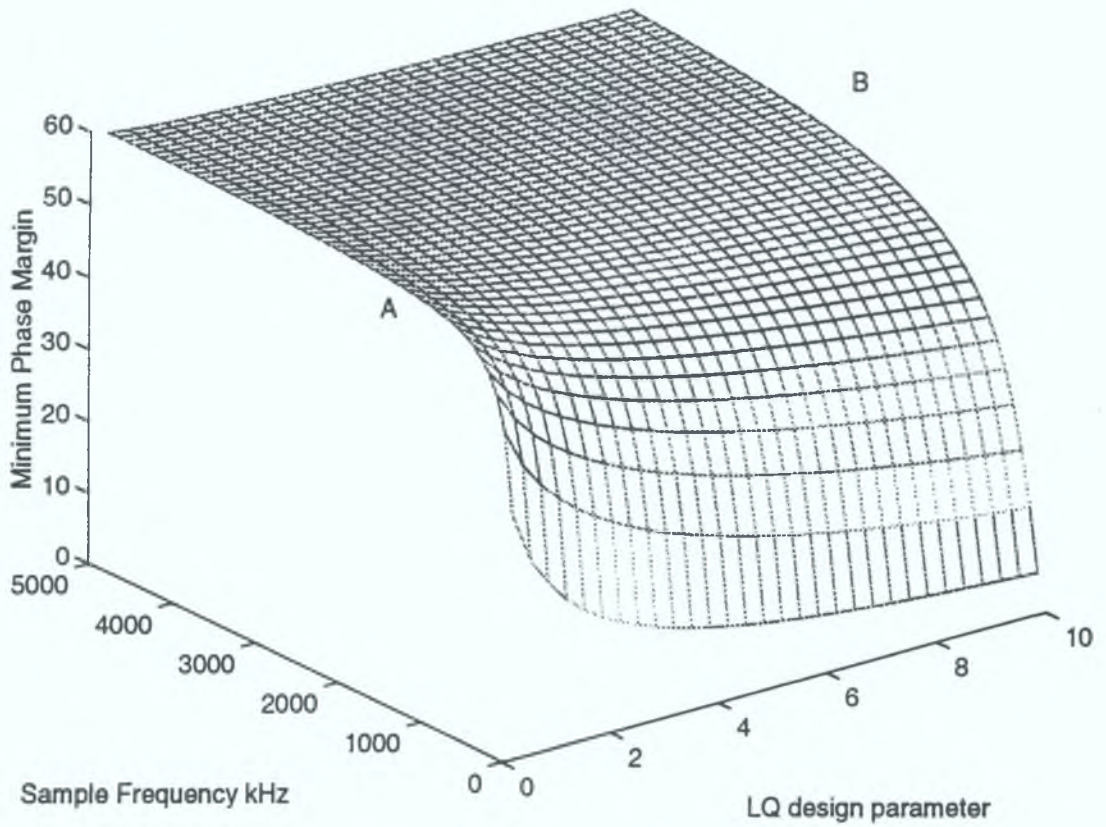

Fig. [3-3] Minimum Phase margin.

Figure **[3-4]** shows a plot of gain margin as a function of sample frequency and the LQ tuning parameter ρ. From the figure it is evident that a low bandwidth and a high sample frequency would provide a good minimum gain margin. This would however be detrimental to the minimum downside gain margins depicted in Figure **[3-5]**. In conclusion the contour from point A to point B in Figure **[3-3]** would represent an overall compromise between the robustness bounds. Such a trade-off will form part of the heuristic tuning procedures. Note that the infinite gain margin can never be reached, because of the nature of the discrete design.

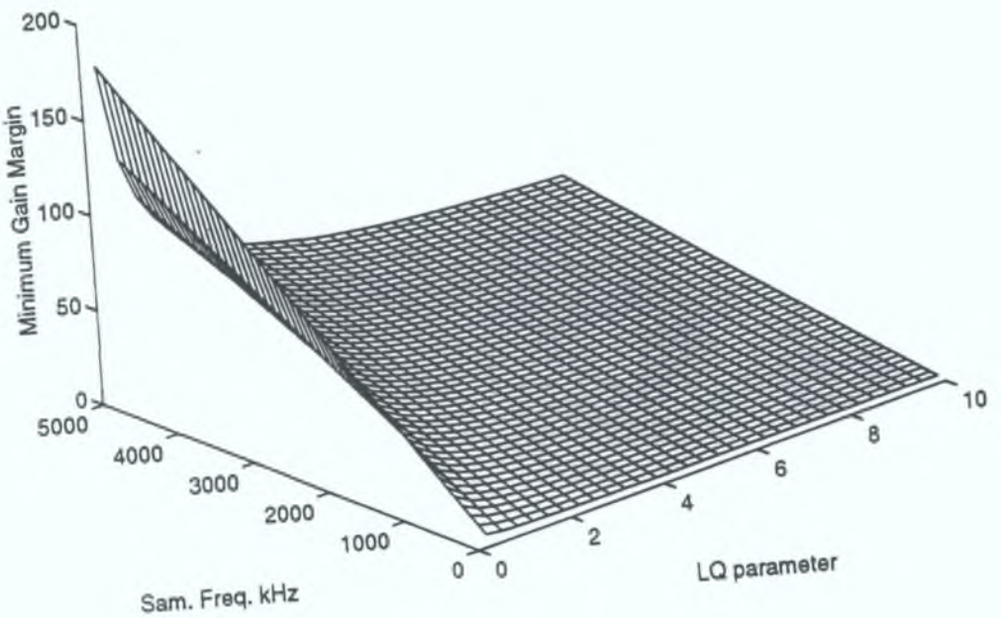

Fig. [3-4] Minimum Gain margin.

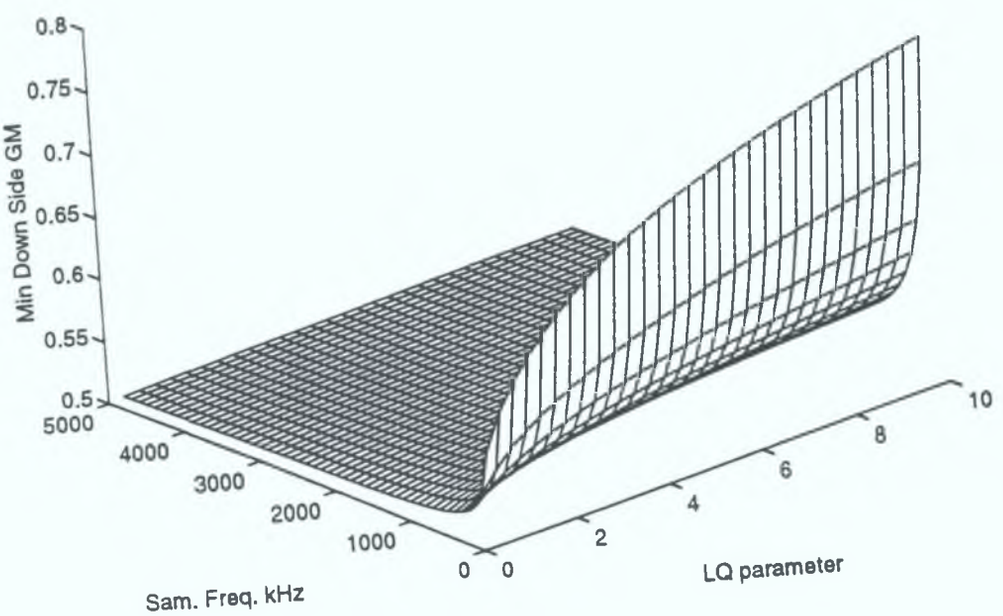

Fig. [3-5] Minimum Down Side Gain margin.

3.2.2 Sensitivity and the Role of the Return Difference.

In this section two important transfer functions will be developed which will help in the examination of the closed loop system for sensitivity to noise, disturbance and parameter variation.

Consider the stable closed loop system depicted by Figure **[3-6]**, equations **[3-25]**, **[3-26]** & **[3-27]** can be easily established. From this the sensitivity and complementary sensitivity functions can be defined **[3-28]**, **[3-29]**.

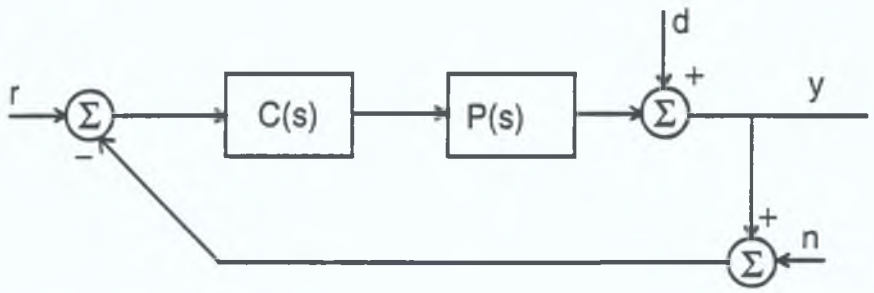

Fig. [3-6] Closed loop system.

$$y = PC(I + PC)^{-1}(r - n) + (I + PC)^{-1}d \qquad \textbf{[3-25]}$$

$$e = r - y - n = (I + PC)^{-1}(r - d) - (I + PC)^{-1}n \qquad \textbf{[3-26]}$$

$$u = C(I + PC)^{-1}(r - n - d) \qquad \textbf{[3-27]}$$

$$S = (I + PC)^{-1} \qquad \textbf{[3-28]}$$

$$T = PC(I + PC)^{-1} \qquad \textbf{[3-29]}$$

Consider equation **[3-26]**, for good tracking performance the tracking error $\|r - y\|$ should be small when d and n are zero. This implies that the sensitivity function **[3-28]** should be 'small'. For good disturbance suppression, that is the effect of the disturbance d on the output of the system, y in equation **[3-25]** should be small. This again implies that the sensitivity function **[3-28]** should be 'small'.

For good noise suppression, that is the effect of the noise n on the output of the system, y in equation **[3-25]**, should be 'small'. This implies that the complementary sensitivity function **[3-29]** should be 'small'. The interpretation of the word 'small' refers to the size of a matrix or its singular value denoted by σ. In the case of a SISO

system **[3-28]** and **[3-29]** are both scalar values and hence the use of singular values can be replaced by absolute values.

The above performance considerations can be summarised by equations **[3-30]** and **[3-31]**. These two conditions are however conflicting which can be readily seen by observing **[3-32]**. Note that condition **[3-30]** agrees with the classical control theory which is to improve tracking and disturbance suppression by keeping the loop gains high.

$$\sigma[S(j\omega)] << 1 \qquad \textbf{[3-30]}$$

$$\sigma[T(j\omega)] << 1 \qquad \textbf{[3-31]}$$

$$S + T = I \qquad \textbf{[3-32]}$$

3.2.3 Robustness and Uncertainty.

While no nominal design model $P(s)$ can emulate a physical plant perfectly, it is clear that some models do so with a greater fidelity than others. Hence no nominal model should be considered complete without some assessment of its error. These errors are called model uncertainties. The representation of the uncertainties depends on the extent to which the uncertainties are known. For example in the case of a waste pump the viscosity of the load can change with temperature. If the manner in which the dynamics of the load change is known for the range over which the temperature will change then this type of uncertainty is known as a structured uncertainty. In this case, if the structure is well known and understood the designer can choose to include a dynamic model for this uncertainty in the nominal design model. This however can present a realisation problem in the system design since now the temperature of the waste has to be measured or estimated. Often, instead the designer will choose to design a system which is stable over all the ranges of this uncertainty. In some systems, the model of the uncertainties can be very structured but at the same time very complex and numerous, in such cases the uncertainties are grouped into unstructured uncertainties.

An important aspect of control systems is its sensitivity to parameter variation. Section 3.2.1 describes the optimal controller from the classical point of view, where its robustness is presented in terms of gain and phase margins. These margins are

bounds on variations in the feedback loop and can be extended to variations in some components of the plant. In particular a variation in the input coupling matrix, with no corresponding variation in the transition matrix could be bounded by the robustness margins described. Consider the practical situation of a current amplifier in a servo system, often these are usually designed with a peak current rating and a continuous current rating. If the amplifier is driven at the peak current for a time greater than the rated time the current amplifier will saturate by clipping the input to the current loop, this reduces the gain of the current amplifier. For the optimal LQ controller design the closed loop system is guaranteed to remain stable if there is no more than a 50% gain reduction in the current amplifier. This however is a worst case scenario, in general the downside gain margin is more favourable. Indeed for low order LQ design the downside gain margin is normally zero. This form of parameter variation is a restrictive set of variations which are bounded by the gain and phase margins discussed.

There are several other sets of variations which can't be bounded by these margins. A great deal of research was carried out in this area during the early eighties particularly in the area of multivariable system [Safonov 81], [Doyle 81, 82] & [Zames 81, 83]. The multivariable results can readily be applied to the SISO system by replacing the singular value constraints with absolute value constraints. Much of the multivariable results are multivariable extensions of the classical control ideas. Safonov and Doyle explored the sensitivity function and the complementary sensitivity function in the presence of structured and unstructured uncertainties.

In general, parameter variation is classified as structured uncertainty. Consider the case of the waste pump, it is the viscosity of the load which is altered with a change in temperature. Thus the number of dynamic modes of the load and their structure still remains the same. It can be shown [Anderson 89], [Grimble 88a] that for structured variations the sensitivity of the output of the closed loop system to parameter variation is the sensitivity function times the sensitivity of the open loop system to the parameter variation **[3-33]**. Thus equation **[3-30]** is a design constraint which minimises sensitivity to structured variations. This constraint agrees with the classical argument for large loop gains.

$$\frac{\partial y_c}{\partial \mu} = S(s)\frac{\partial y_o}{\partial \mu} \qquad \textbf{[3-33]}$$

There are two types of unstructured uncertainties, additive and multiplicative uncertainties. Equation **[3-34]** represents the modified nominal plant in the presence of an additive uncertainty and equation **[3-35]** attaches a bound to this uncertainty, where $l_a(s)$ is a positive scalar function, which confines the plant $P_a(s)$ to a neighbourhood of $P(s)$ with magnitude $l_a(s)$.

$$P_a(s) = P(s) + \Delta P(s) \qquad \textbf{[3-34]}$$

$$\sigma[\Delta P(s)] < l_a(s) \qquad \textbf{[3-35]}$$

Equation **[3-36]** represents the modified plant in the presence of a multiplicative uncertainty and equation **[3-37]** attaches a bound to this uncertainty,

$$P_m(s) = (I + L_m(s))P(s) \qquad \textbf{[3-36]}$$

$$\sigma[L(s)] < l_m(s) \qquad \textbf{[3-37]}$$

where $l_m(s)$ confines $P_m(s)$ to a normalised neighbourhood of $P(s)$. For SISO systems both types of uncertainties can be represented by a multiplicative uncertainty.

It can be shown that a sufficient condition for continued stability under the influence of model uncertainty is the condition of equation **[3-38]** [Doyle 81], from which equation **[3-39]** can be established by observing the singular value inequalities given in equation **[3-40]**. Note the $\underline{\sigma}$ and $\overline{\sigma}$ denote the minimum and maximum singular values, in the case of a SISO system they are equivalent. Using the definition for complementary sensitivity **[3-29]**, condition **[3-39]** becomes **[3-41]**.

$$\underline{\sigma}\left[I + L(s)P(s)C(s)(I + P(s)C(s))^{-1}\right] > 0 \qquad \textbf{[3-38]}$$

$$\overline{\sigma}\left[P(s)C(s)(I + P(s)C(s))^{-1}\right] < \frac{1}{l_m(s)} \qquad \textbf{[3-39]}$$

$$\underline{\sigma}[P] - 1 \le \underline{\sigma}[I + P] \le \underline{\sigma}[P] + 1 \qquad \textbf{[3-40]}$$

$$\overline{\sigma}[T(s)] < \frac{1}{l_m(s)} \qquad \textbf{[3-41]}$$

The term sensitivity and robustness are often used interchangeably, but to be more precise sensitivity refers to the change in the system's response which results from small changes in the system parameters. Robustness refers to the preservation of stability under allowable variations in the nominal system parameters [Grimble 88a].

It must be stressed that unlike other bounds these margins are not conservative estimates of stability bounds. On the contrary, if the uncertainties are truly unstructured and **[3-41]** is violated, then a perturbation $L(s)$ exists within the set allowed by **[3-37]** for which the system is unstable. Hence these stability conditions impose hard limits on the permissible loop gains of a practical feedback system.

Consider the example of a motor and its corresponding current amplifier as depicted in Figure **[3-7]**. Quite often the plant under control **[3-42]** approximated to a first order plant **[3-43]**. The dynamics of the current loop are assumed to be much faster than that of the desired closed loop system. Consequently the nominal plant used for control is **[3-43]**. The question now posed is what are the bounds on the unmodelled dynamics of the current amplifier below which the system can be perturbed into a state of instability? That is, what is the smallest α below which condition **[3-41]** fails? In a practical design problem this question is often reversed, namely what is the largest feedback gains K for which the multiplicative unstructured uncertainty **[3-44]** is bounded by **[3-41]**? Furthermore given the nominal model for the motor and load equation **[3-43]**, what are the bounds on the parameters J and B such that stability is retained? In general the application will dictate these bounds as robustness requirements of the control system. For the purpose of this example assume that the load inertia J_L and damping B_L can vary between zero and three times the nominal motor values. The nominal parameter values are given by equation **[3-46]**. Note that for optimum operation the load and motor parameters are matched, thus the nominal parameters used in the design are twice the motor parameters.

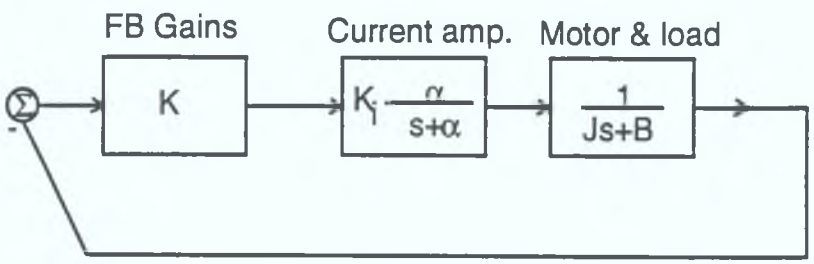

Fig. [3-7] **Example Rig.**

$$P_m(s) = \frac{K_1 \alpha}{(s+\alpha)(Js+B)} \qquad \textbf{[3-42]}$$

$$P(s) = \frac{K_t}{Js + B} \qquad [3\text{-}43]$$

$$L_{Amp}(s) = \frac{-s}{s + \alpha} \qquad [3\text{-}44]$$

$$T(s) = \frac{K_1 s + K_2}{Js^2 + (B + K_1)s + K_2} \qquad [3\text{-}45]$$

$$\begin{aligned} J_{nom} &= J_l + J_m \\ J_{\max} &= 2J_{nom} \\ B_{nom} &= B_l + B_m \\ B_{\max} &= 2B_{nom} \end{aligned} \qquad [3\text{-}46]$$

There are three multiplicative unstructured uncertainties described, namely uncertainties associated with the current loop, the inertia and the viscous damping parameters. Equations **[3-44]**, **[3-47]** and **[3-48]** represents these uncertainties in accordance with equation **[3-36]**.

$$L_{\Delta J}(s) = \frac{(1-\Delta)Js}{\Delta Js + B} \qquad \text{where } P_m = \frac{1}{\Delta J + B} \qquad [3\text{-}47]$$

$$L_{\Delta B} = \frac{(1-\Delta)B}{Js + \Delta B} \qquad \text{where } P_m = \frac{1}{Js + \Delta B} \qquad [3\text{-}48]$$

Using the heuristic tuning procedure of section 3.1.1 and the Hamiltonian solution to Riccati's equation, a full state feedback controller can be designed. $T(s)$ for this controller structure is given in equation **[3-45]**. Figure **[3-8]** depicts the bounded complementary sensitivity function for a Δ in equations **[3-47]** and **[3-48]** equal to 2. From the figure it is apparent that the chosen controller fails the robustness condition of equation **[3-41]**, in the case of the unstructured uncertainty **[3-47]**, between the frequency ranges 10.5 to 11.5 Rad/Sec. By increasing ρ in the tuning procedures the $T(s)$ function migrates along the frequency axis until eventually the robustness condition **[3-41]** again fails but in this case because of the unstructured uncertainty **[3-44]**. By adjusting the ratio of the $q_{i,j}$'s in equation **[3-13]** the amplitude of $T(s)$ can be controlled to some extent and hence the frequency range over which **[3-47]** fails can be reduced. Such adjustments are part of the heuristic robust tuning procedures. It may be found that excessive adjustment of the controller weights may compromise other performance criteria, in which case the controller structure itself may require

adjustment. In this particular example a $\Delta J = 1.25 J_{nom}$ will satisfy the stability criterion **[3-41]**.

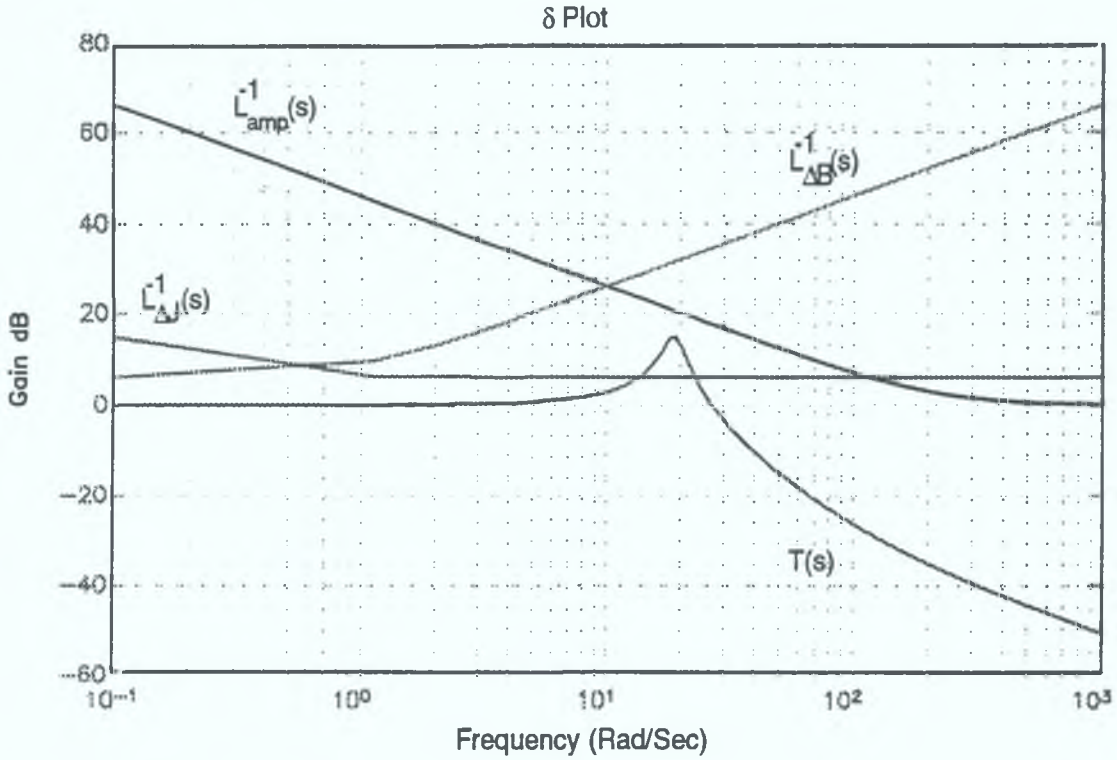

Fig. [3-8] Performance bounds for example .

Thus sensitivity and complementary sensitivity functions provide an effective method for studying the robustness of a given controller structure in the presence of both structured and unstructured uncertainties. They also provide tuning criteria regarding the sensitivity of the closed loop system to measurement noises, disturbance noises and tracking errors. Table **[3-2]** summarises the desirable properties of the sensitivity and complementary sensitivity functions. Figure **[3-9]** depicts these bounds for the example above.

Desirable property	Constraint
Good Tracking Performance	$\sigma[S] << 1$
Good Disturbance Suppression	$\sigma[S] << 1$
Good Noise Suppression	$\sigma[T] << 1$
Good Insensitivity to Structured Uncertainties	$\sigma[S] << 1$
Good Insensitivity to Unstructured Uncertainties	$\sigma[T] << \frac{1}{l_m}$

Table [3-2] Desirable Properties of T(s) and S(s)

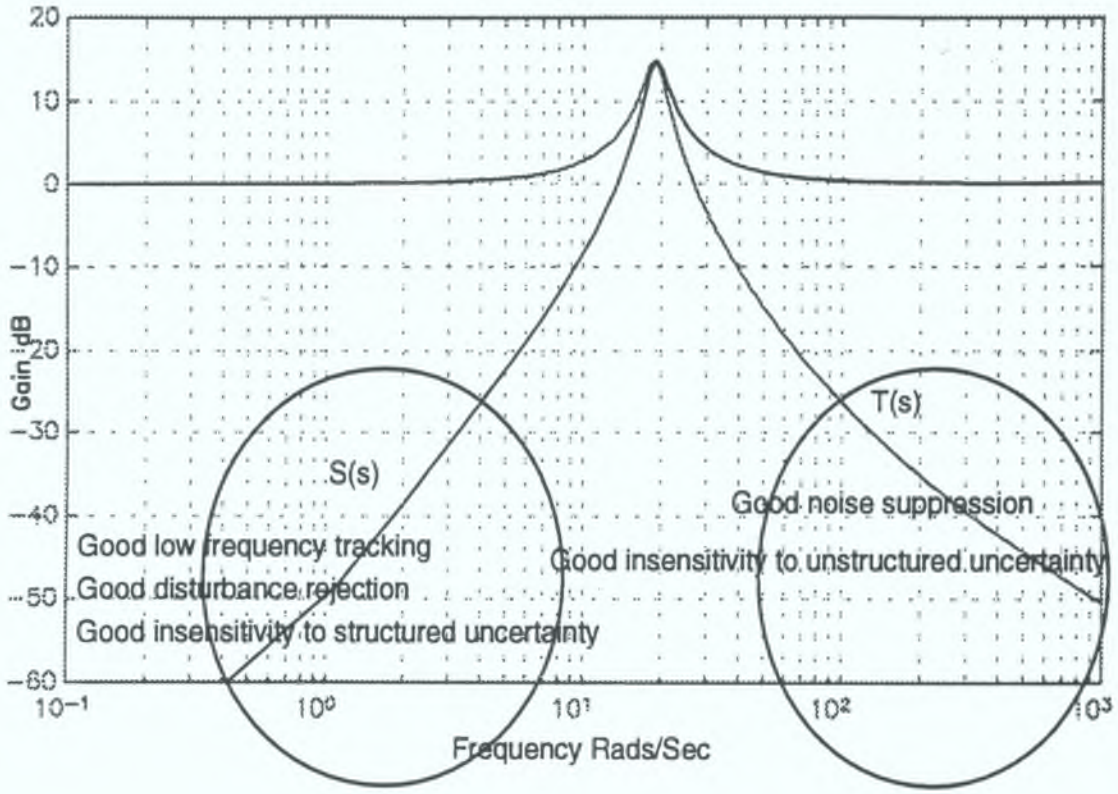

Fig. [3-9] Good Performance bounds.

3.3 The Linear Quadratic Gaussian Controller (LQG)

In the previous sections the LQ controller was presented as an optimal full state feedback controller. The controller is defined by a weighted cost function, the particular weights are chosen using the heuristic tuning procedure. The solution of the controller problem* requires the solving of the discrete *Riccati equation*, a nonrecursive solution of which exists in the form of the Hamiltonian solution. The heuristic tuning procedure describes a series of steps involving manipulation of the cost weights until a satisfactory response is found. Subsequent sections portrayed the LQ controller in a classical light. Using the condition for optimality, namely the return difference inequality, robustness bounds could be established for the LQ controller. The return difference and complementary return difference inequalities are then used to set bounds on structured and unstructured uncertainties. The conflicting bounds on the inequalities are presented in a δ plot, where trade-offs can be made.

The LQ controller is a full state feedback controller and consequently knowledge of all the feedback states are required. As mentioned previously this feedback information will be provided by an estimator. In this particular work, a Kalman estimator is used because it is the optimal estimator, in a Gaussian sense. Chapter 2 explores the development of such an estimator. This section will explore the LQG controller strategy, the basis of which will be the previous work on the LQ controller and the Kalman estimator. It will become apparent in subsequent sections that the LQG controller does not inherit the robustness properties of the LQ controller. In an effort to preserve these robustness properties a loop transfer recovery procedure will be explored. The resulting technique is a linear quadratic Gaussian controller with loop transfer recovery LQG / LTR. Further improvements in robustness to structured and unstructured uncertainties shall be made with the use of frequency shaped cost functions. The resulting controller strategy is a FS-LQG / LTR controller, a subset of which is the PI-LQG / LTR controller. The controller and estimator problems define a two-degrees-of-freedom design problem, the design of which can be integrated using a H^{∞} design strategy.

The LQG controller consists of a linear quadratic controller with a Kalman filter in the feedback path. The LQG controller has two-degrees-of-freedom in its design, the *separation principle* provides this two-degrees-of-freedom. This important principle is now developed.

3.3.1 The Separation Principle.

Consider a plant description **[3-49]** and the availability of a full state feedback controller **[3-50]**. The gain vector K can be an arbitrary gain, but in this application of the separation principle, the gain K will be derived through some linear quadratic performance constraints such as **[3-1]**. A closed loop description of this plant and controller can be readily obtained **[3-51]**, the characteristic equation of which is defined by equation **[3-52]**.

$$\begin{aligned} x_{k+1} &= \Phi x_k + \Gamma u_k \\ y_k &= H x_k \end{aligned} \qquad \textbf{[3-49]}$$

$$u_k = -K x_k \qquad \textbf{[3-50]}$$

$$x_{k+1} = (\Phi - \Gamma K) x_k \qquad \textbf{[3-51]}$$

$$|\Phi - \Gamma K| = 0 \qquad \textbf{[3-52]}$$

In practice all the states are not available to implement the control law **[3-50]**, instead this control law is replaced with equation **[3-56]**, where the plant states are replaced with an estimate of the states. The LQ controller is thus implemented as a LQG controller because of practical and physical constraints. The estimates of the states are obtained using a Kalman estimator. A time invariant implementation of the Kalman estimator is described by equations **[3-53]**, **[3-54]** and **[3-55]**, where the gain vector L is the steady state Kalman gain.

$$\hat{x}_k^- = \Phi \hat{x}_{k-1} + \Gamma u_{k-1} \qquad \textbf{[3-53]}$$

$$\hat{x}_k = \hat{x}_k^- + L(y_k - \hat{y}_k^-) \qquad \textbf{[3-54]}$$

$$\hat{y}_k^- = H \hat{x}_k^- \qquad \textbf{[3-55]}$$

$$u_k = -K \hat{x}_k \qquad \textbf{[3-56]}$$

A closed loop description of this estimator can be found by rewriting the Kalman equations in terms of the estimated error, defined by equation **[3-57]**. By substituting equations **[3-49]**, **[3-53]**, **[3-54]** and **[3-55]** into **[3-57]**, the closed form description **[3-58]** follows, the characteristic equation of which is given in **[3-59]**

$$\tilde{x} = x - \hat{x} \qquad \textbf{[3-57]}$$

$$\begin{aligned}\tilde{x}_k &= \Phi x_{k-1} + \Gamma u_{k-1} - \hat{x}_k^- - L\left(y_k - \hat{y}_k^-\right) \\ &= \Phi x_{k-1} - \Phi\hat{x}_{k-1} - LH\left(x_{k-1} - \Phi\hat{x}_{k-1} - \Gamma u_{k-1}\right) \\ &= \Phi\left(x_{k-1} - \hat{x}_{k-1}\right) - LH\left(\Phi x_{k-1} - \Phi\hat{x}_{k-1}\right) \\ &= \left(\Phi - LH\Phi\right)\tilde{x}_{k-1}\end{aligned} \qquad \textbf{[3-58]}$$

$$\left|\Phi - LH\Phi\right| = 0 \qquad \textbf{[3-59]}$$

The combined estimator and controller form a LQG controller. A closed form solution of the LQG controller and plant is required. This can be obtained by augmenting the plant and controller as a linear combination of the plant states and the estimated error defined by **[3-57]**. Equation **[3-58]** already describes the estimator as a linear combination of the estimated error. The plant **[3-49]** and controller **[3-56]** can be rewritten is terms of the estimated error by substituting **[3-57]** into **[3-56]** and then the result into **[3-49]**. The resulting description is given in **[3-60]**.

$$\begin{aligned}x_{k+1} &= \Phi x_k - \Gamma K\left(x_k - \tilde{x}_k\right) \\ &= \left(\Phi - \Gamma K\right)x_k + \Gamma K\tilde{x}_k\end{aligned} \qquad \textbf{[3-60]}$$

Augmenting **[3-60]** and **[3-58]** gives the closed loop description of the closed loop system **[3-61]**, the characteristic equation of which is given by **[3-62]**, using the relationship that the determinant of a product is the same as the product of determinants. It is thus evident from **[3-63]** that the dynamic response of the closed loop LQG system is the cascaded response of the Kalman estimator **[3-59]** and the LQ controller **[3-52]**. This allows the design of such an estimator / controller combination to be carried out separately and then combined at a final stage. This relationship is not restricted to the LQG controller, indeed any similarly derived estimator and controller can be combined in such a manner.

$$\begin{bmatrix} x_{k+1} \\ \tilde{x}_{k+1} \end{bmatrix} = \begin{bmatrix} \left(\Phi - \Gamma K\right) & \Gamma K \\ 0 & \left(\Phi - LH\Phi\right) \end{bmatrix} \begin{bmatrix} x_k \\ \tilde{x}_k \end{bmatrix} \qquad \textbf{[3-61]}$$

$$\left|\left(\Phi - \Gamma K\right)\left(\Phi - LH\Phi\right)\right| = 0 \qquad \textbf{[3-62]}$$

$$\left|\left(\Phi - \Gamma K\right)\right|\left|\left(\Phi - LH\Phi\right)\right| = 0 \qquad \textbf{[3-63]}$$

It must be emphasised however that the separation principle does not allow completely separate design of the estimator and controller. If the estimator were designed with a 'small' error covariance the response of the closed loop system is dominated by the dynamics of the estimator **[3-59]**. Thus the designed response will not be the optimal LQ response desired. As a general rule the estimator bandwidth is chosen to be sufficiently 'larger' than that of the controller bandwidth. This insures that the closed loop response of the augmented system will be dominated by the dynamics of the LQ controller and thus will approximate to the optimal LQ response **[3-52]**. In subsequent sections the interdependence between the estimator and the controller will be explored, with particular regard to robustness implications.

3.3.2 The Loss of Robustness.

This section will examine the input and output robustness of the closed loop system. Consider the effect on robustness of a non-linearity or unmodelled dynamics inserted at points X and Y in Figure **[3-10]**. Note the chosen points X and Y are outside the bounds of the nominal plant and controller. If this nonlinearity were inside the bounds of the plant, it would come under the heading of an unstructured uncertainty. However there is a large overlap between these classifications.

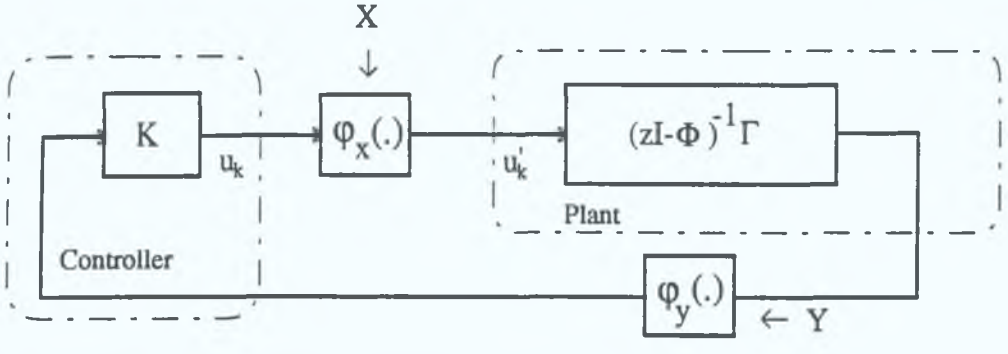

Fig. [3-10] System with nonlinearities.

The guaranteed passband robustness properties established in section 3.2.1 for the LQ full state feedback controller simply evaporate with the introduction of a state estimator [Doyle 78]. In this section the effect of the state estimator on the return difference inequality and corresponding effects on the robustness properties will be shown by example. This example will form the basis for a robustness recovery procedure featured in subsequent sections [Doyle 79].

The loss of the robustness property can be shown by comparing two systems, one without and the other with the state estimator. Consider the discrete time system

depicted in Figure **[3-11]**, from an input robustness point of view the transfer function for the closed loop system broken at point X is of interest. Equation **[3-64]** represents such a transfer function. Note that point X is outside both the controller and plant.

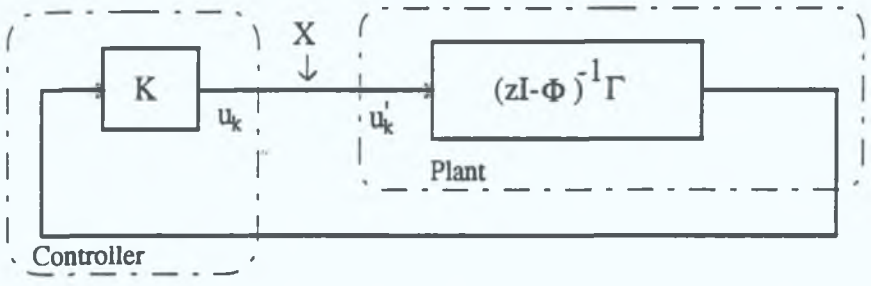

Fig. [3-11] Discrete time system.

$$\frac{u_k}{u_k'} = -K(zI-\Phi)^{-1}\Gamma \qquad \textbf{[3-64]}$$

Now consider this system with a full state feedback controller and a Kalman predictor-corrector state estimator depicted in Figure **[3-12]**. Again by breaking the loop at an equivalent point X, an equivalent transfer function can be derived.

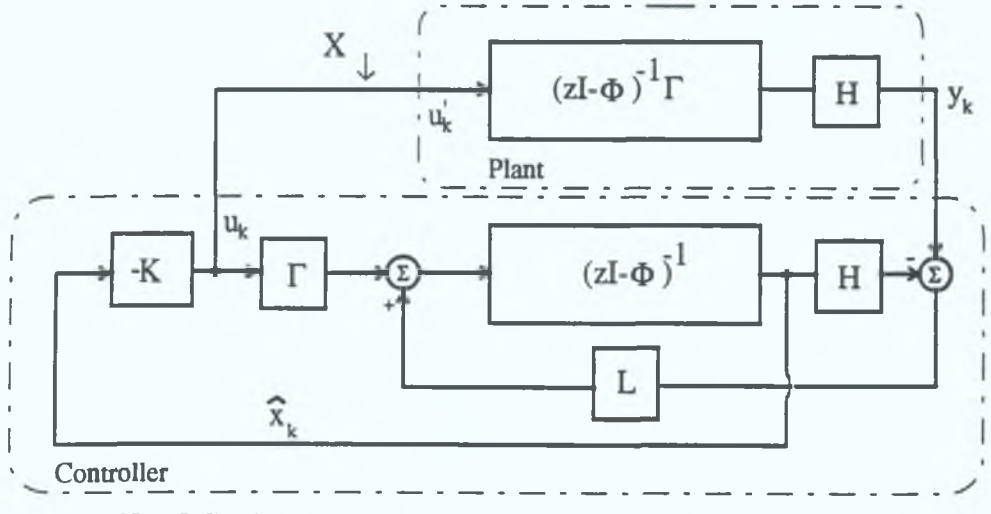

Fig. [3-12] LQG with DTIK predictor-corrector form.

This transfer function is readily derived by first evaluating the transfer function from the output of the plant y_k to the output of the state estimator $\hat{x}_k$. Using the time invariant predictor-corrector Kalman estimator defined by equations **[3-53]**, **[3-54]**, **[3-55]** and then substituting **[3-56]** evaluated at time *k-1*, for u_{k-1}, gives equation **[3-65]**. Taking the $\tilde{z}$ transform of **[3-65]** and expressing it as a transfer function gives **[3-66]**. Using the definition for the full state feedback controller **[3-56]** and equation

[3-66], the LQG controller can now be formally defined as **[3-67]**, where K in **[3-67]** is derived from some LQ constraint.

$$\begin{aligned}\hat{x}_k &= \Phi\hat{x}_{k-1} + \Gamma u_{k-1} + L(y_k - H\Phi x_{k-1} - H\Gamma u_{k-1}) \\ &= \Phi\hat{x}_{k-1} - \Gamma K\hat{x}_{k-1} + L(y_k - H\Phi\hat{x}_{k-1} + H\Gamma K\hat{x}_{k-1}) \\ &= (\Phi - LH\Phi - \Gamma K + LH\Gamma K)\hat{x}_{k-1} + Ly_k\end{aligned} \qquad \textbf{[3-65]}$$

$$\frac{\hat{x}_k}{y_k} = (zI - \Phi + LH\Phi + \Gamma K - LH\Gamma K)^{-1} L \qquad \textbf{[3-66]}$$

$$u_k = -K(zI - \Phi + LH\Phi + \Gamma K - LH\Gamma K)^{-1} Ly_k \qquad \textbf{[3-67]}$$

The transfer function for the open loop plant is given by equation **[3-68]**. Substituting for y_k into **[3-67]** gives the desired transfer function for the closed loop system broken at point X **[3-69]**.

$$\frac{y_k}{u_k} = H(zI - \Phi)^{-1}\Gamma \qquad \textbf{[3-68]}$$

$$\frac{u_k}{u_k} = -K(zI - \Phi + LH\Phi + \Gamma K - LH\Gamma K)^{-1} LH(zI - \Phi)^{-1}\Gamma \qquad \textbf{[3-69]}$$

The output robustness can be derived in a similar manner by breaking the loop at point Y. In this case the output robustness transfer function for the LQ and LQG controllers are given in equation **[3-70]** and **[3-71]**. For SISO systems equation **[3-64]** is the same as equation **[3-70]** and equation **[3-69]** is the same as equation **[3-71]**. Thus the SISO input / output robustness can be described using one set of equations.

$$\frac{y_k}{y_k} = -(zI - \Phi)^{-1}\Gamma K \qquad \textbf{[3-70]}$$

$$\frac{y_k}{y_k} = -H(zI - \Phi)^{-1}\Gamma K(zI - \Phi + LH\Phi + \Gamma K - LH\Gamma K)^{-1} L \qquad \textbf{[3-71]}$$

For the purpose of this example the continuous time motor model is used with parameters given by equations **[3-72]**. The controllers to be implemented are discrete time LQ and LQG controllers for which a sample frequency of 1kHz is chosen. Using the heuristic tuning procedures of section 3.1.1, a LQ gain $K = [17.6 \quad 1451.8]$ is

chosen. This gain corresponds to controller roots located at $z = 0.9082 \pm 0.0780i$ and provides a settling time of about 30ms. The LQG controller is designed using the LQ gain just described and a Kalman estimator with gain $L = [79.73 \quad 0.3615]^T$. This gain corresponds to estimator poles at $z = 0.7792 \pm 0.1764i$. The gain L in this case is chosen such that the estimator roots are 'faster' then the controller roots.

$$x = \begin{bmatrix} \omega \\ \theta \end{bmatrix}, \quad \Phi_c = \begin{bmatrix} -0.5 & 0 \\ 1 & 0 \end{bmatrix}, \quad \Gamma_c = \begin{bmatrix} 10 \\ 0 \end{bmatrix}, \quad H = [0 \quad 1] \qquad \textbf{[3-72]}$$

Figure **[3-13]** shows a portion of the Nyquist plot for the two controllers just described centred around the -1 point. The first observation that can be readily made from the plot is the reduced size of the exclusion region, which pertains to the discrete nature of the design. The circle labelled 'Gamma Circle' inscribes a region of exclusion for the Nyquist contour. This circle is a consequence of the condition for optimality (see section 3.2.1.1). The minimum guaranteed robustness bounds for the discrete time system are less than that for the equivalent continuous time system. For this particular choice of sample frequency and controller bandwidth the minimum robustness bounds are given in Table **[3-3]**. Recall that the phase margin is given by the angle F-O-B, the gain margin is given by the ratio of F-O over F-G. The downside gain margin is the reciprocal of the point at which the second[5] crossing of the real axis occurs.

From the figure it is also further evident that the Nyquist plot for the LQ controller, remains outside the Gamma circle, and hence it is optimal. The robustness bounds for this controller are also contained in Table **[3-3]**. In contrast however the Nyquist plot for the LQG controller falls inside the Gamma circle, consequently the controller is no longer an optimal controller. As a result of this loss in optimality the robustness bounds have been greatly reduced (Table **[3-3]**).

[5]The crossing at the origin is not considered in this case to be a crossing.

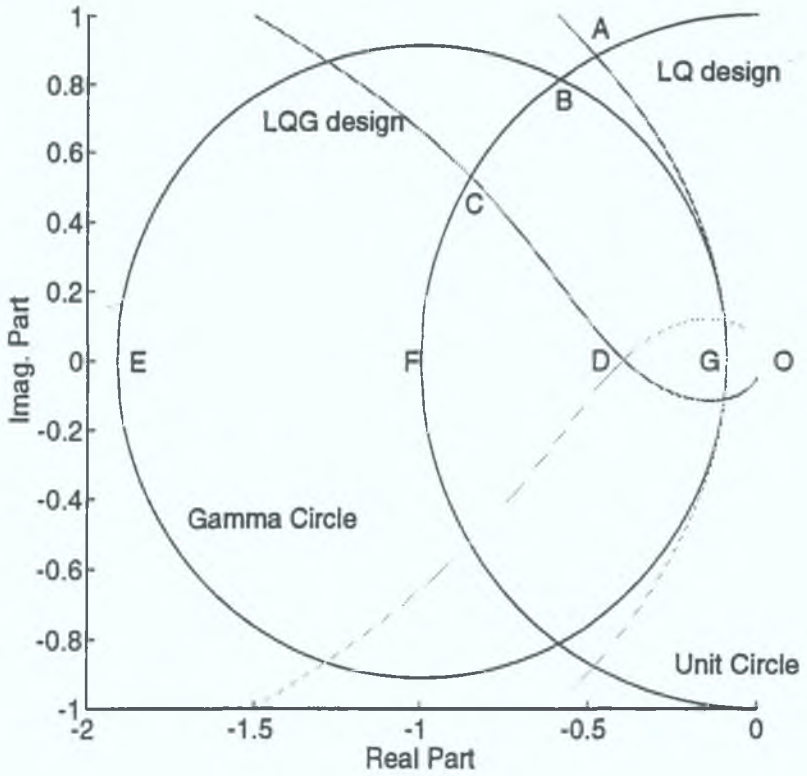

Fig. [3-13] Nyquist plot for LQ and LQG controllers.

Implementation	Phase Margin	Gain Margin (GM)	Down Side GM
Minimum	54.2°	21.09 dB	-5.628 dB
LQ	61.5°	21.09 dB	0
LQG	31.8°	7.80 dB	0
LQG/LTR	43.5°	16.0 dB	0
LQG/LTR DKS	53.2°	(∞)	0

Table [3-3] Robustness properties.

3.3.3 Robustness Recovery.

Doyle and Stein in [Doyle 79] devised a relatively simple procedure for estimator design such that full loop recovery takes place for minimum phase plant models. This robustness recovery procedure is referred to as 'Loop Transfer Recovery' (LTR). The procedure exploits the asymptotic properties of the continuous time equivalent of equation **[3-69]** [Athans 86]. That is, the open loop gain transfer function for the LQG design converges to that of the LQ design as the estimator design parameter approaches infinity. The difference between the LQG loop transfer and the LQ loop transfer is referred to as the recovery error. A dual recovery procedure also exists for

LQG controller design in order to recover output robustness. This section will outline the philosophy behind these recovery procedures and present a discrete time equivalent recovery procedure. It will be shown that full robustness recovery is not necessarily available for the discrete implementation. The procedures themselves will become part of the heuristic tuning procedure for the overall closed loop system. Subsequent sections will provide improved recovery procedures which limit the bandwidth of the estimator, thereby improving noise attenuation.

3.3.3.1 Loop Transfer Recovery (LTR).

The cause of the LQG design's robustness degradation is a mismatch between the actual input to the plant and the input to the estimator. This is because of the presence of the nonlinearity or an unmodelled dynamic. The recovery procedure minimised the dependence of the estimator on the output from the controller. Figure **[3-14]** clearly depicts this dependence, where the controller output is feeding back into the estimator. The continuous LTR procedure involves applying a fictitious noise source to the input of the plant in the estimator design. As the amplitude of the injected noise becomes infinite in intensity, the LQG open loop transfer function approaches that of the LQ design and with this loop recovery takes place. This results in an estimator that weights the measure information more heavily, thus reducing the dependence on the plant input. The discrete time LTR procedure is much the same as the continuous time, except in this case full recovery is only available for particular Kalman forms.

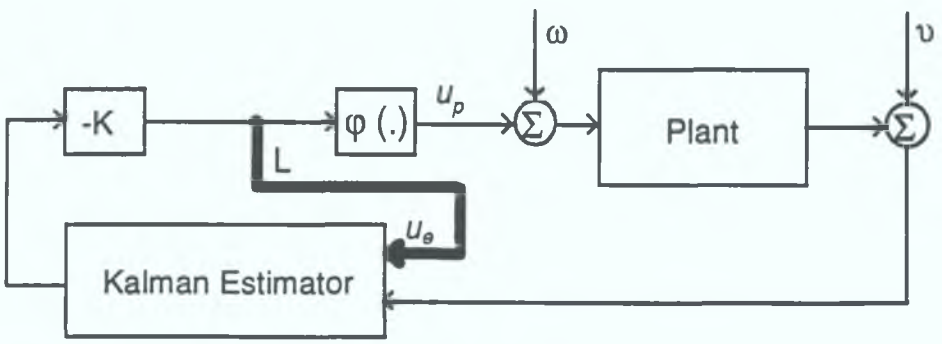

Fig. [3-14] LQG Robustness degradation.

The LQG design and robustness recovery procedure for a SISO system can be summarised as follows:

- Design a LQ controller given the available nominal plant information. Choose a LQ design parameter that gives a satisfactory response.
- Design a Kalman estimator given available nominal plant information, and stochastic process and measurement noise information.
- Examine the passband input / output robustness of the combined LQG system using equation **[3-69]**.
- To recover robustness, increase the process noise covariance matrix using equation **[3-73]**, where k describes the recovery iteration, B the plant input coupling matrix and Q_n is the nominal plant noise covariance matrix. Use this updated noise covariance matrix in a redesign of the Kalman estimator, and repeat the examination process above.
- If robustness recovers to within a satisfactory limit of the passband input robustness of LQ design given by equation **[3-64]**, halt the recovery procedure.

$$Q_k = Q_n + q_k BB^T \quad for \quad q_k = [1 \quad 10 \quad 100 \quad \ldots \quad \infty] \qquad \textbf{[3-73]}$$

Note that if the bandwidth of the nominal estimator design is less than the bandwidth of the nominal LQ design it is quite likely that robustness will disimprove until such time as the recovery procedure drives the estimator bandwidth beyond that of the LQ design. The robustness bounds have a local minimum in a region where the estimator and LQ bandwidth are similar. For the LQG system, where the bandwidth of the estimator is less than that of the LQ controller, the response of the cascaded system is dominated by the estimator design

A dual recovery procedure exists for recovering output robustness or sensitivity. This recovery procedure involves manipulating the LQ cost function weights and using these new weights in the LQ redesign. Equation **[3-74]** represents the quadratic cost function weight update for the $k^{th.}$ iteration, where H is the measurement coupling matrix. For SISO systems the input robustness and output robustness or sensitivity, can be represented by the same set of equations. Thus the output sensitivity recovery procedure really works against the input robustness recovery procedure. For good sensitivity the controller loop gain must be high (see Table **[3-2]**), whereas for good LQG robustness the estimator bandwidth must be higher than the bandwidth of the LQ controller.

The sensitivity recovery procedure in this particular application is viewed as a means of setting or selecting a suitable response and/or performance. Equation **[3-74]** will feature as a refined version of the LQ heuristic tuning parameter ρ, of section 3.1.1.

$$Q_{1,k} = Q_{1,n} + q_k H^T H \quad for \quad q_k = [1 \quad 10 \quad 100 \quad ... \quad \infty] \qquad \textbf{[3-74]}$$

Figure **[3-15]** shows loop recovery taking place for the LQG design example of section 3.3.2. It becomes apparent from the figure that full robustness recovery does not take place. There is however a significant improvement in robustness, the robustness properties are contained in Table **[3-3]** (LQG/LTR). A further limiting factor in the recovery of robustness is a reduction in the noise attenuation properties of the estimator. Robustness improvements are sought at the expense of the noise suppression.

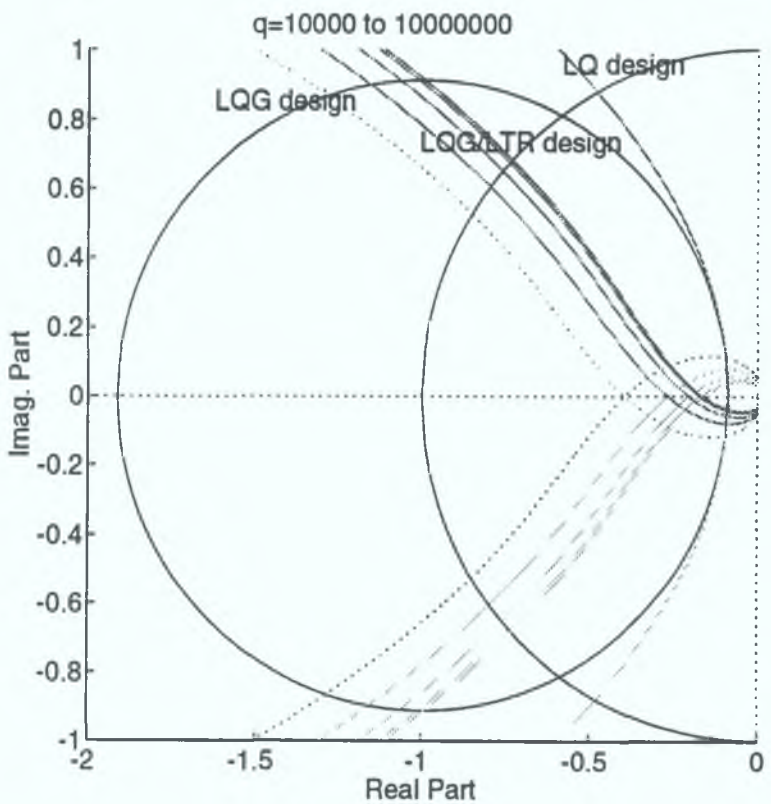

Fig. [3-15] LQG/LTR predictor corrector estimator.

The absence of full recovery is again a consequence of the discrete nature of the design. Further robustness can be obtained, by reviewing the choice or form of the Kalman estimator. Section 3.4 reviews the available Kalman filter forms. Three forms are described, the Kalman single-stage predictor, the Kalman predictor-corrector and

the Kalman smoother. The predictor-corrector implementation exhibits a superior time response over the other implementations. Maciejowski in [Maciejowski 86] showed that full robustness recovery can take place for any stable observer of the form given by equations **[3-75]** and **[3-76]** provided that the gains L^p and L^c satisfy equation **[3-77]**. The Kalman smoother[6] is a subset of this robust observer design. Maciejowski and Ishihara in [Ishihara 86] show that full robustness is not available for the Kalman predictor and predictor-corrector implementations.

At this stage in the design, a design trade-off has to be made between disturbance response and system robustness / sensitivity margins. The decision will lead to a particular discrete Kalman filter (DKF) implementation. In some situations the designer may not even have a say in this decision making process. If the computational time for the compensator is a significant portion of the sample interval, the designer may be forced to use the single-stage predictor Kalman implementation and accept finite recovery margins.

$$\hat{x}_{k+1|k} = \Phi\hat{x}_{k|k-1} + \Gamma u_k + L^p\left(z_k - H\hat{x}_{k|k-1}\right) \qquad \textbf{[3-75]}^7$$

$$\hat{x}_{k|k} = \hat{x}_{k|k-1} + L^c\left(z_k - H\,\hat{x}_{k|k-1}\right) \qquad \textbf{[3-76]}$$

$$L^p = \Phi L^c \qquad \textbf{[3-77]}$$

For the discrete time invariant Kalman (DTIK) smoother implementation the LQG controller is depicted in Figure **[3-16]**. By substituting the controller description given in equation **[3-78]** into equation **[3-75]** and then using equations **[3-76]** and **[3-77]**, a state space realisation of the compensator can be found **[3-79]**. The transfer function representation for this LQG controller is given by equation **[3-80]**. The corresponding loop transfer for this system with the loop broken at the point X is given by equation **[3-81]**. It is this equation which is used in the LTR state of the LQG design.

$$u_k = -K\hat{x}_{k|k} \qquad \textbf{[3-78]}$$

---

[6] Note that in the context of control the Kalman gain is represented by the symbol L to avoid confusion with the controller feedback gain K.

[7] Note that there is a slight change in notation $\hat{x}_{k|k} \equiv \hat{x}_k$ and $\hat{x}_{k|k-1} \equiv \hat{x}_k^-$. This more conventional notation is clearer at representing more than two events in time, as is the case with the Kalman smoother implementation.

$$\hat{x}_{k+1|k} = (\Phi - \Gamma K)(I - L^c H)\hat{x}_{k|k-1} + (\Phi - \Gamma K)L^c y_k$$
$$u_k = K(I - L^c H)\hat{x}_{k|k-1} + KL^c y_k \qquad \textbf{[3-79]}$$

$$u_k = K(I - L^c H)\left\{\left\{zI - (\Phi - \Gamma K)(I - L^c H)\right\}^{-1}(\Phi - \Gamma K)L^c + KL^c\right\} y_k \qquad \textbf{[3-80]}$$

$$\frac{u_k}{u_k} = H(zI - \Phi)^{-1}\Gamma K(I - L^c H)\left\{\left\{zI - (\Phi - \Gamma K)(I - L^c H)\right\}^{-1}(\Phi - \Gamma K)L^c + KL^c\right\}$$

[3-81]

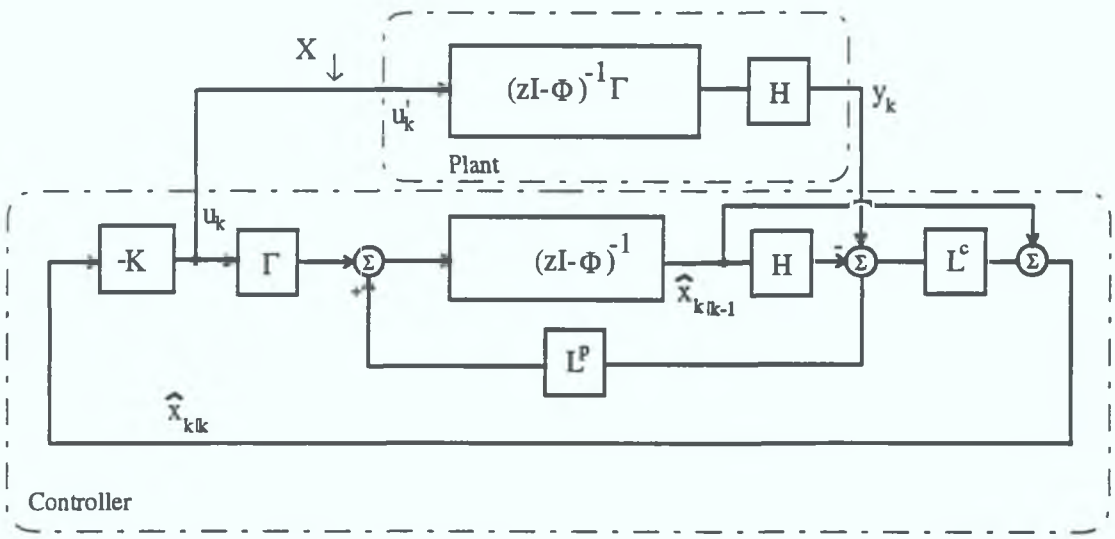

Fig. [3-16] LQG with DTIK Smoother.

Figure **[3-17]** represents a Nyquist plot as robustness recovery takes place for the LQG controller with the Kalman predictor-corrector smoothing compensator. From the plot it is apparent that this compensator structure exhibits superior robustness recovery properties when compared against the other structures. The final robustness values are contained in Table **[3-3]**. Note that the infinite gain margin has been realised in this particular implementation. Figure **[3-18]** shows the realisation of this infinite gain margin more clearly. This figure is a clearer plot of the Nyquist contour around the origin of Figure **[3-17]**, only the final LQG/LTR Nyquist plot is shown.

Although the gain margin in this example has been fully recovered, the cost of this recovery is felt in terms of a reduced disturbance noise attenuation in the closed loop system. In a practical situation the designer must often sacrifice full recovery for improved disturbance attenuation. The estimator gain used in the two LQG/LTR

designs is the same. It is thus evident that the Kalman smoother implementation exhibits superior robustness properties for a given disturbance noise attenuation level.

If the computational overhead is not a primary consideration in the design then the designer could improve the robustness bounds by increasing the sample frequency. Note that as the sample frequency in increased, all three Kalman forms become better approximations to the continuous time implementation. Indeed it would appear that the robustness convergence properties of the Kalman implementation are a function of γ from section 3.2.1.1. Thus for a high sample frequency and a low controller bandwidth the robustness convergence properties of the Kalman predictor-corrector filter implementation can be improved.

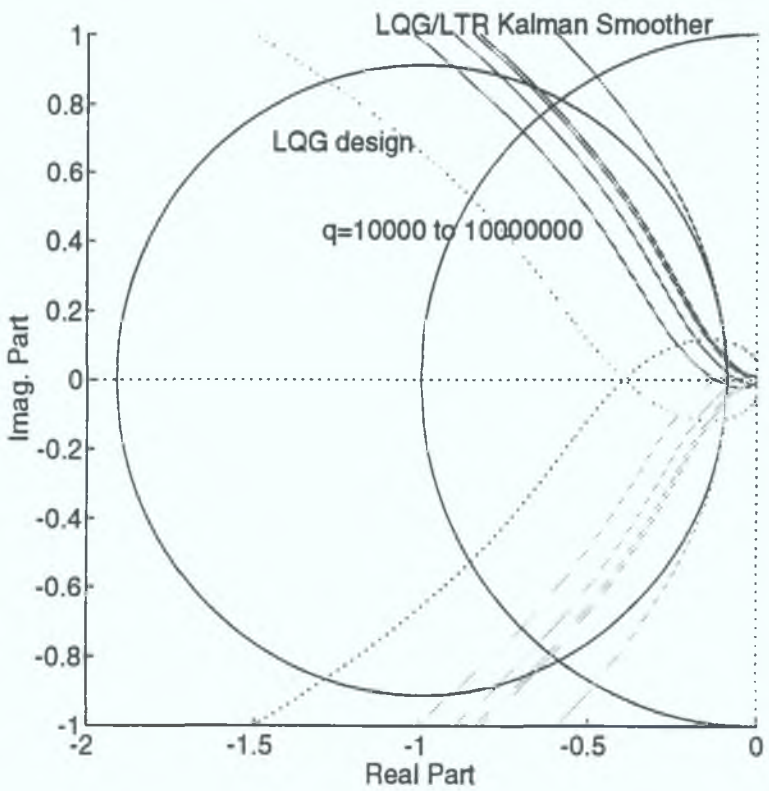

Fig. [3-17] Nyquist plot for LQG/LTR with DTIK Smoother.

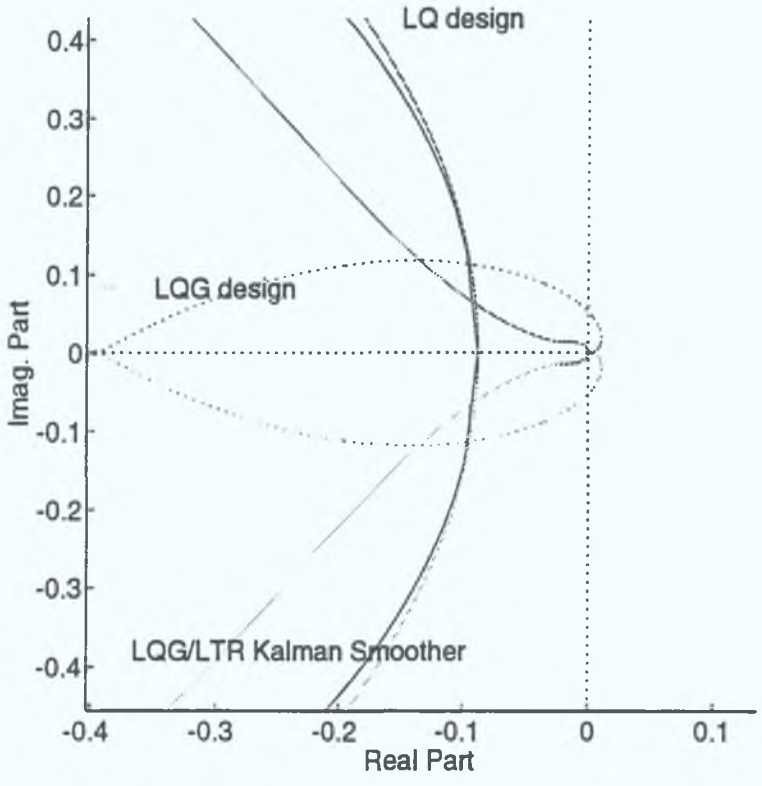

Fig. [3-18] Nyquist plot at the origin showing infinite gain margin recovery .

3.3.3.2 Performance Costs.

In the preceding sections, the existence of a trade-off between robustness / performance has been stated. Using the Nyquist plot for the different controller structures, robustness comparisons can be drawn between the structures. This section develops the techniques required to make performance comparisons between different systems. Three aspects of performance will be considered cost, disturbance attenuation and noise suppression.

Recall that the philosophy surrounding the design of a LQ controller involves the minimisation of a linear quadratic cost function **[3-1]**. Thus for a given sequence $[x_k \; u_k]$ the performance cost based on this cost function can be evaluated. The nominal LQ controller will be used as a basis for this cost evaluation. The LQ cost function represents the time domain cost of a controller's response. The output disturbance response of each system will be used as a common reference from which cost comparisons can take place.

The state space realisation of the predictor, predictor-corrector and smoother compensator structures are reproduced below for clarity in equations **[3-82]**, **[3-83]** and **[3-84]**. The closed loop response to a step change in output disturbance can be readily obtained by augmenting these state space implementations with the plant model. Equation **[3-85]** describes this augmented system, where each compensator is described by an ABCD state space system model and the plant is described by a ΦΓH state space model. The performance costs are obtained by summing the resulting $\begin{bmatrix} x_k & u_k \end{bmatrix}$ response, subject to their respective controller weightings[8].

Tables **[3-5]** to **[3-7]** show the costs of the three compensator implementations, at different stages of the LTR procedure for the preceding example. The costs in these tables are normalised by the cost of the nominal LQ controller. The information in the tables can be summarised as follows. For the discrete Kalman smoother (DK-Smoother) implementation the performance costs increase as recovery takes place whereas for the predictor and predictor-corrector implementations costs reduce as recovery takes place.

Predictor compensator[9]:

$$\begin{aligned} \hat{x}_k &= \left(\Phi - L^p H - \Gamma K\right)\hat{x}_{k-1} + L^p y_{k-1} \\ u_k &= -K\hat{x}_k \end{aligned} \qquad \textbf{[3-82]}$$

Predictor-corrector compensator:

$$\begin{aligned} \hat{x}_k &= \left(\Phi - L^c H\Phi - \Gamma K + L^c H\Gamma K\right)\hat{x}_{k-1} + L^c y_k \\ u_k &= -K\hat{x}_k \end{aligned} \qquad \textbf{[3-83]}^{10}$$

Smoother compensator:

$$\begin{aligned} \hat{x}_{k+1|k} &= (\Phi - \Gamma K)\left(I - L^c H\right)\hat{x}_{k|k-1} + (\Phi - \Gamma K)L^c y_k \\ u_k &= K\left(I - L^c H\right)\hat{x}_{k|k-1} + KL^c y_k \end{aligned} \qquad \textbf{[3-84]}^{11}$$

---

[8] See Matlab function costs.m, listed in Appendex B.

[9] The Predictor compensator, hasn't appeared in this text before, but can be readly derived using the Kalman form #1 structure.

[10] This equation is a redraft of equation **[3-65]**.

[11] This equation is a copy of equation **[3-79]**

$$\hat{x}_{k+1} = \begin{bmatrix} A & BH \\ -\Gamma C & \Phi - \Gamma DH \end{bmatrix} \hat{x}_k + \begin{bmatrix} BH \\ -\Gamma DH \end{bmatrix} y_r \qquad \textbf{[3-85]}$$

$$u_k = \begin{bmatrix} DH & -C \end{bmatrix} \hat{x}_k + Dy_r$$

The disturbance attenuation and noise suppression aspects of performance can be described in terms of the sensitivity and complementary sensitivity functions developed in section 3.2.2. Table **[3-2]** contains a summary of the desirable properties of these functions. Figure **[3-19]** shows a delta plot for the sensitivity (S) and complementary sensitivity function (T) at different stages of the loop recovery for the Kalman smoother implementation. Figure **[3-20]** is the corresponding sensitivity plot for the LQ controller. Several important observations can be made from these plots.

As recovery takes place both the sensitivity and complementary sensitivity plots advance forward in frequency. Consider two fixed points in frequency at 20 Rad/Sec and 500 Rad/Sec. As recovery takes place the disturbance attenuation properties of the LQG system improve. Tables **[3-5]** to **[3-7]** reflect the improvement in disturbance attenuation for the three LQG compensator implementations. The attenuation figures given, are those for a disturbance with a frequency of 20 Rads/Sec.

However as recovery takes place the noise suppression properties of the LQG controller deteriorate. The tables also reflect this deterioration as seen for a noise signal with a frequency of 500 Rads/Sec. For a system specification expressed in terms of noise or disturbance attenuation values, the sensitivity and complementary sensitivity functions can be used to halt the LTR procedure. This design process would maximise sensitivity for a given disturbance attenuation or vice versa.

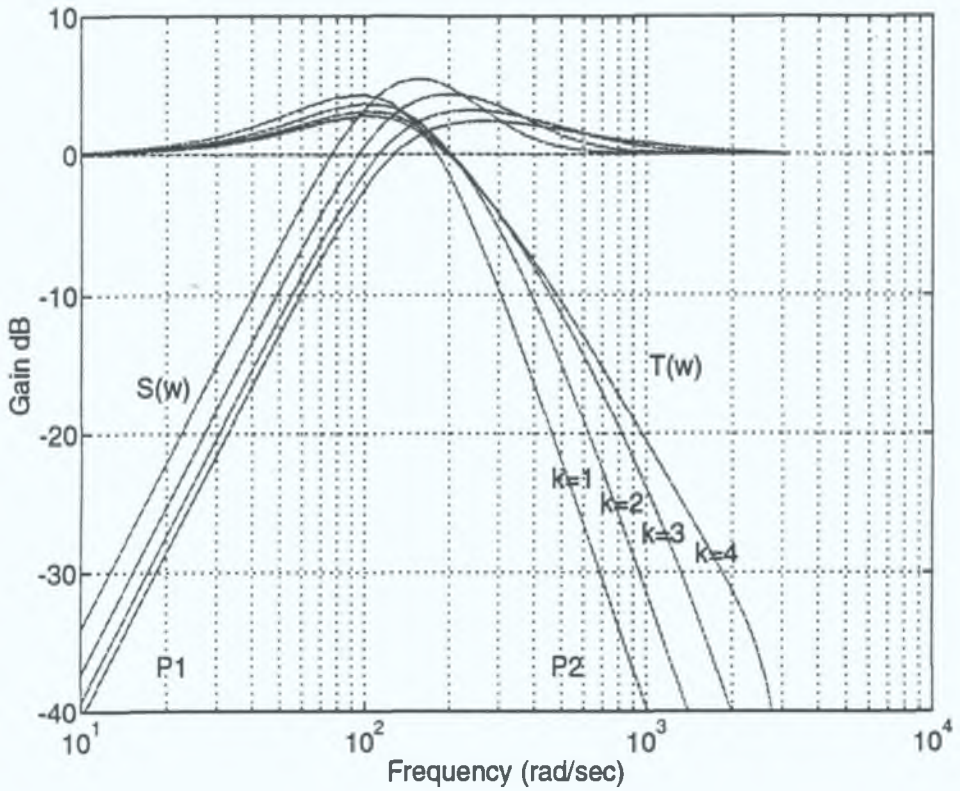

Fig. [3-19] Sensitivity plot for LQG(DK-Smoother)/LTR

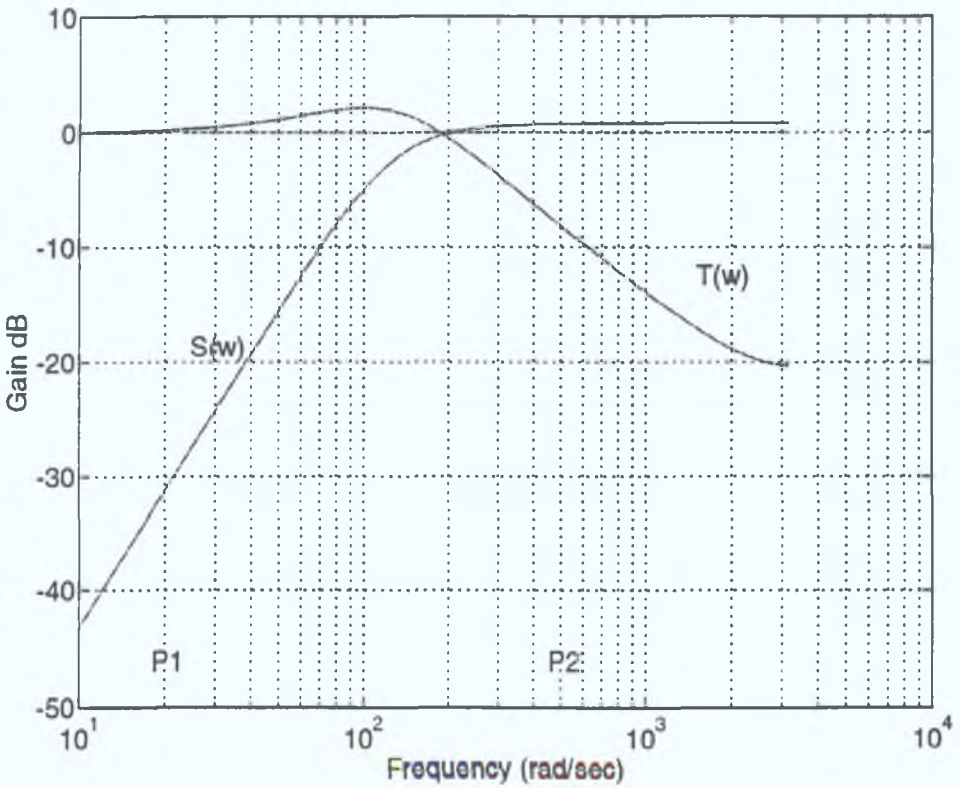

Fig. [3-20] Sensitivity plot for LQ compensator

From the two figures a further very important observation can be made, regarding the respective roll-off rates of complementary sensitivity functions for the LQ and LQG designs. It is immediately obvious that the LQG design exhibits superior roll-off rates. This would make intuitive sense in light of the increased order of the LQG design. As recovery takes place this superiority of the LQG design is lost at or around the cross-over frequency. It is later regained for frequencies outside the bandwidth of the estimator. The loss of this superiority yet again poses another halting constraint in the LTR design procedure.

The robustness improvements as the LTR procedure advances is further evident from the reduced overshoot of the sensitivity and complementary sensitivity functions. Recall the reason for the failure of the design example in section 3.2.3. The robustness bounds established in section 3.2.3, when used as a design criterion, provide another halting criterion for the LTR design procedure.

The sensitivity plots for the predictor-corrector and predictor implementations are given in figures **[3-21]** and **[3-22]**. By comparing the plots or comparing the equivalent tables, it becomes apparent that the disturbance and noise suppression properties of these three implementations are more or less the same. The only notable difference between the three implementations occurs at the cross-over frequency. The DK-Smoother implementation at each stage in the recovery has a smaller overshoot compared with the other implementations. The DK-Predictor compensator has the greatest overshoot.

Using the results from tables **[3-4]** to **[3-7]** the designer is faced with a design choice. The robustness results obtained for the DK-Smoother compensator for the third and fourth LTR iteration are very attractive, see Table **[3-5]**. Although the phase margin hasn't fully recovered to that of the optimum LQ design, it is still within the bounds for 'good' design using classical synthesis techniques. The gain margin on the other hand exceeds the minimum requirements for optimality and the margins for the optimum LQ design. However, the costs of this robustness for most applications is too high. Consequently robustness sacrifices will have to be made to meet satisfactory performance costs.

Consider the DK-Smoother/LTR iteration #2 or the DK-Current/LTR iteration #4 designs, here the robustness bounds are more or less the same for the two systems and they are still 'good' in terms of classical merits. Furthermore the performance costs are now satisfactory, although the DK-Current compensator's costs are

superior. If noise suppression is a primary consideration the DK-Smoother/LTR #2 provides superior noise suppression, whereas the DK-Current/LTR #4 provides superior disturbance attenuation.

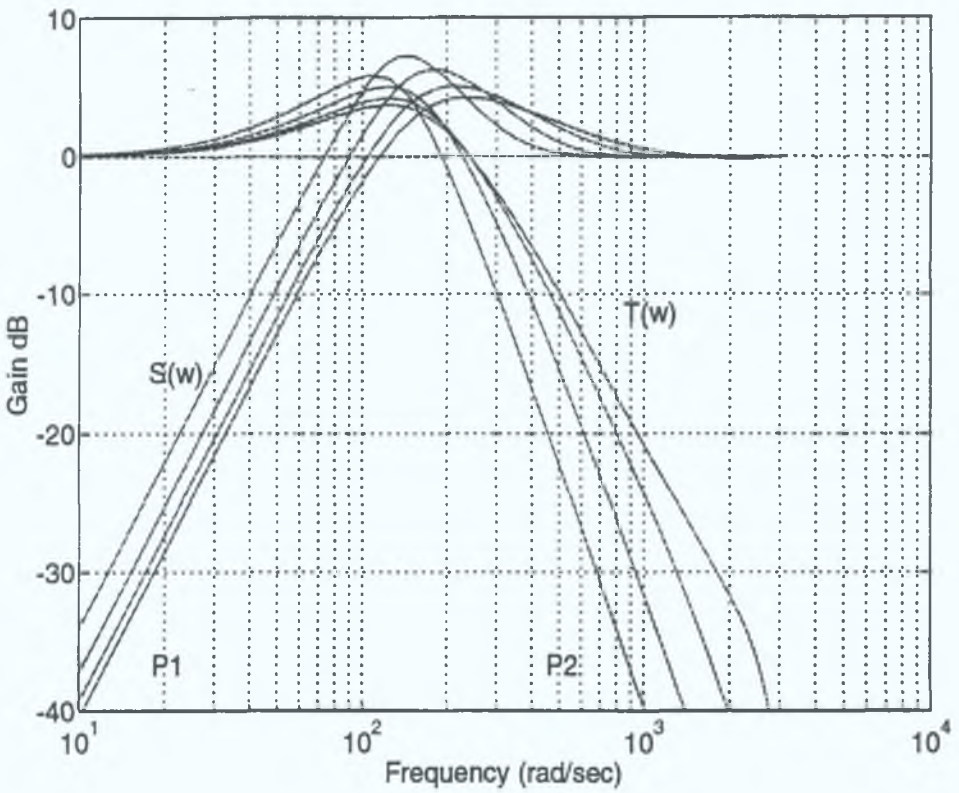

Fig. [3-21] Sensitivity plot for LQG(DK-predictor-corrector)/LTR compensator

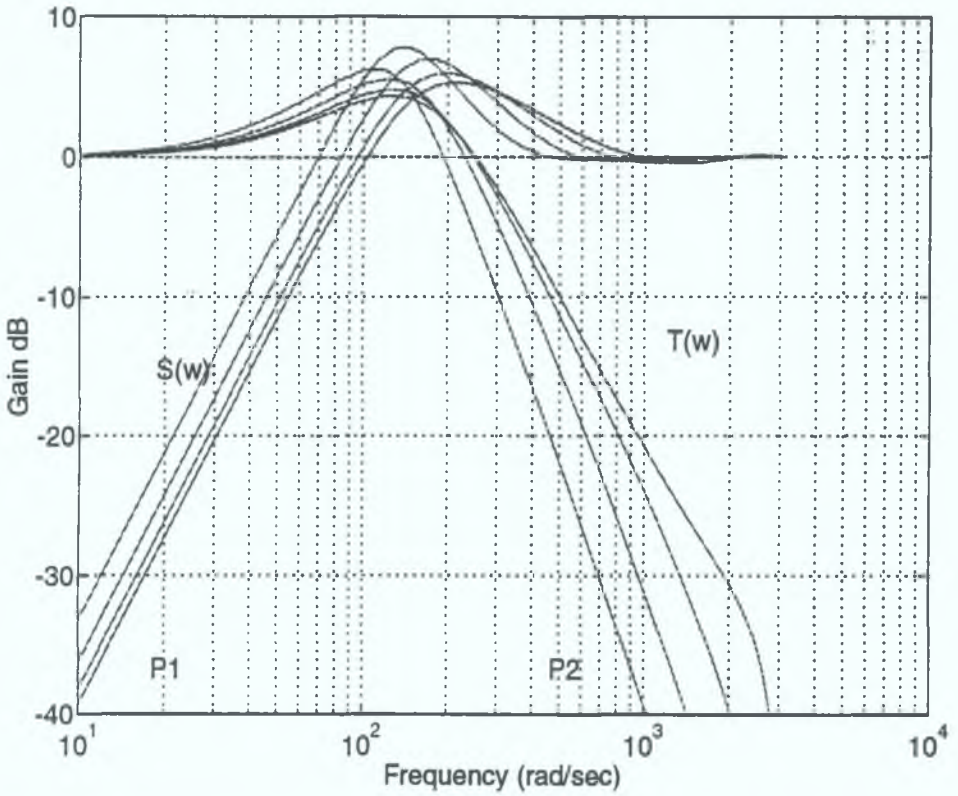

Fig. [3-22] Sensitivity plot for LQG(DK-predictor) compensator

Normalised Cost	1
Gain Margin	21.09 dB
Phase Margin	61.5°
Disturbance Atten. @ P1	31.32 dB
Noise Suppression @ P2	8.15 dB

Table [3-4] Performance results for LQ compensator

LTR Iteration (k)	1	2	3	4
Est. Root Location	54±54i	97±96i	174±170i	318±293i
Normalised Cost	1.2197	1.4460	2.4764	6.3997
Gain Margin	10.9 dB	13.5 dB	18.36 dB	24.5 dB
Phase Margin	35.85°	40.40°	45.80°	50.00°
Disturbance Atten. @ P1	22.05 dB	25.35 dB	27.32 dB	28.59 dB
Noise Suppression @ P2	22.00 dB	15.07 dB	11.39 dB	10.59 dB

Table [3-5] Performance results for LQG(DK-Smoother)/LTR

LTR Iteration (k)	1	2	3	4
Est. Root Location	54±54i	97±96i	174±170i	318±293i
Normalised Cost	1.2229	1.2166	1.2048	1.1969
Gain Margin	7.9 dB	9.28 dB	11.5 dB	13.8 dB
Phase Margin	29.48°	32.69°	37.2°	40.5°
Disturbance Atten. @ P1	22.18 dB	25.29 dB	27.32 dB	28.59 dB
Noise Suppression @ P2	22.30 dB	15.39 dB	11.26 dB	10.00 dB

Table [3-6] Performance results for LQG(DK-Current)/LTR

LTR Iteration (k)	1	2	3	4
Est. Root Location	54±54i	97±96i	174±170i	318±293i
Normalised Cost	1.2402	1.2361	1.2252	1.2176
Gain Margin	6.57 dB	7.51 dB	8.9 dB	10.1 dB
Phase Margin	27.9°	30.28°	33.7°	36.2°
Disturbance Atten. @ P1	21.24 dB	24.27 dB	26.18 dB	27.38 dB
Noise Suppression @ P2	21.88 dB	15.18 dB	11.45 dB	9.96 dB

Table [3-7] Performance results for LQG(DK-Predictive)/LTR

3.3.3.3 Frequency Shaped Loop Transfer Recovery (FS-LTR).

In the previous section an approach to improve the robustness of the LQG system was adopted. This approach increased the degree of stability in the estimator design by applying an appropriately constructed fictitious noise source in the state model, during the estimator design. The intensity of this fictitious noise source is increased until robustness is recovered. The gain in robustness properties of the LQG/LTR system is at the expense of the reduced closed loop performance for the nominal plant. This section provides a modified approach to the LTR design procedure which limits the performance costs of the LTR design.

The technique in this section is to construct a noise process so that the effective energy is primarily in the frequency bands where the robustness properties are lacking, thus robustness improvements can be achieved in the necessary frequency bands without affecting the closed loop characteristics outside this band. This technique will provide a systematic approach to achieving improved robustness and performance trade-offs.

This improved approach was developed by Moore *et al* in [Moore 81], they extended the work of Doyle *et al* [Doyle 79]. Moore *et al* proposed replacing the fictitious noise which has a white distribution with an appropriately constructed noise source with a coloured distribution. The fictitious coloured noise is represented formally, as the output of a linear asymptotically stable system driven by a white noise source **[3-86]**. This noise model is then augmented with the stochastic model for the plant given by equation **[3-87]**, the resulting augmented system is described by equation **[3-88]**. The augmented model given by equation **[3-88]** is subsequently used in the estimator design.

$$\begin{aligned} x_{k+1} &= \Phi_n x_{k+1} + \Gamma_n \omega_k \\ \xi_k &= H_n x_k + G_n \omega_k \end{aligned} \qquad \textbf{[3-86]}$$

$$\begin{aligned} x_{k+1} &= \Phi x_{k+1} + \Gamma(u_k + \xi_k) + G\omega_k \\ y_k &= H x_k + \upsilon_k \end{aligned} \qquad \textbf{[3-87]}$$

$$\begin{aligned} x_{k+1} &= \begin{bmatrix} \Phi & \Gamma H_n \\ 0 & \Phi_n \end{bmatrix} x_k + \begin{bmatrix} \Gamma \\ 0 \end{bmatrix} u_k + \begin{bmatrix} \Gamma G_n + G \\ \Gamma_n \end{bmatrix} \omega_k \\ y_k &= \begin{bmatrix} H & 0 \end{bmatrix} x_k + \upsilon_k \end{aligned} \qquad \textbf{[3-88]}$$

The next stage in the design is to parameterise the colour noise model **[3-86]**. In practice, if there are unacceptably poor phase margins in the LQG design, it is reasonable to inject fictitious plant noise in the vicinity of the cross-over frequency, and possibly in a frequency band where there is high plant input (actuator) uncertainty, during the recovery procedure [Anderson 79]. Recall that robustness is measured in terms of gain and phase margins, these margins are defined at the cross-over frequency of the closed loop system. In a LQG design, the LQ design defines this desired cross-over frequency, provided the nominal estimator doesn't dominate the closed loop response.

It is usual to use low-order high-pass, low-pass or band-pass filters driven by white noise in the construction of a coloured noise source. In particular the LTR procedure requires the plant to be minimum phase. Since this noise model will be augmented with the plant model in the estimator design, it is required that this noise model is also minimum phase. A Butterworth filter design is an all-pole filter, its zeros are all at infinity and its poles lie on the unit circle. The inverse of a Butterworth filter is also stable and as a consequence the filter is minimum phase. Thus a Butterworth filter would represent a suitable choice of filter design for this application. The order and

choice of frequency band for the filter is a function of the particular application. In general, a low pass filter with a cut-off frequency close to that of the desired closed loop system would provide better robustness / performance trade-off than the white noise case. The improved roll-off rate characteristics of the original LQG design are preserved when loop recovery takes place in a low frequency band. Thus in the absence of additional information such a low-pass filter would be the first stage in the design. The success of a given LQG design will be rated in terms of its robustness and performance compared to those properties of the original LQ design.

Figures **[3-23]** and **[3-24]** show the Nyquist and sensitivity plots, for a second order low pass frequency shaping filter. Each figure contains two plots which correspond to the two choices of cut-off frequency. Table **[3-8]** summarises the performance and robustness properties obtained from these plots. In the previous examples, the LTR index k was used to correlate the performance results for the different implementations. In this situation the model used in the estimator design has changed and hence this index can no longer be used for correlating the results. Instead the estimator's root locations will be used. By comparing these results with Table **[3-5]** it is apparent that the first frequency shaped design (120Hz) corresponds approximately to k=4, and the second frequency shaped design (40Hz) corresponds approximately to k=3. From the results it is apparent that the frequency shaped design with a low order low pass filter exhibits superior phase margin properties for a given estimator bandwidth. However the gain margin has suffered during this design. The noise suppression properties about P2 have also disimproved. However this degradation is local to P2 and for higher frequency noise the noise attenuation improves.

In conclusion the FS-LTR design approach provides, in general, superior robustness properties than the LTR approach. The superior roll-off rate of the LQG design is further improved with the increase in estimator order. However, there is a loss of noise suppression local to the cut-off frequency of the frequency shaped filter. The use of a frequency shaped filter with a flatter pass-band response would lessen this degradation. There is also a degradation in the time response of the closed loop system which is a consequence of the increased order of the compensator.

In section 4.4 the current amplifier model is used in the estimator design, this model acts as a frequency shaping filter for the loop transfer recovery procedure. The current amplifier focuses recovery at the crossover frequency for the closed loop system.

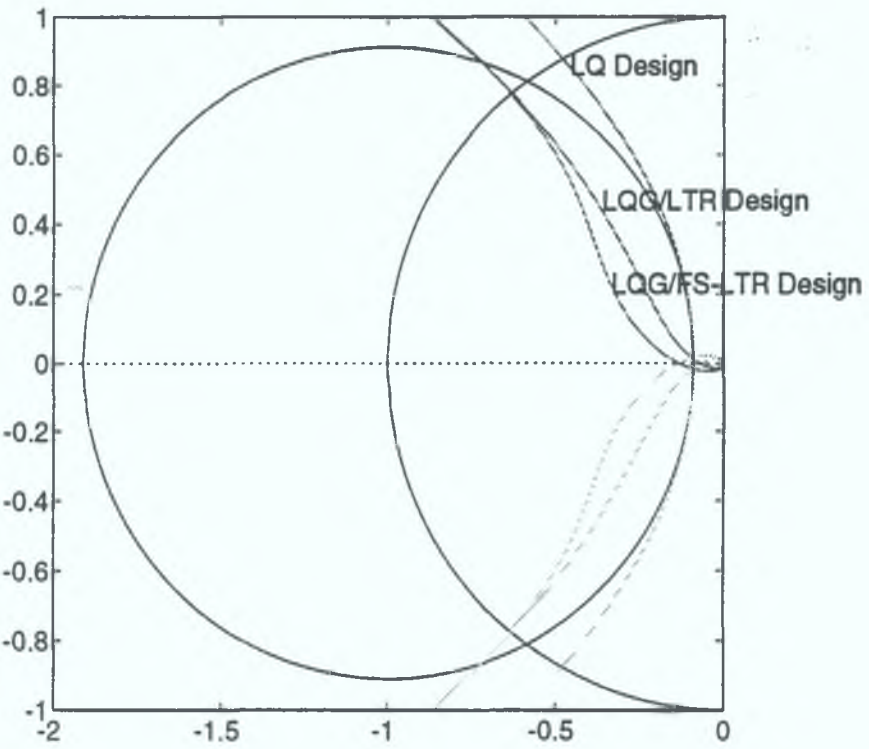

Fig. [3-23] Nyquist plot for LQG/FS-LTR(DK-Smoother) compensator

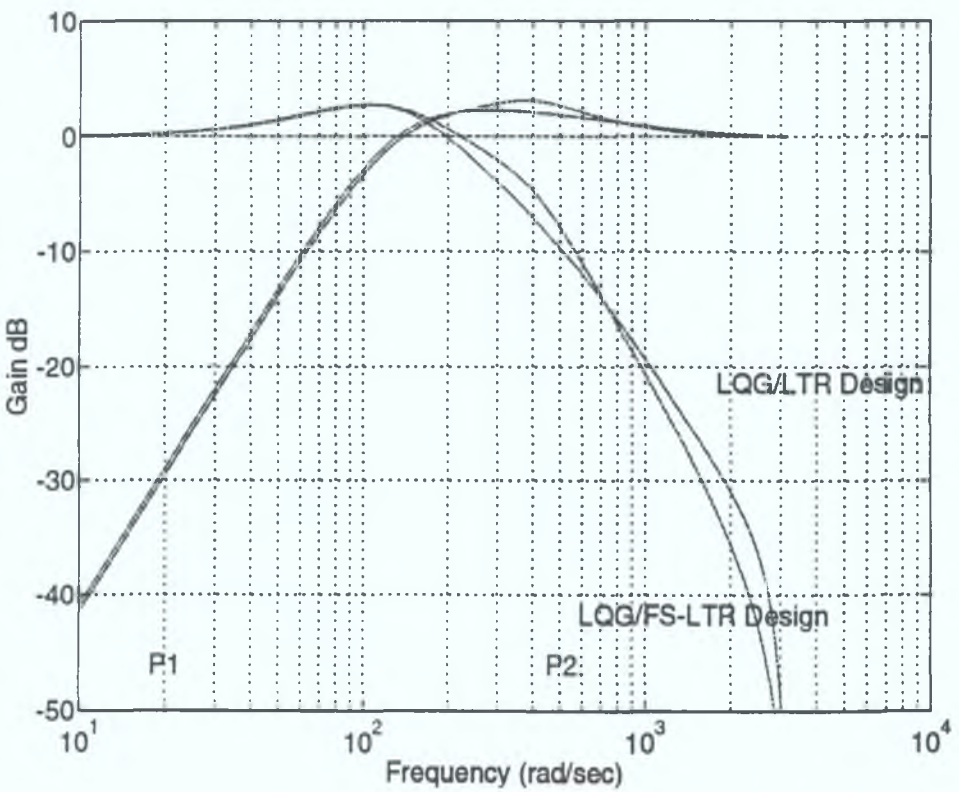

Fig. [3-24] Sensitivity plot for LQG/FS-LTR(DK-Smoother) compensator

FS Cut-off	120Hz	40Hz
Est. Root Location	342±190i,159±343i	220±8.7i,8.5±200i
Normalised Cost	NA	NA
Gain Margin	23.07 dB	17.42 dB
Phase Margin	50.7°	50.97°
Disturbance Atten. @ P1	28.9 dB	29.45 dB
Noise Suppression @ P2	9.7 dB	8 dB

Table [3-8] Performance results for LQG/FS-LTR(DK-Smoother) compensator

3.3.3.4 Frequency Shaped Linear Quadratic Gaussian Control (FS-LQG).

Often in control problems there is the need to overcome the effects of external forces and unmodelled inputs into the plant. These inputs can cause steady state and tracking errors in the closed loop design. In classical control these forces are often overcome with the use of integral action. Such integral action is a subset of frequency shaped control. This section describes at the extension of LQ design to include frequency shaping. In particular proportional plus integral frequency shaping will be considered.

The LQ controller is a full state feedback controller. The control law is simply a constant times the feedback states. Frequency shaped control involves replacing the LQ controller gains with a dynamic frequency shaped filter. Equation **[3-89]** describes the modified controller equation for a proportion plus integral frequency shaping filter, where H is the output coupling matrix.

$$\begin{aligned} u_k &= K(s)\hat{x}_k \\ &= \left\{K_p + \frac{K_i H}{s}\right\}\hat{x}_k \end{aligned} \qquad \textbf{[3-89]}$$

By augmenting the plant model with the frequency shaping filter in the controller design, linear quadratic control gains can be established for the proportional and integral components of the frequency shaped filter. Equation **[3-90]** describes this augmented model for a PI-LQ controller. The quadratic cost function for the augmented system is given by **[3-91]**. The LQ controller gains can now be calculated in the usual manner. The estimator design for the LQG controller is performed using the unaugmented model.

The resulting compensator for the LQG design can be established using the compensator models **[3-82]**, **[3-83]** or **[3-84]** depending on the discrete Kalman filter

form used for the implementation, where the plant model used in the compensator design is the augmented model. Note that the estimator gain L must be padded with as many zeros as there are states in the frequency shaped filter.

$$x_k = \begin{bmatrix} \Phi & 0 \\ HT & 1 \end{bmatrix} x_{k-1} + \begin{bmatrix} \Gamma \\ 0 \end{bmatrix} u_{k-1}$$
$$y_k = \begin{bmatrix} H & 0 \end{bmatrix} x_{k-1} \qquad \textbf{[3-90]}$$

$$J = \sum_{k=0}^{N} \left[\begin{bmatrix} x_k & x_k' \end{bmatrix} \begin{bmatrix} Q_1 & 0 \\ 0 & Q_1' \end{bmatrix} \begin{bmatrix} x_k \\ x_k' \end{bmatrix} + u_k^T Q_2 u_k \right] \qquad \textbf{[3-91]}$$

The use of the frequency shaped filter introduces additional poles into the closed loop system. These poles affect the dynamic response of the system to reference inputs in the case of a servo system. This degradation of the command response is an undesirable side effect from using frequency shaping or integral control. To overcome this degradation the use of disturbance feedforward is often considered. In this configuration the estimator model is augmented with a disturbance estimate, the resulting disturbance estimate is then fed forward into the input of the plant, cancelling out the effects of external disturbance. Placing the integrator into the estimator removes it from the forward path of the reference signal, thus eliminating the degradation in performance. An application of this technique can be seen in [Kettle 93].

The disturbance estimate is an estimate of a bias at the input to the plant. A bias can be modelled as an integrator driven by a white noise source. This noise source couples into the system in much the same way as the fictitious noise source in the FS-LTR design. Indeed the disturbance estimate is a subset of FS-LTR. However in the FS-LTR design the states of the frequency shaped filters are not used in the control law. Equation **[3-92]** describes the augmented model used in the estimator design. Equation **[3-94]** described the augmented control law which includes the disturbance feedforward.

$$\hat{x}_{k+1} = \begin{bmatrix} 1 & 0 \\ \Gamma & \Phi \end{bmatrix} x_k + \begin{bmatrix} 0 \\ \Gamma \end{bmatrix} u_k$$
$$y_k = \begin{bmatrix} 0 & H \end{bmatrix} x_k \qquad \textbf{[3-92]}$$

$$Q_e' = \begin{bmatrix} \sigma_\omega & 0 \\ 0 & Q_e \end{bmatrix} \qquad \textbf{[3-93]}$$

$$K' = \begin{bmatrix} 1 & K \end{bmatrix}, \quad u_k = K'\hat{x}_k \qquad \textbf{[3-94]}$$

Figure **[3-25]** depicts a graphical interpretation of the PI-LQG design. Figure **[3-26]** depicts an LQG controller with disturbance feedforward. Both implementations provide similar disturbance suppression properties, although the disturbance feedforward approach has superior command response properties. The choice of a given disturbance rejection technique will depend on the precedence of these features in the given application.

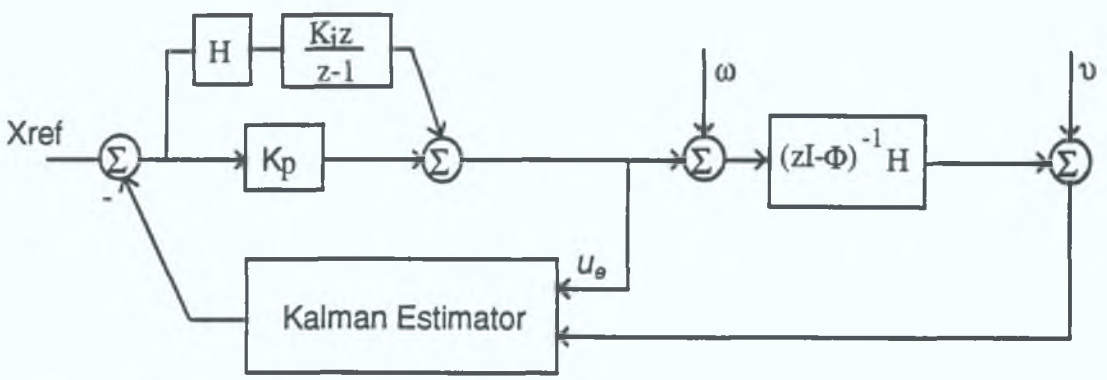

Fig. [3-25] PI-LQG design.

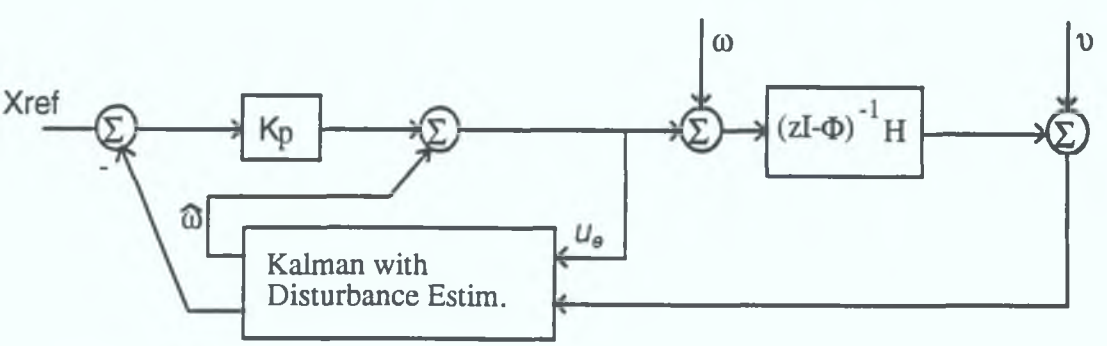

Fig. [3-26] LQG Disturbance feedforward design.

There exists a dual frequency shaping procedure for estimator design. Here the constant estimator gain is replaced by a frequency shaped filter. This procedure provides rejection of constant plant disturbances entering with the process noise.

3.4 Discrete-Time Kalman (DKF) Forms.

The discrete-time optimal stochastic filter was derived by Kalman in [Kalman 60] and has since been called the Kalman filter. The Kalman filter problem can be formulated as follows, given a discrete time stochastic state space description of a system **[3-95]** and an observation model **[3-96]**, where Φ, Γ and H in equations **[3-95]** and **[3-96]** have their usual state space interpretation and where ω_k and υ_k denote process noise and measurement noise sequences respectively, then the Kalman filter is the optimal filter for gaussian signal models. The noises ω_k and υ_k are assumed to be uncorrelated with zero means and gaussian distributions, formally these can be mathematically described using equations **[3-97]** and **[3-98]**, where δ denotes the Kronecker delta function which is defined by equation **[3-99]**. The matrices Q_k and R_k are defined as positive definite symmetric matrices.

$$x_{k+1} = \Phi_k x_k + \Gamma_k u_k + G_k \omega_k \qquad \textbf{[3-95]}$$

$$z_k = H x_k + \upsilon_k \qquad \textbf{[3-96]}$$

$$\mathrm{cov}\{\omega_t, \omega_k\} = Q_k \delta_{t,k}\,,\; E\{\omega_k\} = 0 \qquad \textbf{[3-97]}$$

$$\mathrm{cov}\{\upsilon_t, \upsilon_k\} = R_k \delta_{t,k}\,,\; E\{\upsilon_k\} = 0 \qquad \textbf{[3-98]}$$

$$\delta_{i,j} = \begin{cases} 1 & i = j \\ 0 & i \neq j \end{cases} \qquad \textbf{[3-99]}$$

The optimal discrete linear filter is required to minimise the estimation error criterion defined by **[3-100]**, where the estimation error is defined by **[3-101]**. Kalman in his paper [Kalman 60] presented an estimator of the form given in equation **[3-102]**, this structure is often called a single-state predictor, since the current estimate at time **k+1** depends only upon past observations. The subscript notation used, for example $\hat{x}_{k|k-1}$ reads as follows, the estimate of x denoted $\hat{x}$, at time k given information up to and including time k-1.

$$J = \mathrm{E}\left\{\tilde{x}_{k|k-1}\tilde{x}^T_{k|k-1}\right\} \qquad \textbf{[3-100]}$$

$$\tilde{x}_{k|k-1} = x_k - \hat{x}_{k|k-1} \qquad \textbf{[3-101]}$$

$$\hat{x}_{k+1|k} = \Phi_k \hat{x}_{k|k-1} + K_k\left(z_k - H_k \hat{x}_{k|k-1}\right) \qquad \textbf{[3-102]}$$

The *predictive* Kalman filter as described in Kalman's paper is summarised below [Kalman form #1]. Subsequent work in the area as outlined by Grimble in [Grimble 88b], brought about alternative forms of the DKF. There forms are based on a slightly different estimation error minimisation criterion **[3-103]**,

$$J = \mathrm{E}\left\{\tilde{x}_{k|k}\tilde{x}_{k|k}^{T}\right\} \qquad \textbf{[3-103]}$$

$$\tilde{x}_{k|k} = x_k - \hat{x}_{k|k} \qquad \textbf{[3-104]}$$

where the processing time is considerably smaller than the sample period the *current* or *predictor-corrector* form of the DKF can be used [Kalman form #2][Jazwinski 70]. In this form the current estimator is based on the current measurement, hence the name. There are two common versions of this filter [#2a, #2b], both of which are equivalent. The latter is the most attractive form because it separates the estimate into two portions, those dependent on the current measurement and those dependent on the previous estimate. This approach aids the design of a practical algorithm. Prior to the next sample interval the processor can evaluate equation **[3-118]**, on the next sample interval when a measurement has been made the processor evaluates equation **[3-119]**. This is more attractive than evaluating equation **[3-112]** on the next sample interval. Note that any known inputs to the plant, become inputs to the estimator, this includes process noise or measurement noise non zero biases.

The third form of the DKF is the predictor-corrector smoother form [Kalman form #3]. This filter form is presented here because it exhibits superior robustness properties over the other forms. The filter construction uses present and past measurements in the evaluation of a new estimate.

Kalman Form #1: *Discrete linear time-varying (DLTV) single-stage predictor:*

Plant model: $$x_{k+1} = \Phi_k x_k + \Gamma_k u_k + G_k \omega_k \qquad \textbf{[3-105]}$$

Observation model: $$z_k = H_k x_k + \upsilon_k \qquad \textbf{[3-106]}$$

Estimate: $$\hat{x}_{k+1|k} = \Phi_k \hat{x}_{k|k-1} + \Gamma_k u_k + K_k\left(z_k - H_k \hat{x}_{k|k-1}\right) \qquad \textbf{[3-107]}$$

Gain: $$K_k = \Phi_k P_{k|k-1} H_k^T \left\{H_k P_{k|k-1} H_k^T + R_k\right\}^{-1} \qquad \textbf{[3-108]}$$

A priori cov.:

$$P_{k+1|k} = \Phi_k P_{k|k-1} \Phi_k^T + G_k Q_k G_k^T - \Phi_k P_{k|k-1} H_k^T \left\{H_k P_{k|k-1} H_k^T + R_k\right\}^{-1} H_k P_{k|k-1} \Phi_k^T \qquad \textbf{[3-109]}$$

Kalman Form #2a: *DLTV Kalman filter Classical:*

Plant model: $x_{k+1} = \Phi_k x_k + \Gamma_k u_k + G_k \omega_k$ **[3-110]**

Observation model: $z_k = H_k x_k + \upsilon_k$ **[3-111]**

Estimate: $\hat{x}_{k|k} = \Phi_{k-1}\hat{x}_{k-1|k-1} + \Gamma_{k-1}u_{k-1} + K_k\left(z_k - H_k\Phi_{k-1}\hat{x}_{k-1|k-1}\right)$ **[3-112]**

Gain: $K_k = P_{k|k-1}H_k^T\left\{H_k P_{k|k-1}H_k^T + R_k\right\}^{-1}$ **[3-113]**

A priori cov.: $P_{k+1|k} = \Phi_k P_{k|k}\Phi_k^T + G_k Q_k G_k^T$ **[3-114]**

A posteriori cov.: $P_{k|k} = P_{k|k-1} - K_k H_k P_{k|k-1}$ **[3-115]**

Kalman Form #2b: *DLTV Kalman filter Predictor-corrector or Current estimator:*

Plant model: $x_{k+1} = \Phi_k x_k + \Gamma_k u_k + G_k \omega_k$ **[3-116]**

Observation model: $z_k = H_k x_k + \upsilon_k$ **[3-117]**

Predictive Est.: $\hat{x}_{k+1|k} = \Phi_k\hat{x}_{k|k} + \Gamma_k u_k + G_k\varpi_k$ **[3-118]**

Current Est.: $\hat{x}_{k|k} = \hat{x}_{k|k-1} + K_k\left(z_k - H_k\hat{x}_{k|k-1}\right) - \overline{\upsilon}_k$ **[3-119]**

Gain: $K_k = P_{k|k-1}H_k^T\left\{H_k P_{k|k-1}H_k^T + R_k\right\}^{-1}$ **[3-120]**

A priori cov.: $P_{k+1|k} = \Phi_k P_{k|k}\Phi_k^T + G_k Q_k G_k^T$ **[3-121]**

A posteriori cov.: $P_{k|k} = P_{k|k-1} - K_k H_k P_{k|k-1}$ **[3-122]**

Kalman Form #3: *DLTV Kalman smoother, Predictor-corrector:*

Plant model: $x_{k+1} = \Phi_k x_k + \Gamma_k u_k + G_k \omega_k$ **[3-123]**

Observation model: $z_k = H_k x_k + \upsilon_k$ **[3-124]**

Predictive Est.: $\hat{x}_{k+1|k} = \Phi_k\hat{x}_{k|k-1} + \Gamma_k u_k + G_k\varpi_k + K_k^P\left(z_k - H_k\hat{x}_{k|k-1}\right)$ **[3-125]**

Current Est.: $\hat{x}_{k|k} = \hat{x}_{k|k-1} + K_k^c\left(z_k - H_k\hat{x}_{k|k-1}\right) - \overline{\upsilon}_k$ **[3-126]**

Gains: $K_k^c = P_{k|k-1}H_k^T\left\{H_k P_{k|k-1}H_k^T + R_k\right\}^{-1}$ **[3-127]**

$K_k^P = \Phi_k K_k^c$ **[3-128]**

A priori cov.: $P_{k+1|k} = \Phi_k P_{k|k}\Phi_k^T + G_k Q_k G_k^T$ **[3-129]**

A posteriori cov.: $P_{k|k} = P_{k|k-1} - K_k^c H_k P_{k|k-1}$ **[3-130]**

4. Robust Optimal DC Motor Controller (Implementation).

4.1 The Test Rig.

The development platform for the implementation of the motor controller featured in this document, consists of two 4kW permanent magnet DC motors coupled back to back. The coupling between the two motors is rigid. The second motor is used as an active load, which is used to simulate changes in inertia and viscosity of the motor and its load and to simulate external disturbance or excitations applied to the closed loop system.

In order to design a controller for this system, a reasonable model of the system is required. This section deals with the identification of a mathematical model for the test rig. This is accomplished in several ways, the first of which is to use available information from the data sheets for the motor and inverter. This data is then complemented with an analytical model obtained by modelling the system in full, from a circuit component level. Where possible, each stage of this analytical model is verified using empirical procedure. Finally the overall system is identified using time domain response procedures and recursive identification procedures. It is imperative that the models at this stage in the design are reasonably accurate. Although the controller design is in itself robust, the model at this stage will represent the nominal model in the final design. From an optimality and efficiency point of view this nominal design should be as close to the actual physical system as possible. Hence, where possible, each parameter is double checked and cross checked using other empirical and analytical techniques.

The open loop system under investigation can be described by Figure **[4-1]**. This describes the entire open loop system from the DSP output, to the DSP input. Some of the intermediate elements are approximated by gains. The bandwidth of the post-sampling and anti-aliasing filters are selected such that their gains and phase roll-offs are well outside the frequency of interest during control, consequently they can be neglected during the design. Equation **[4-1]** describes this open loop system. In order to successfully design a controller the parameters and components given in equation **[4-1]** must be identified.

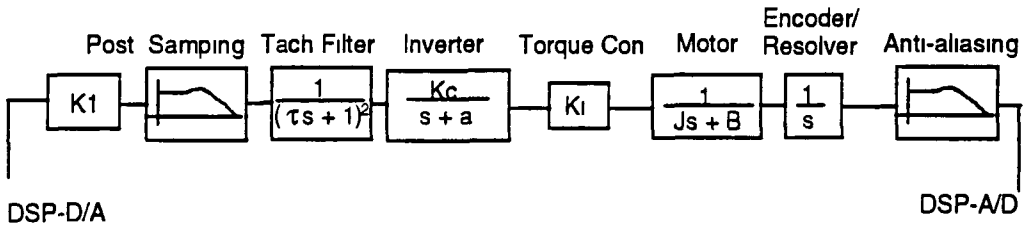

Fig. [4-1] Open Loop System.

$$\frac{DSP-A/D}{DSP-D/A}=\frac{\theta}{Command}=K_1\frac{1}{(\tau_1 s+1)^2}\frac{Kc}{s+a}\frac{K_t}{Js+B}\frac{1}{s} \qquad \textbf{[4-1]}$$

The Tachogenerator filter component of the open loop system is available from the analytical modelling of the open loop system described in Appendix A.

The motor model component of equation **[4-1]** can be described by equation **[4-2]**. The numerical values for this equation are available from the manufacturer of the motor. Table **[4-1]** summarises this information

$$\frac{\omega}{Current}=\frac{K_t}{Js+B} \qquad \textbf{[4-2]}$$

Parameter	Sym	Units	Value
Motor inertia	J	Nm	0.0014
Viscous damping	B	Nm/rad	0 0007163
Torque sensitivity	Kı	Nm/Amp	0.506

Table [4-1] Basic Motor-Tachometer Constants from Data Sheet

The open loop system described by equation **[4-1]** can be simplified by approximating the current amplifier to a gain K2 The system can be further simplified by replacing the Tachogenerator filter with a unity gain. With these simplifications the open loop system can be described by a second order approximation given by equation **[4-3]**. A numerical approximation can be found by using empirical measurements of the gains. Table **[4-2]** contains these empirically derived gains

Parameter	Sym	Units	Value
Inverter Command to current	K2	Amp/Volt	10
DSP (A/D) to Inverter Command.	K1	Volt/Float	10

Table [4-2] Empirical gains, average of several measurements.

$$\frac{\theta}{Command} = K_1 K_2 \frac{K_i}{Js+B}\frac{1}{s} \qquad \textbf{[4-3]}$$

This model is a second order approximation of the plant under investigation. It is however very much a simplification, insofar as the dynamics of the current amplifier are assumed to be outside the bandwidth[12] of the desired closed loop system. Thus the current loop is approximated by a gain K2. Furthermore, the mechanical constants for the motor are based on the data sheet values. The gains are based on the average of several measurements.

In order to arrive at a better model of the open loop system two approaches are followed. Firstly develop an analytical model of existing controller to determine the gain and dynamics of the current controller and secondly identify the motor and current controller using off-line identification techniques. These results are further confirmed using empirical time domain response analysis.

The following sub-sections describes the identification of the current amplifier and mechanical motor model in turn.

4.1.1 The Current Amplifier.

The analytical modelling of the current amplifier component of the open loop system can be found in Appendix A. From the appendix it is apparent that the current amplifier has fourth order dynamics. The loop can however be approximated to a

---

[12] At this stage in the design the actual bandwidth of the closed loop system is not defined. Thus the elimination of a dynamic component from the open loop system is only possible if the designer can choose the dynamics of this component. In this particular case the designer chooses to work with the existing current loop design. The dynamics of the current loop are thus fixed parameters. It will become evident in subsequent sections that these current loop dynamics are the limiting factors in the choice of the bandwidth of the closed loop system.

second order system by using pole zero cancellation. Equation [A-3] describes this second order approximation. Figure [4-2] shows a plot of the fourth order and the second order approximation of the current loop. As can be seen from the figure the second order approximation retains all the necessary dynamic properties of the current loop, the apparent discrepancy in steady state gains is a consequence of cancelling a slow pole corresponding to the mechanical motor dynamics. Although not apparent from the figure, both plots converge to a steady state value of 10 as time approached infinity (and the motor reached its terminal velocity). Thus the steady state gains of the two systems are the same. The second order approximation is really an approximation of the current loop in the absence of the mechanical dynamics of the motor. By neglecting these dynamics the current amplifier model is only thoroughly valid for low to moderate speed ranges. For higher speed ranges the use of a third order model which contains the mechanical dynamics of the system should be considered. At this stage in the design it is the fast modes of the current amplifier that are of particular interest, as it is these modes which will define the limiting factors in the choice of the bandwidth for the closed loop system. From the figure it is further evident that the second order approximation does not account for finite phase delays inherent in the fourth order model.

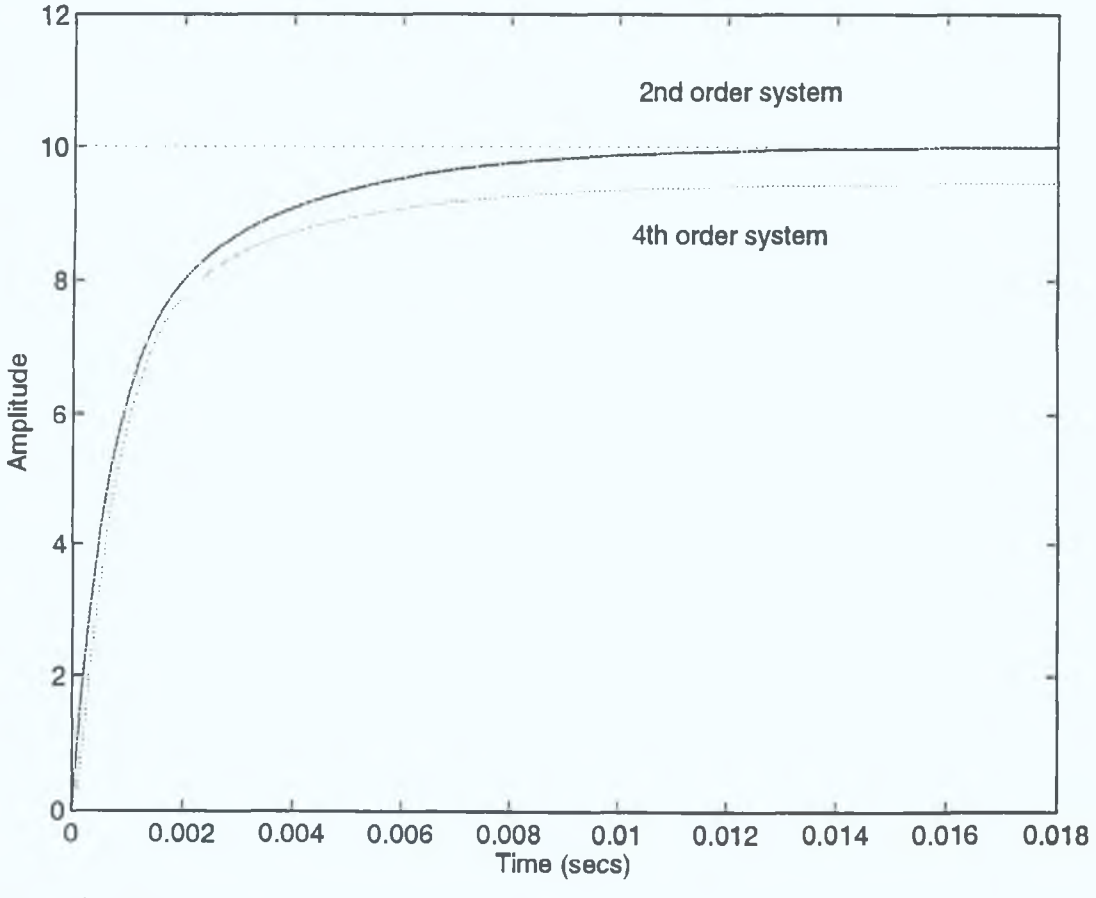

Fig. [4-2] Step response of current loop.

The theoretical model developed in the preceding section is only an accurate representation of the physical system if it truly represents the physical system. In this particular case the step response will be used as a basis for comparison. Figure **[4-3]** depicts several step responses of the physical system, for input voltages between the ranges of 0 to 10 Volts. From the figure several important observations can be made, the first of these is that the maximum current available from the current amplifier is 50 Amps, this occurs for a command voltage of 5V. Thus, although the input is between the range of ± 10V the current limiting circuits limit the effective input range to ± 5V. These ranges set the saturation bounds for the current amplifier. Furthermore the response of the physical amplifier closely approximates that of a first order system. This implies that the zero of the theoretical system is indeed faster in the physical system. The overall bandwidth of the physical system is however slower than its theoretical counterpart. Table **[4-3]** summarises the time domain characteristics of the physical and theoretical models. Figure **[4-4]** depicts the step response of the physical and the theoretical systems. From this figure it is apparent that the theoretical second order model is a reasonably accurate model for the physical system. Note that the theoretical response in this figure is driven by the measured input to the current loop, which in effect is the step response of the Tachogenerator and the anti-aliasing filters.

From the figure it is further evident that an unmodelled delay in the current loop exists. This delay is in the order of 0.3ms. It is not unreasonable to attribute this delay to switching delays inherent in the PWM and power circuits and indeed to approximations made during the modelling of the current loop as described. By accounting for this delay in the theoretical model an improved theoretical model is available. Figure **[4-5]** takes a closer loop at these delays. For a velocity controller implemented at a sample frequency of 5kHz, a delay of 0.2ms represents a one sample delay. If the Tachogenerator and anti-aliasing filters are omitted from the final design an additional one sample delay must be accounted for in the current loop model.

Model	Rise Time (ms)	Settling Time (ms)	Delay (ms)
Theoretical[13]	4	14	0
Physical	6	16	0.5 [14]

Table [4-3] Time domain specification.

[13] Driven by ideal step input

[14] 0.2ms of a delay attributed to the tachogenerator and anti-alaising filters phase delay.
0.3ms of a delay attributed to delays inherent in PWM.

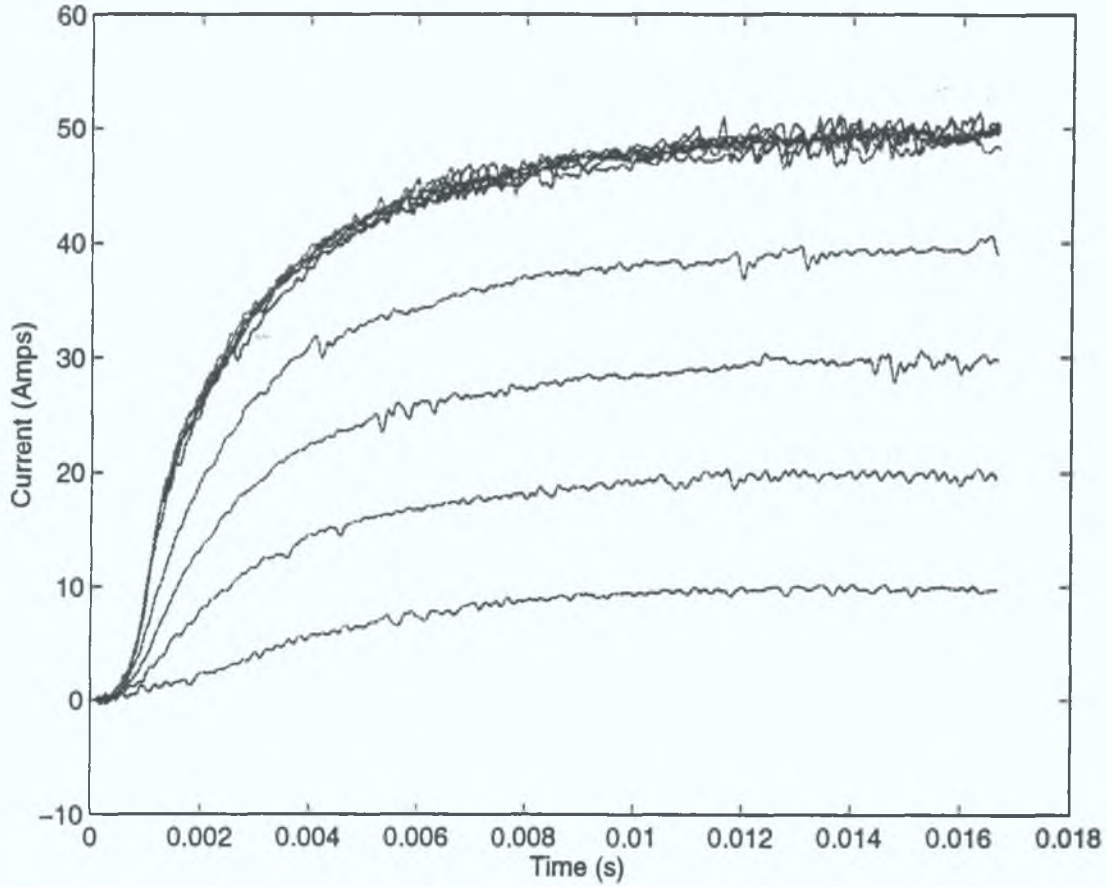

Fig. [4-3] Measured step response (commands in the range from 0-10V).

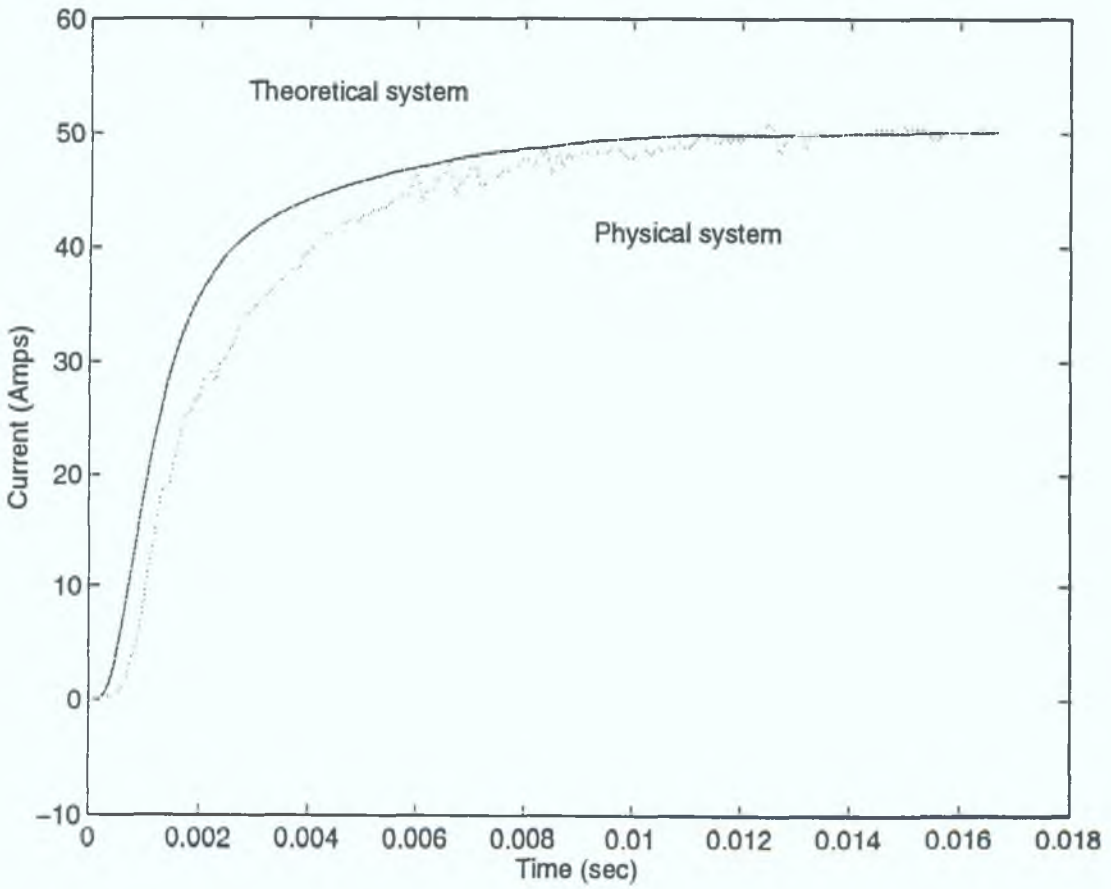

Fig. [4-4] Theoretical and Physical step responses.

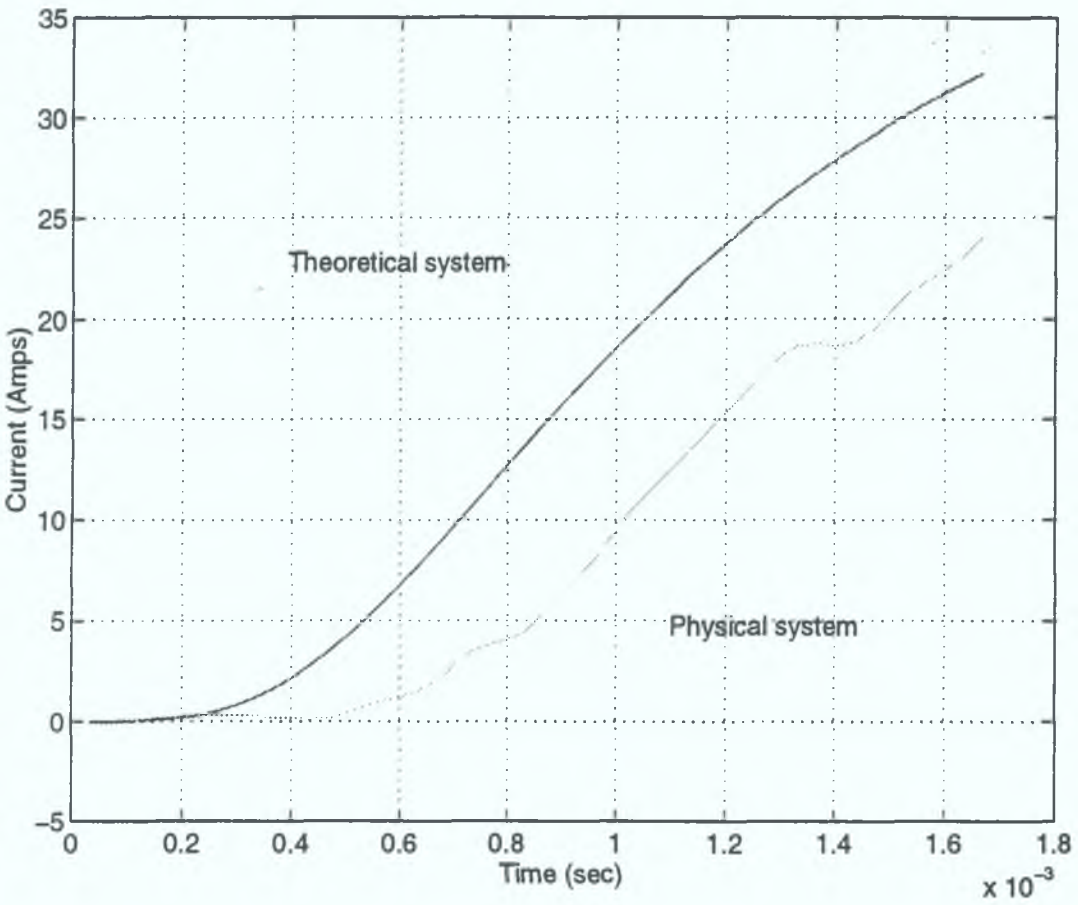

Fig. [4-5] Delays between theoretical and physical step responses.

4.1.1.1 Identification of the Current Amplifier

To resolve the bandwidth discrepancies between the theoretical and physical models, the system is identified using an off-line recursive identification algorithm. This identification is performed using the Matlab identification toolbox. From the preceding work the dynamics of the current loop can be accurately described by a second order system. The model used for identification purposes is a second order auto regressive model with a first order disturbance model, described by equation **[4-4]**.

$$\text{AR model} \quad A(z^{-1})y(t) = B(z^{-1})u(t) + \upsilon(t)$$
$$\text{MA model} \quad \upsilon(t) = C(z^{-1})e(t) \qquad \textbf{[4-4]}$$

$$\text{where} \quad A(z^{-1}) = 1 + a_1 z^{-1} + a_2 z^{-2}$$
$$B(z^{-1}) = b_1 z^{-1} + b_2 z^{-2}$$
$$C(z^{-1}) = 1 + c_1 z^{-1}$$

The general requirements on the choice of an excitation signal, for identification purposes, is that the signal have a zero mean and is constructed so that it excites all modes of the plant under investigation. To this end a staggered square wave excitation signal is chosen. Figure [4-7] depicts the excitation signal and the resulting current loop response. As is evident from the figure the current measurement has a low signal to noise ratio and the effective current resolution is only realistically 10 bits of information. This observation will aid the choice of measurement covariance in an estimation configuration which includes current feedback information. In particular, model based current information should be weighted more heavily than measurement based current information.

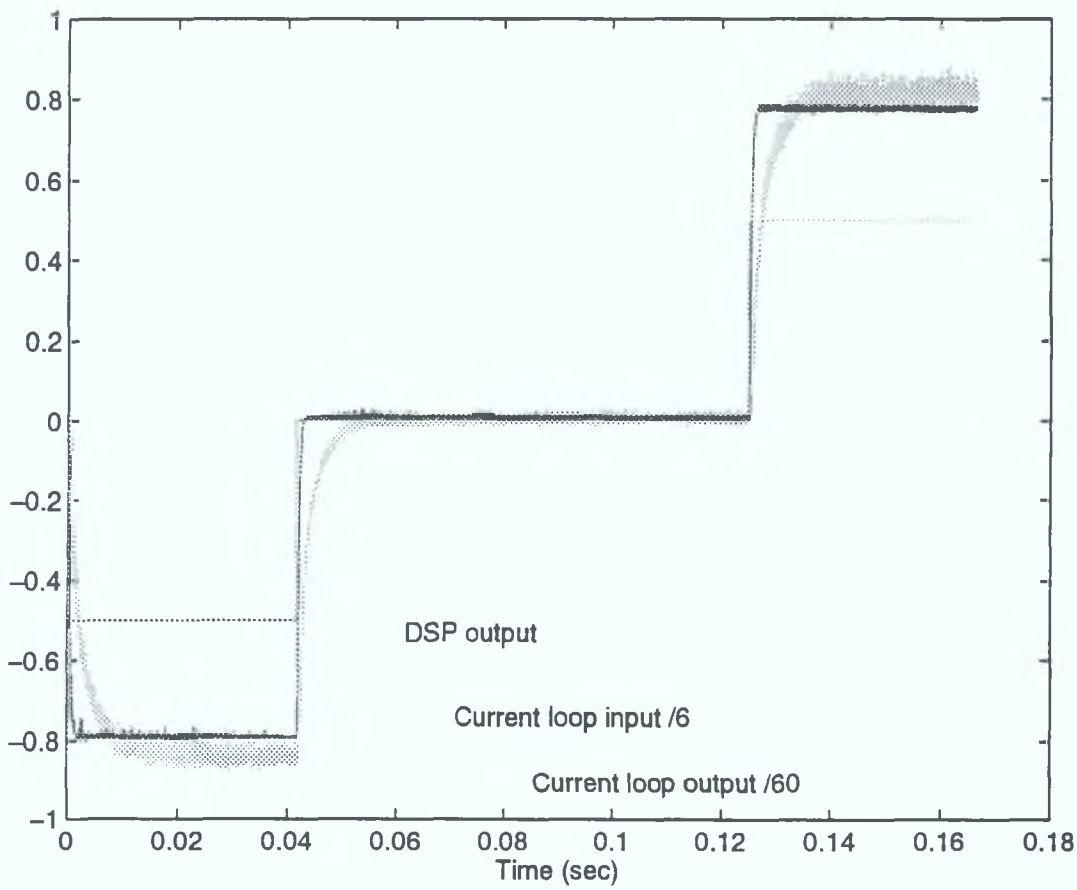

Fig. [4-6] Excitation signal and current loop response.

The identification of the current loop is broken up into two stages, the first of which involves the identification of a model for the actual current loop. The second stage involves the identification of the open loop system which consists of the cascaded combination of anti-aliasing filters. Tachogenerator filters and current loop. The latter model is a more realistic model for the purpose of control.

Equations [4-5] and [4-6] represent the results of the identification procedure. Both models are discrete time ARMAX models for a sample frequency of 30kHz. The corresponding continuous time poles and zeros are given in Table [4-4]. From the table it would appear that the relative spacing of the poles and zeros would agree with those for the theoretical model. However the zero of the cascaded system is in the right half plane, causing the step response to start off in the wrong direction. This discrepancy is an indication that the order of the model under identification is indeed greater than the model used for the identification. Indeed the Tachogenerator and antialiasing filters introduce an additional six poles into the model. The order of the model used for the identification can be increased to accommodate for the additional dynamics. The bandwidth of the antialiasing and Tachogenerator filters are parameters in the controller design and can be altered at the discretion of the designer. In general the bandwidth of these filters are chosen such that they are outside the bandwidth of the closed loop system. Figure [4-7] shows the step response of the identified current loop model. From this figure it is apparent that the identified model fits the physical response better then the theoretical model.

$$
\begin{aligned}
a_1' &= -0.9410, \sigma = 0.0160 \\
a_2' &= -0.0404, \sigma = 0.0157 \\
b_1' &= -0.3752, \sigma = 0.1064 \\
b_2' &= \ \ 0.1815, \sigma = 0.1083 \\
c_1' &= -0.8745, \sigma = 0.0072
\end{aligned}
\qquad \textbf{[4-5]}
$$

$$
\begin{aligned}
a_1' &= -0.9671, \sigma = 0.0160 \\
a_2' &= -0.0172, \sigma = 0.0158 \\
b_1' &= -15.556, \sigma = 0.6993 \\
b_2' &= 12.0860, \sigma = 0.7145 \\
c_1' &= -0.8665, \sigma = 0.0072
\end{aligned}
\qquad \textbf{[4-6]}
$$

Model	Poles	Zeros
Current loop	s=-9.5726e4	s=-23200
	s=-542	
Cascaded system	s=-1.2139e5	s=2740.9
	s=-470	

Table [4-4] Continuous time root locations.

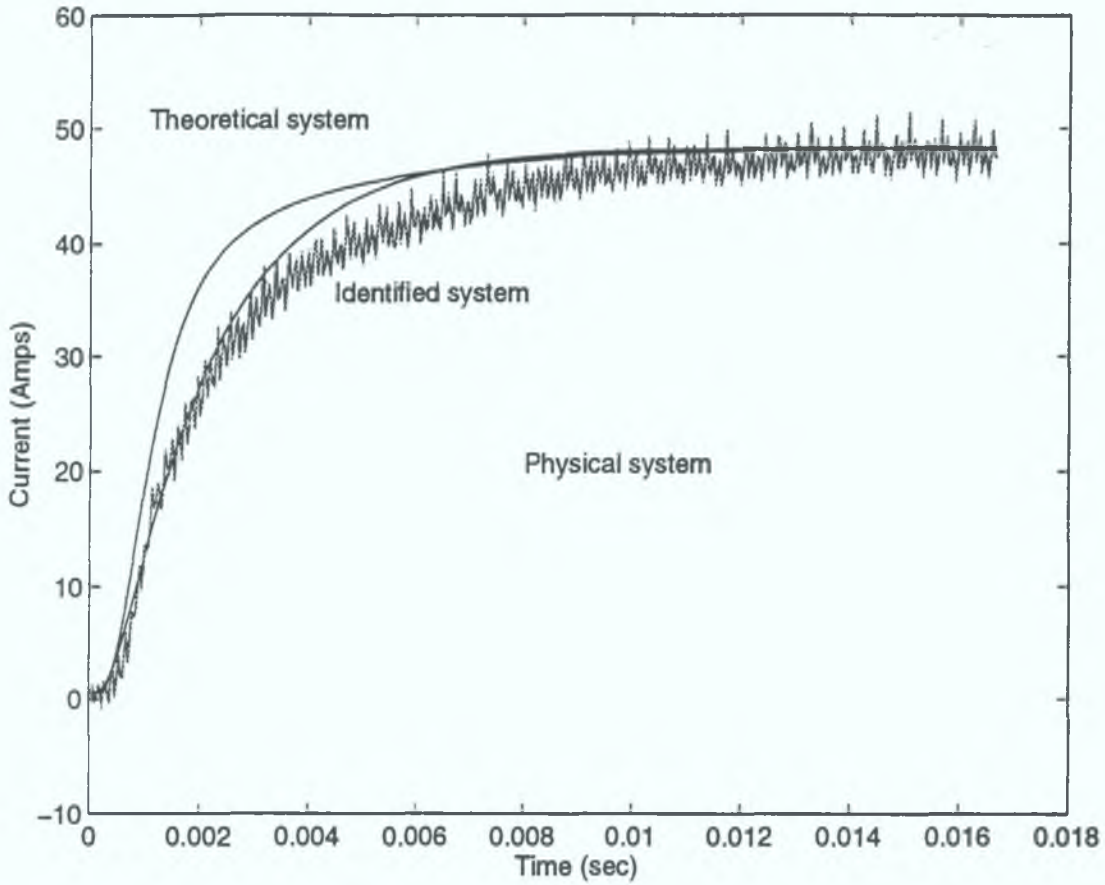

Fig. [4-7] Comparison of step responses.

Table **[4-5]** contains the DC gain values for the two identified models. These gains correspond to the unsaturated current amplified. When saturation takes place the input voltage to the current loop is limited and the effective torque command is reduced. The DC gain for the saturated amplifier is required for stability analysis, Table **[4-5]** also contains worst case saturation gains for the current amplifier. Figure **[4-8]** shows the current amplifier saturating after approximately three seconds of peak current. The saturated current corresponds to the rated continuous current rating of the amplifier.

Model	Sym	**DC-Gain**	**Saturated Gain**
Current loop	K2	10.38	5.19
Cascaded system	K2.K1	97.70	48.85

Table [4-5] DC gains of current amplifier.

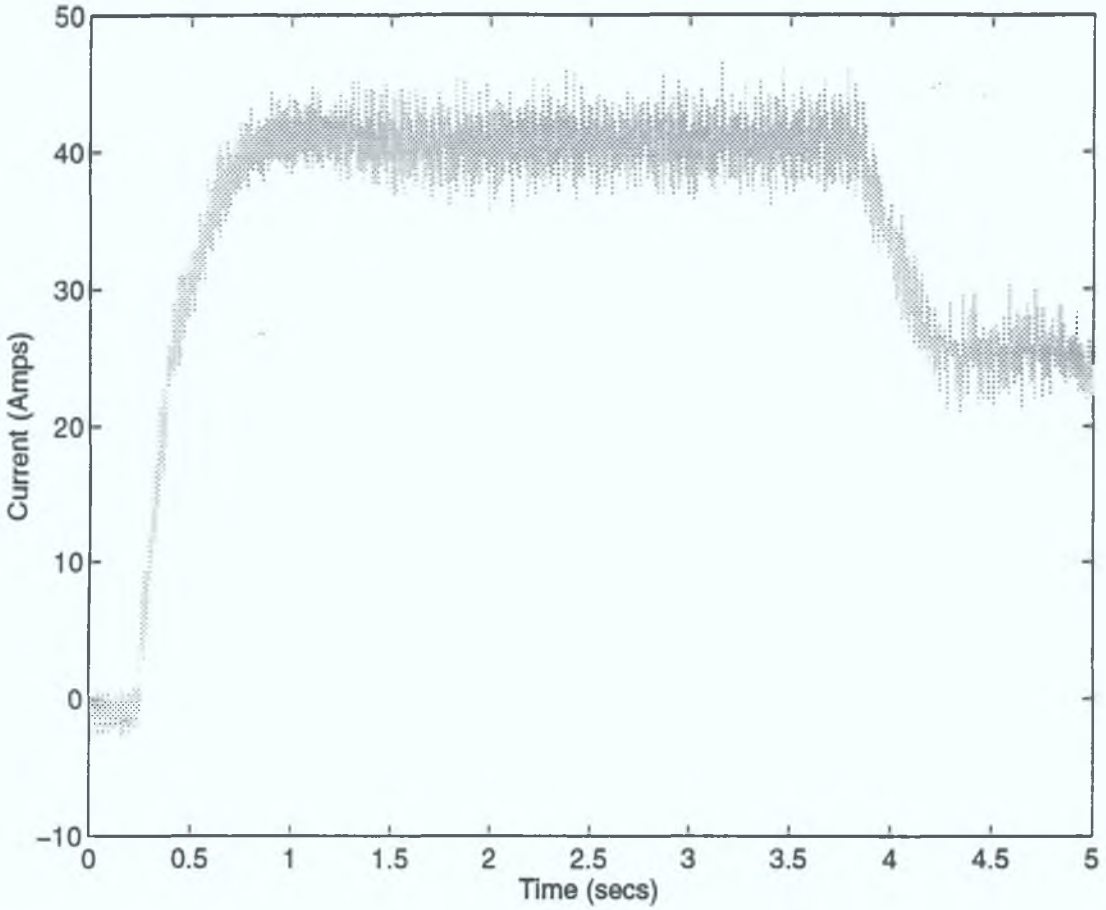

Fig. [4-8] Saturation of Current amplifier.

4.1.2 The DC Servo Motor

Identification of the motor model was performed using closed loop input-output data. Current and velocity measurements were chosen as the input-output data used during the identification of the motor model. Note that in this case the motor model is a transfer function from current to velocity and not from torque to velocity. To obtain the latter the torque constant is assumed to be known.

The choice of a perturbation signal has a large impact on the accuracy of the identified system. In order to successfully identify the models a suitable set of data is required. This data must excite all the modes of the system being identified. Again the most obvious choice is to use a square wave perturbation signal. This contains an infinite number of frequency components and hence in theory will excite all the required modes of the system. For the closed loop system a square wave perturbation signal is used. Several batch measurements were taken, for different amplitudes and frequencies of the perturbation signal. Each batch of sampled data was scaled, and a first order ARMAX model identified. An average for the parameter was then

obtained. It was found that the viscous damping parameter had the largest variation for the closed loop data. The viscous parameter is in general very small and often varies as a function of temperature. Instead this parameter was obtained using steady state analysis of the open-loop system. By disabling the over-speed protection and driving the motor to its terminal velocity, measurements of current combined with the electrical characteristics of the motor provide a reliable value for the cascaded viscous damping[15]. The average results for the identification are given in equation **[4-7]** and the corresponding continuous time equivalent model for the identified plant is given in equation **[4-8]**. Using the value for the torque constant specified in the data sheets, the motor model parameters can be specified see Table **[4-6]**. The identified mechanical parameters are the combined inertia and viscosity for the motor, its load and the coupling. The inertia parameters obtained from the identification are approximately twice the size of those obtained from the data sheets, this accounts for the two motors and the inertia of the coupling. The viscosity parameter is approximately equal to that obtained from the data sheets.

$$\begin{aligned} a_1' &= -0.999895, \sigma = 0.0001 \\ b_1' &= 0.0, \sigma = 0 \\ b_2' &= 0.0241, \sigma = 0.0003 \\ c_1' &= -0.4537, \sigma^2 = 0.0129 \end{aligned} \qquad \textbf{[4-7]}$$

$$\frac{\omega}{I_a} = \frac{100.17}{s + 0.2824} \qquad \textbf{[4-8]}$$

Parameter	Sym	Units	Value
Motor inertia	J	Nm	0.00505
Viscous damping	B	Nm/rad	0.001445

Table [4-6] Identified Motor and load parameters[16]

---

[15] $B = K_i\left(\frac{V_a - V_b}{R_a}\right)\Big/\omega = 0.506\left(\frac{1}{1.226}\right)/285.6 = 0.001445$

[16] Note that the data sheet parameter values correspond to the values for a single motor. The values presented here are for the identified motor and its load. In this case the load is an equivalent motor, so the parameter values for an individual motor are approximately half those given in this table.

4.2 Controller Design (Nominal system).

This section describes the design of a LQG/LTR velocity servo for the test rig featured in the previous section. This will represent the nominal design which will be used as a benchmark for subsequent designs. In this design the dynamics of the current amplifier are neglected during the controller design. These dynamics are modelled as structured uncertainties which will be used to establish stability bounds on this particular controller implementation.

Equation **[4-3]** describes a first order model for the system where the current amplifier is approximated by a gain. Numerical values for these gains are obtained from the results of the identification procedures, Table **[4-5]** contains these results. The motor parameters used for this design are those identified, the results for which are presented in Table **[4-6]**.

For this design example it is assumed that the availability of ample processing power is not an issue. Consequently implementation issues regarding the sample rate selection are ignored for now. A sample rate of 5kHz is chosen. This sample rate selection issue will be dealt with at a later stage.

Following the heuristic tuning procedures of section 3.1.1 a LQ controller can be designed. For this design Bryson's inverse square method of weighted matrices selection is used [Bryson 75]. The maximum allowable deviations for each of the states is thus required, Table **[4-7]** contains these deviation values. The cost weighting matrices parametrised by ρ are given in equation **[4-9]**. Using equations **[3-11]**, **[3-12]** and **[3-9]** a set of controller gains can be found for a given value of ρ. The value of ρ is increased until a satisfactory response is realised, in this case a satisfactory response shall be one with a settling time of approximately 60ms.

On examining the step response of the resulting controller design, based on Bryson's inverse square method, it is apparent that the controller exhibits a damped response. The target settling time cannot be realised without an excessive increase in ρ. However by increasing the maximum deviation on the velocity state in equation **[4-9]**, a less damped response can be obtained. This process in effect de-emphasises the velocity state during the controller design. Bounds on the extent to which these states can be de-emphasised will be established by example. Figure **[4-9]** depicts an impulse response for the modified controller weight matrices described by equation **[4-10]**.

This design corresponds to a design parameter $\rho = 800$. Table **[4-8]** summarises some of the properties of the resulting controller design.

State name	Units	Deviation (max.)	Mean Value
Position	Rads	$\pm\pi$	0
Velocity[17]	Rads/s	± 265	0
Current	Amps	± 50	0

Table [4-7] Max. Deviation values.

$$Q_1 = \begin{bmatrix} \rho/(265)^2 & 0 \\ 0 & \rho/\pi^2 \end{bmatrix} \qquad \textbf{[4-9]}$$

$$Q_2 = 1$$

$$Q_1 = \begin{bmatrix} \rho/(1000)^2 & 0 \\ 0 & \rho/\pi^2 \end{bmatrix} \qquad \textbf{[4-10]}$$

Property	Description	Values
ρ	LQ design parameter	800
γ	Anderson's Gamma	0.9510
Roots	Discrete time LQ roots	$z = 0.9684 \pm 0.0306i$
Ts	Settling time	64 ms

Table [4-8] Summary of LQ controller properties (under-damped).

The gamma parameter for this controller design is very close to unity, which is a consequence of the choice of a high sample frequency. Recall the sample frequency trade-off of section 3.2.1.1. With a gamma value close to unity, the advantages of the Kalman-Smoother implementation over the Kalman Predictor-corrector implementation become insignificant. For this reason the Kalman Predictor-corrector form will be used for this LQG controller implementation.

During the design of a Kalman filter, plant and measurement noise covariance information is required. This stochastic information specifies the bandwidth of the Kalman filter in the classical sense. When the Kalman filter is used as a Kalman

[17] The deviation on the velocity state is based on measurements from the test rig.

estimator this stochastic specification becomes less significant. Although in most cases the estimator still has a filtering role to perform, this role is surpassed by the estimator's need for a wide bandwidth, in the classical sense. Thus the Kalman filters noise covariance's often forms the basis for a nominal Kalman estimator design. As seen in section 3.3.3, the bandwidth of the Kalman estimator is often widened by injecting additional fictitious noise covariance's into the design model, in which case one could argue that the estimator's noise covariances bears no similarities to the physical system's noise covariance.

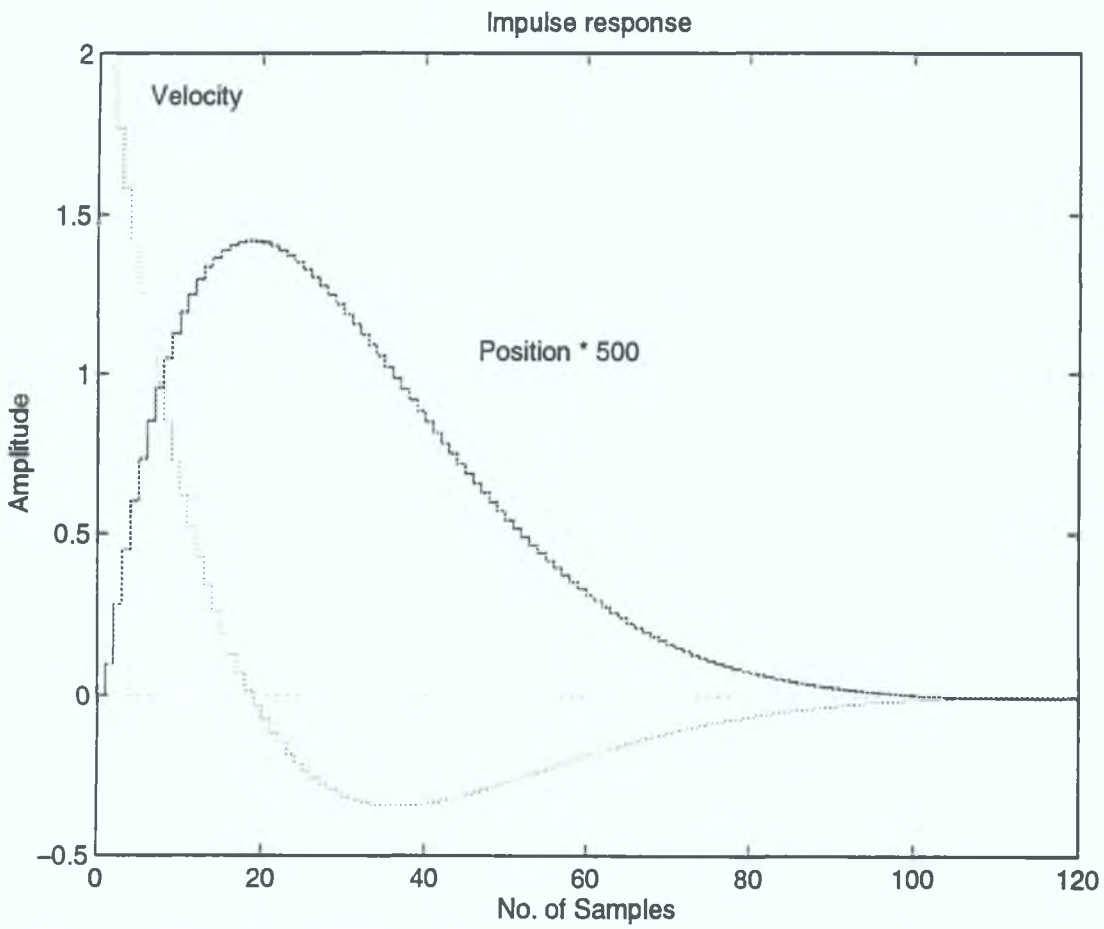

Fig. [4-9] Impulse response of LQ controller.

Equation **[4-11]** describes the nominal covariance matrices used in this design. The magnitude of these covariances have no bearing on the physical model. The bandwidth of the estimator will be set during the LTR procedure, equation **[4-12]** contains the recovery parameters used. Figure **[4-10]** shown the Nyquist plot for the LQG compensator as the recovery procedure unfolds, Figure **[4-11]** shows the corresponding sensitivity and complementary sensitivity functions. From these two figures robustness and performance information can be obtained. Table **[4-9]** summarises this performance information.

$$Q_n = \begin{Bmatrix} 1 & 0 \\ 0 & 0 \end{Bmatrix} \quad \text{[4-11]}$$

$$R_n = 1$$

$$q_k = [100 \quad 10000 \quad 100000 \quad 10000000] \quad \text{[4-12]}$$

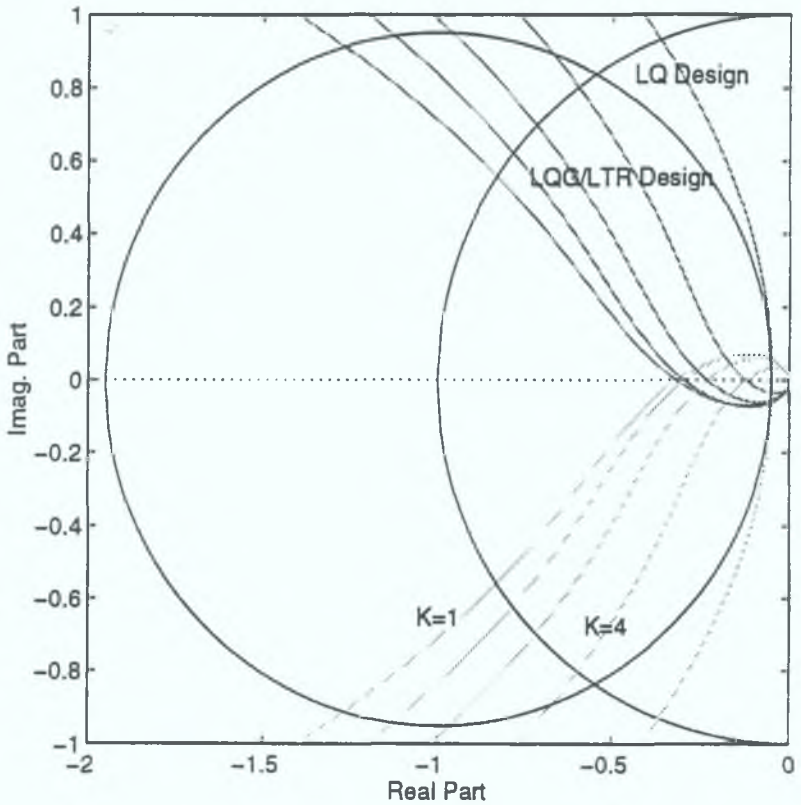

Fig. [4-10] Nyquist plot as recovery unfolds.

LTR Iteration (k)	1	2	3	4
Est. Root Location[18]	0.968±0.0307i	0.900±0.090i	0.8236±.148i	0.4082±0.292i
Normalised Cost	1.1785	1.1745	1.1675	1.1585
Gain Margin	9.82 dB	10.5 dB	12.7 dB	18.0 dB
Phase Margin	34.0°	38.4°	44.0°	53.2°
Distur. Atten. @ P1[19]	-43 dB	-51.8 dB	-54.0 dB	-58.8 dB
Noise Suppr. @ P2[20]	-53.8 dB	-37.9 dB	-29.4 dB	-19.6 dB

Table [4-9] Performance results for LQG(DK-Predictor-corrector)/LTR.

[18] These are the discrete time root locations.

[19] The test point P1 corresponds to a disturbance frequency of 10Hz.

[20] The test point P2 corresponds to a noise frequency of 3kHz.

From the table it is apparent that robustness is at its lowest when the roots of the estimator are the same as the roots of the LQ controller. As recovery takes place the robustness of the design improves. However the noise suppression properties of the design disimproves. The Kalman filter becomes more of an estimator and less of a filter as recovery takes place. This is a fundamental trade-off in the design of a LQG controller. The greater the robustness requirement of the design the greater the corresponding signal to noise requirement of the sensors.

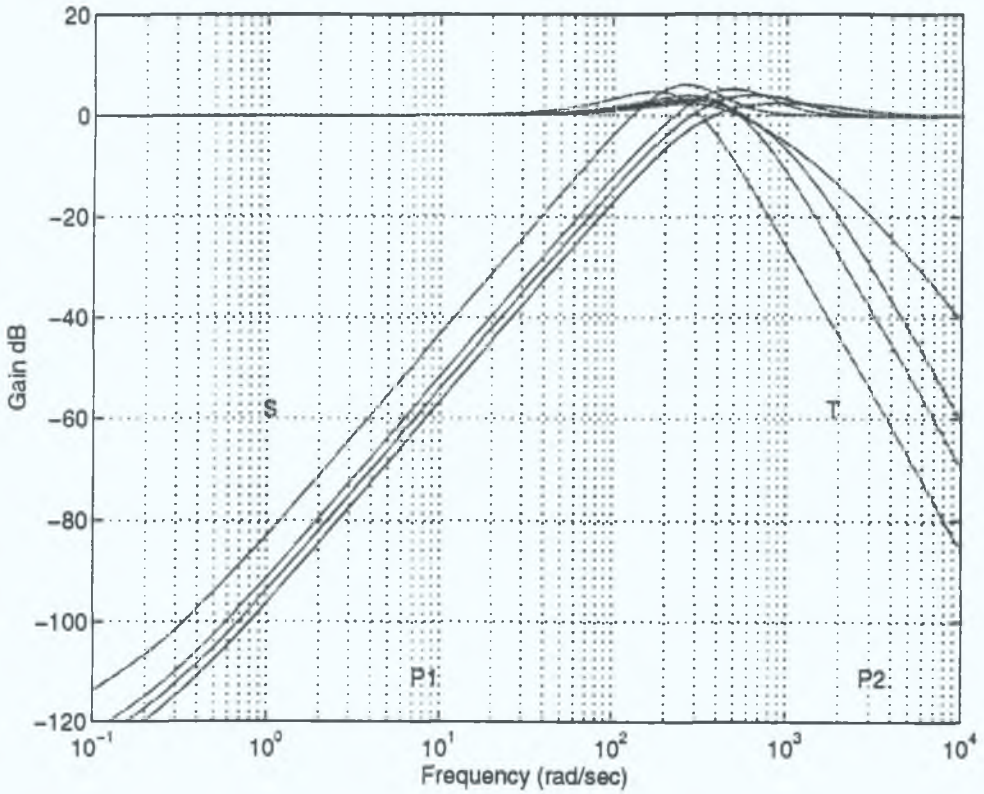

Fig. [4-11] Delta plot as recovery unfolds.

The next stage in the design is to establish stability bounds on the robustness of the design to model uncertainty. The controller designed in this section is a nominal design based on a nominal plant model. In reality the physical model will deviate from this nominal model. For example, in an application such as a servo system the dynamic properties of the load can vary for different servo states. In this section allowable bounds on these variations are established.

From the identification of the plant, important non-linear properties of the plant were observed. In particular, the saturation of the current amplifier halves the forward gain of the open loop system. It will be necessary to establish stability bounds for such an event. Furthermore this design neglects the dynamics of the current amplifier. At what stage in the design will such an approximation affect the stability of the closed

system? To address these problems, the stability bounds procedure established in section 3.2.3 will be applied. In all, stability bounds for four uncertainties need to be established, namely variation an load inertia, variation in load viscosity, saturation of the current amplifier and the unmodelled dynamics of the current amplifier. In a practical situation the bounds on these variations are often part of the design specification. In particular, Table **[4-10]** specifies bounds on the load dynamic parameters for this design example.

Parameter	Min.	Max.
J_L	0	$3J_n$
B_L	0	$3B_n$

Table [4-10] Load dynamic bounds specification.[21]

Each of the uncertainties can be modelled as a multiplicative structured uncertainty, from which a bounding function can be derived using equation **[3-36]**. Stability is preserved when the complementary sensitivity function and the multiplicative uncertainty bounding function satisfy condition **[3-41]**. In the case of the unmodelled current amplifier dynamics, the identified model for the current loop is used. This model bounds all the other current loop models. The multiplicative uncertainty model for the current loop dynamics is given by equation **[4-13]**, this is the cascaded combination of the current loop dynamics and the nominal plant model. The multiplicative bounds for this model can be calculated using the Matlab function 'perbou.m' given in Appendix B. The resulting multiplicative uncertainty bounding model is not reproduced here.

$$P_m = \frac{-2.323e4s - 5.3912e8}{s^2 + 9.6268e4s + 5.177e7} \cdot \frac{K}{Js + B} \qquad \textbf{[4-13]}$$

The multiplicative uncertainty model and corresponding multiplicative uncertainty bounding model for a variation in load viscosity is given in equation **[4-14]**. These models are parametrised as a function of Δ. The corresponding models for variations in load inertia and amplifier gain are given in equations **[4-15]** and **[4-16]** respectively.

$$P_m = \frac{K}{Js + \Delta B} \quad , \qquad L_{\Delta B} = \frac{(1-\Delta)B}{Js + \Delta B} \qquad \textbf{[4-14]}$$

[21] The subscript 'n' stands for nominal. The nominal inertia is the nominal load inertia plus the nominal motor inertia

$$P_m = \frac{K}{\Delta Js + B} \quad , \qquad L_{\Delta J}(s) = \frac{(1-\Delta)Js}{\Delta Js + B} \qquad \textbf{[4-15]}$$

$$P_m = \frac{\Delta K}{Js + B} \quad , \qquad L_{\Delta K}(s) = \Delta - 1 \qquad \textbf{[4-16]}$$

Figure **[4-12]** shows frequency plots for the complementary sensitivity functions at each stage of the LTR procedure and the reciprocal of each of the multiplicative uncertainty bounding models for each uncertainty. Table **[4-11]** contains the legend for this figure. From the figure it can be seen that stability condition **[3-41]** fails, recall from section 3.2.3 that stability fails if the complementary sensitivity function is above[22] the reciprocal of a multiplicative uncertainty bounding. This condition fails on the first and second LTR iteration for a structured variation in load inertia (L3). Failure also occurs for all LTR iterations when all the structured variations events occur at once (L5).

Failure in each case occurs at the peak frequency of the complementary sensitivity functions. The magnitude of the overshoot can be controlled by selecting a more damped LQ controller design. Indeed the LQG design is at best only as good as the LQ design. Thus the LQ design must first satisfy the stability bounds outlined above. Figure **[4-13]** contains the complementary sensitivity functions for the original inverse square design and the less damped inverse square LQ design. From the figure it is apparent that the original inverse square design satisfies the stability bound specifications. This design, on the other hand, fails to satisfy the settling time specification. A controller between these two design could meet the stability specifications and minimise the settling time of the design.

As the bandwidth of the LQ controller is widened the complementary sensitivity function will advance in frequency. This advance is constrained or bounded by the multiplicative uncertainty bounds attributed to the current amplifier dynamics. This bound sets the maximum available bandwidth for the closed loop system.

Using these techniques the designer is presented graphically with all the necessary information to make an informed decision about the choice of estimator and controller designs. In many cases the designer may be forced to relax the design specifications.

---

[22] The word above is used as a graphical interpertation of the condition $|A| > |B|$.

For example the specified settling time can't be realised for the given load variation specification. However the settling time can be realised if the specified variations in load parameters are no more than twice the nominal load parameters. Alternatively relaxing the settling time specification would insure a design which meets the load specifications

Relaxing the design specifications for the load may seem like a senseless design strategy however in a real system if the variation on load parameters are in the order of three times the nominal plant values, perhaps it is the motor specifications that should be reviewed. This would have a knock on effect reducing the controller design specifications. The performance of the resulting controller would not be sacrificed to meet the unrealistic load specifications

Figure [4-14] shows that stability bounds are satisfied for the third and fourth stage of the LTR procedure for the damped LQ design, however the settling time requirements is not realised m this design

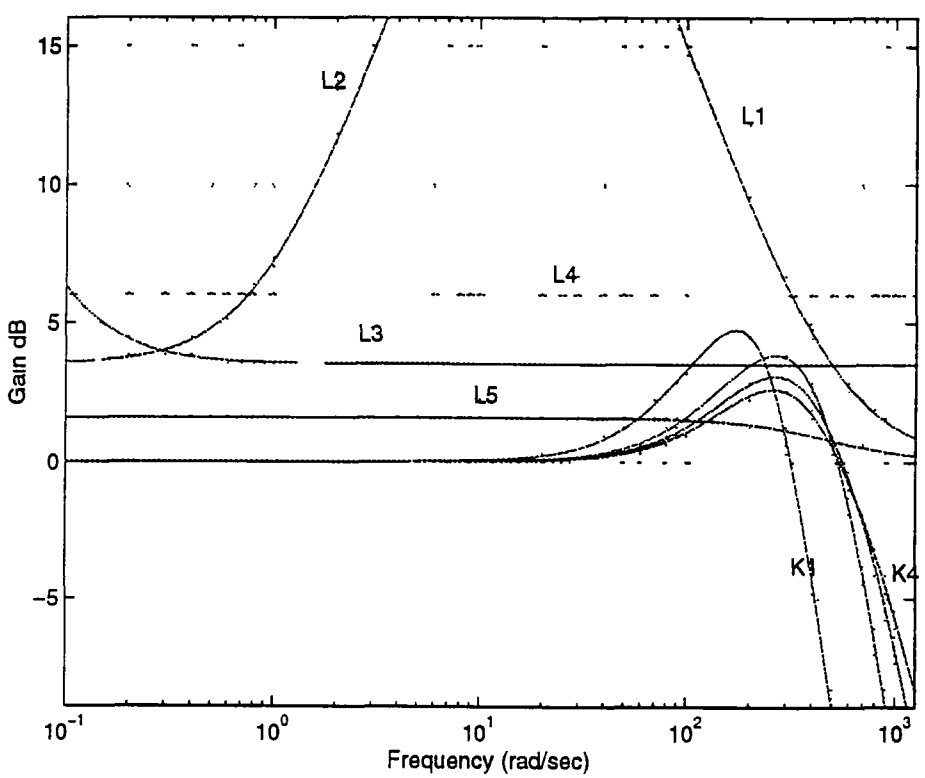

Fig. [4-12] Stability Bounds LQG designs. (under-damped).

Label	Description	Δ
L1	Multiplicative uncertainty current amplifier.	
L2	Multiplicative uncertainty load viscosity.	3
L3	Multiplicative uncertainty load inertia.	3
L4	Multiplicative uncertainty saturation gain.	0.5
L5	All multiplicative uncertainties	
L6	Multiplicative uncertainty Tachogenerator filters	
LQ1	Inverse square method (damped)	
LQ2	Inverse square method (under-damped)	
K(1 to 4)	Complementary sensitivity function for each LTR iteration.	

Table [4-11] Legend for Figure [4-12], [4-13] and [4-14].

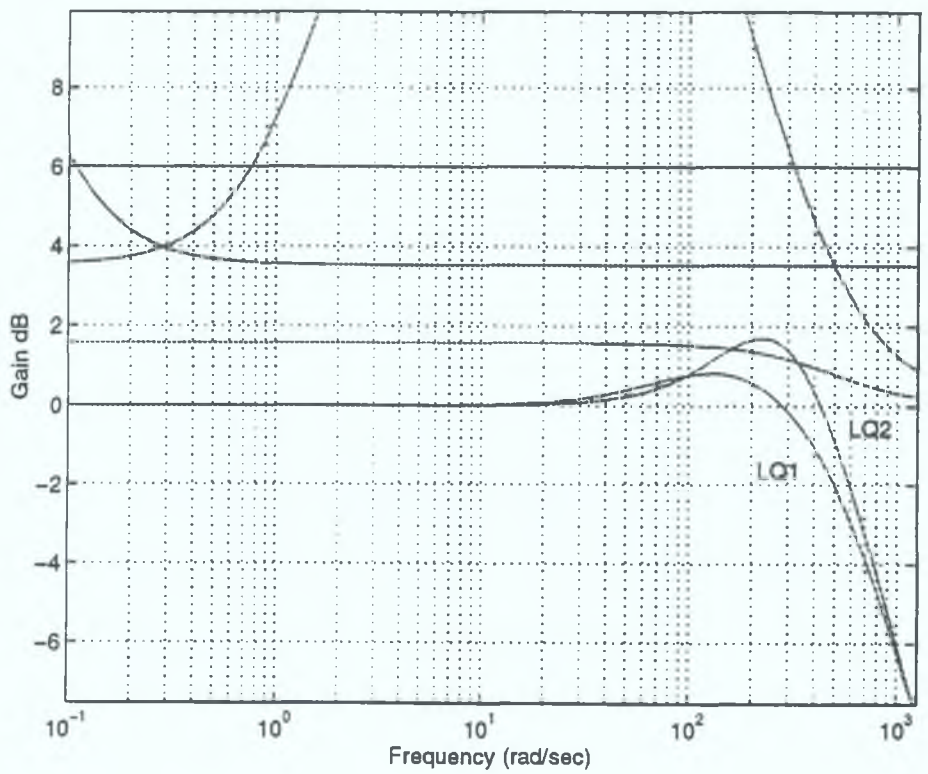

Fig. [4-13] Stability Bounds LQ designs.

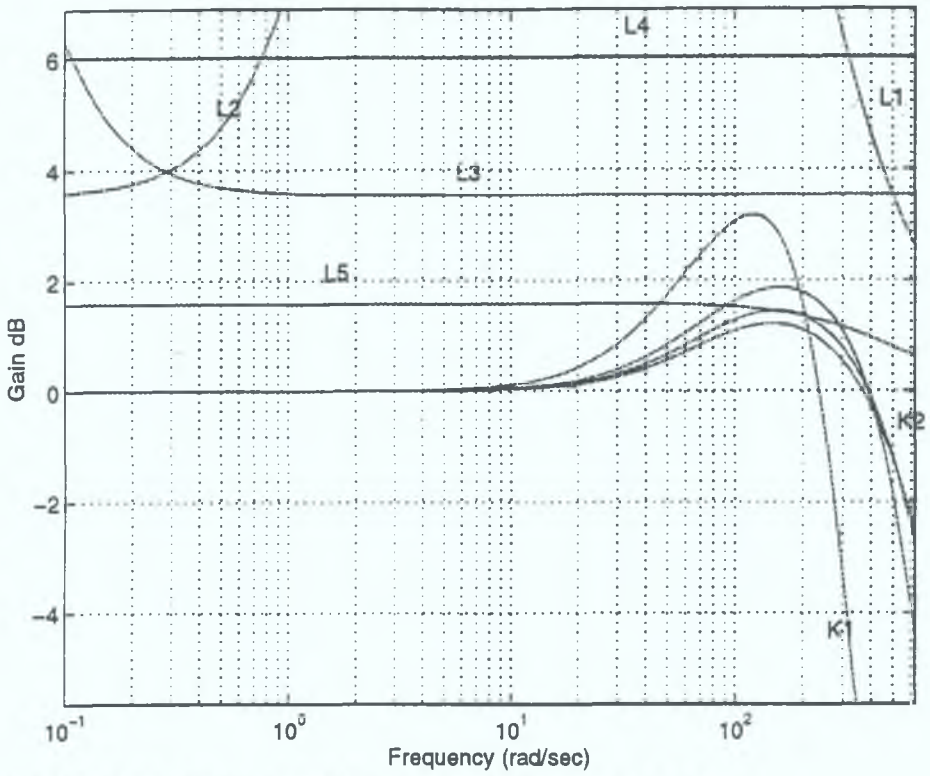

Fig. [4-14] Stability Bound LQG designs (damped design).

4.3 Noise Attenuation and Disturbance Suppression .

In the previous example a concise systematic procedure is applied in the design of a LQG/LTR controller. The design procedure should result in an optimal controller which satisfies the robustness constraints of the design specification. As a general rule when these two criteria conflict, robustness will hold precedence over optimality. Once the robustness and optimality issues have been resolved, the disturbance suppression and noise attenuation issues then hold precedence. The precedence of the latter issues depends on the particular application. If the design fails to resolve these issues, the structure of the controller and/or design specifications should be reviewed.

In this section, variations on the controller structure will be examined with particular attention towards the disturbance suppression and noise attenuation issues.

In section 3.3.3.3 the use of a frequency shaped recovery procedure is adopted. An important property of this procedure is the increased roll-off rate of the resulting compensator. Thus the FS-LTR procedure provides superior noise attenuation for frequencies above the cut-off frequency of the frequency shaping filter. Furthermore the FS-LTR procedure injects fictitious noise at the frequencies where recovery is required. Thus the cut-off frequency of the estimator is often reduced allowing the superior roll-off rates of the LQG compensator to occur at a lower frequency. This in turn further enhances the noise attenuation properties of the resulting compensator design.

In section 3.3.3.4, the use of frequency shaped LQG design, in particular proportional plus integral frequency shaping was introduced to provide improved disturbance suppression. In this section this procedure will be applied to the nominal design to enhance the suppression properties of the design.

In this design the LTR procedure is implicitly used. Two designs are considered, a LQG controller with proportional plus integral frequency shaping (PI-LQG) and a LQG controller with disturbance feedforward (DE-LQG). In each case a new design parameter is introduced into the design.

In the PI-LQG design an additional cost-index weight is introduced to the cost function, this weight sets the cost of the integral state during the LQ design. The design procedure for the selection of this free design parameter is to increase the

parameter until the integral state makes an equal contribution to the overall cost. In practice, as the controller design parameter ρ is increased the response time of the LQ design should increase, however the relative response characteristics should remain the same. This design parameter will determine the speed at which a disturbance is suppressed. Normally in servo applications, the disturbance suppression time should be at a minimum. In general the robustness bounds will set a limit on this parameter, thus limiting the disturbance suppression performance of the controller. By altering the remaining cost-index weights a compromise can often be reached.

In the DE-LQG design a similar free parameter exists for the estimator design. This parameter is the variance of the white noise driving the bias estimate. Again the amplitude of this parameter is increased until a satisfactory response is obtained. The size of this parameter will determine the speed at which a disturbance is suppressed. Again the choice of this parameter is governed by the stability bounds.

For the purpose of comparison between designs a model for the system excited by a disturbance is required. In this case a disturbance is assumed to be entering the system at the input to the plant. Figure **[3-25]** depicts this situation. A model from disturbance to plant output can be described by equation **[4-17]**, where ABCD describes the compensator and ΦΓH describes the plant.

$$\hat{x}_{k+1} = \begin{bmatrix} A & BH \\ -\Gamma C & \Phi - \Gamma DH \end{bmatrix} \hat{x}_k + \begin{bmatrix} BH \\ -\Gamma DH \end{bmatrix} y_r + \begin{bmatrix} 0 \\ \Gamma \end{bmatrix} \omega_k \qquad \textbf{[4-17]}$$
$$u_k = \begin{bmatrix} 0 & H \end{bmatrix} \hat{x}_k$$

From the results of section 3.2.3 it is known that for good disturbance suppression the singular value of the sensitivity function must be small for a given disturbance frequency. This property will be used for comparison of different implementations. From the section on controller loop recovery it is apparent that the disturbance attenuation properties of the design improve as the bandwidth of the controller is widened. This improvement can be seen through the migration of the sensitivity function forward in frequency. Figure **[4-15]** contains the sensitivity and complementary sensitivity functions for the LQG, PI-LQG and DE-LQG implementations. From the figure it is apparent that the PI-LQG and DE-LQG designs offer superior disturbance rejection properties.

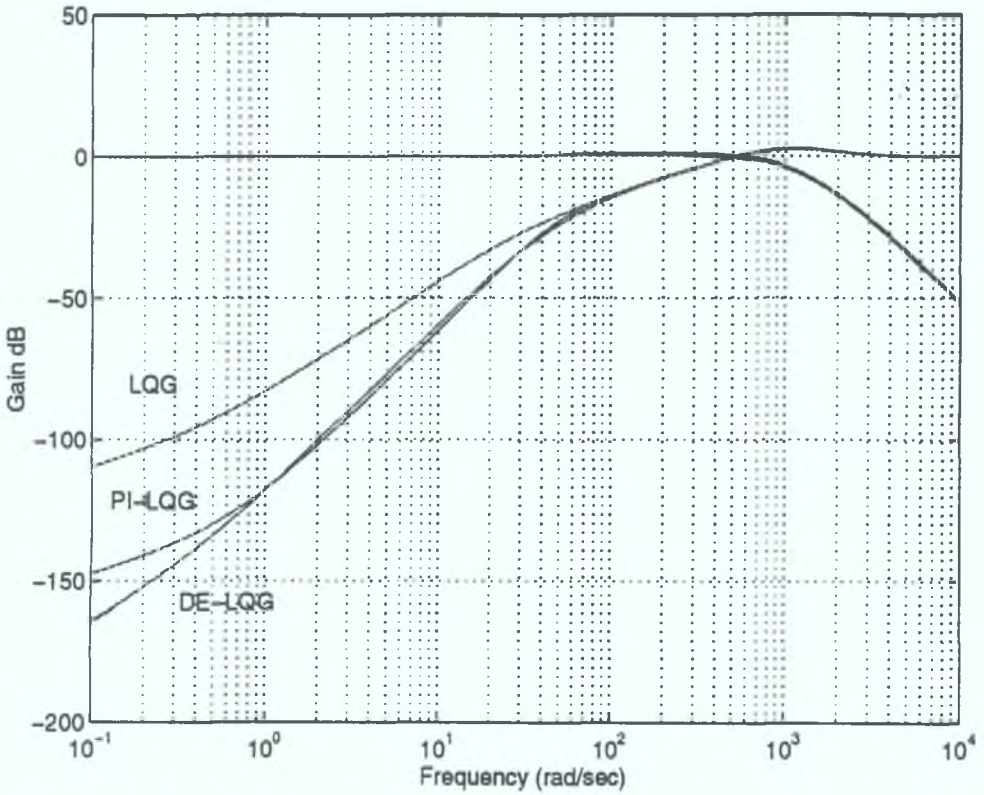

Fig. [4-15] Sensitivity plots for LQG, PI-LQG & DE-LQG designs.

The corresponding stability bound plot for the system is given in Figure **[4-16]**, here only the worst case bound is presented (L5). Note that the PI-LQG and DE-LQG designs are equivalent insofar as each design can perform as well as the other given a suitable choice of the design parameters. Figure **[4-16]** shows how these design parameters are bounded by a worst case multiplicative uncertainty[23]. If the free design parameters are further increased the stability condition will fail. Thus the disturbance suppression response time is set by these stability bounds. Figure **[4-17]** shows the corresponding disturbance response for each design. A disturbance suppression response time of approximately 160ms can be realised with the DE-LQG and PI-LQG designs. Figure **[4-18]** depicts the Nyquist plots for these designs.

[23] In this implementation the load variation specifications are relaxed. A Δ=2 is used in the multiplicative uncertainty specifications.

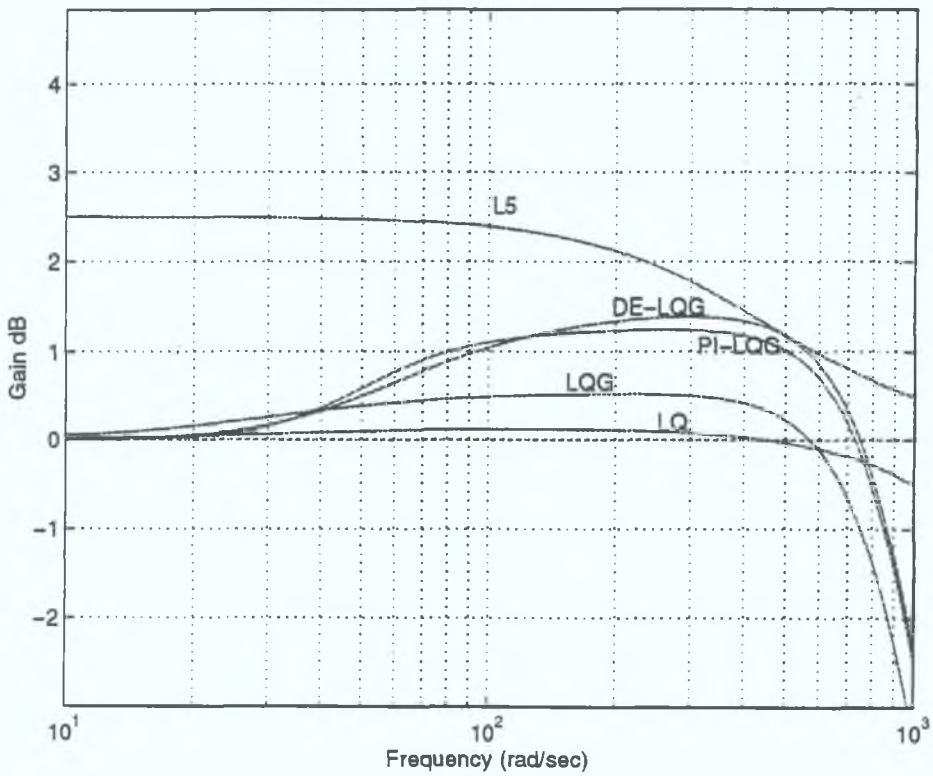

Fig. [4-16] Stability Bounds 5kHz.

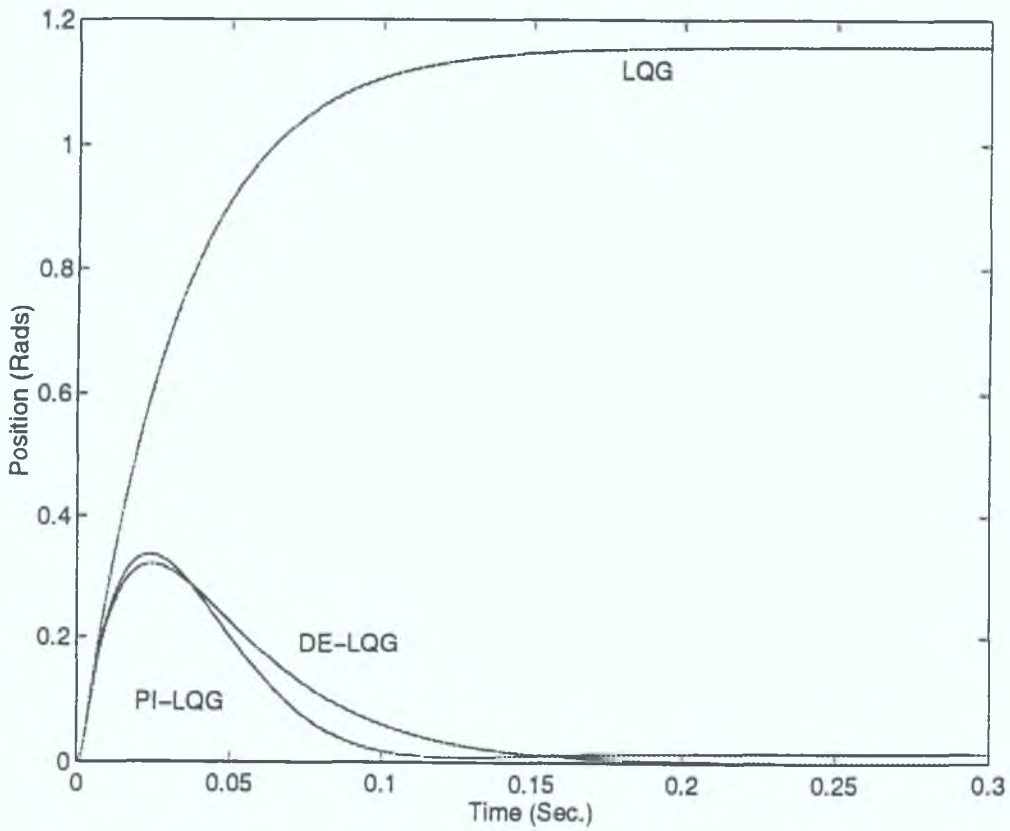

Fig. [4-17] Disturbance response.

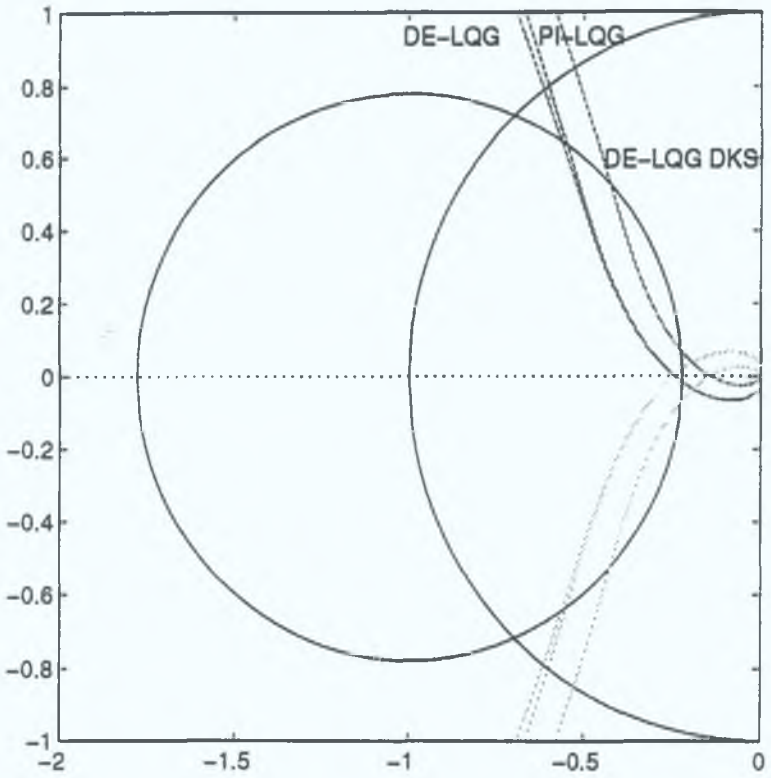

Fig. [4-18] Nyquist plots.

Table **[4-12]** summarises the design parameters and Table **[4-13]** summarises the performance properties of the resulting designs. From the design parameters it is apparent that the gamma value for the controller design is relatively small. Recall the results established in section 3.2.1.1, the gamma value can be used to establish a suitable choice of sample frequency for a given choice of bandwidth. Thus if there is ample processing resources available, the designer has the option to increase the sample frequency and avail of the improved robustness margins. Figure **[4-19]** shows the complementary sensitivity functions bounded by the worst case stability bound for a sample frequency of 20kHz. Observe that the margins between stability and instability have increased. This increase can be exploited by increasing the free design parameter in the PI-LQG or DE-LQG designs, thus improving the disturbance suppression response time of the designs. Table **[4-14]** contains the performance results for the increased sample frequency.

Alternatively, the designer may choose to use this increased stability margin to reduce the bandwidth of the estimator, thus improving the noise attenuation properties of the design. Recall that as the bandwidth of the estimator is reduced, the robustness of the LQG design is reduced. This reduction in robustness manifests itself with increased overshoot in the complementary sensitivity function. Table **[4-15]** contains the performance results for an estimator design parameter, $\rho_e = 200$.

Parameter	Description	Value
1/T	Sample frequency	5000 Hz
γ	Gamma	0 7786
ρ_c	Controller design param.	200
ρ_e	Estimator design param.	40000
Q_1	State cost weights matrix. For PI-LQG design	$\begin{Bmatrix} 1/100^2 & 0 & 0 \\ 0 & 1/\pi^2 & 0 \\ 0 & 0 & 600 \end{Bmatrix}$
Q_2	Input cost weight matrix	1
Q_e	State noise covariance matrix For DE-LQG design	$\begin{Bmatrix} 0\ 000011 & 0 & 0 \\ 0 & 1 & 0 \\ 0 & 0 & 0 \end{Bmatrix}$
R_e	Measurement noise cov	1

Table [4-12] Design parameters PI-LQG and DE-LQG.

Property	PI-LQG	DE-LQG
Gain Margin	12.18 dB	12 18 dB
Phase Margin	52.19°	53.12°
Distur. Atten. @ P1	-61.1 dB	-59.4 dB
Noise Suppr. @ P2	-22.7 dB	-22.7 dB

Table [4-13] Performance results 5kHz.

Property	PI-LQG	DE-LQG
Gain Margin	13 36 dB	13.36 dB
Phase Margin	58.09°	58.9°
Distur. Atten @ P1	-66.1 dB	-54 5 dB
Noise Suppr @ P2	-11.6 dB	-11.6 dB

Table [4-14] Performance results 20kHz.

Property	PI-LQG	DE-LQG
Gain Margin	17.2 dB	17.2 dB
Phase Margin	52.1°	50.63°
Distur. Atten. @ P1	-54.8 dB	-56.3 dB
Noise Suppr. @ P2	-31.6 dB	-31.6 dB

Table [4-15] Performance results 20kHz $\rho_e = 200$.

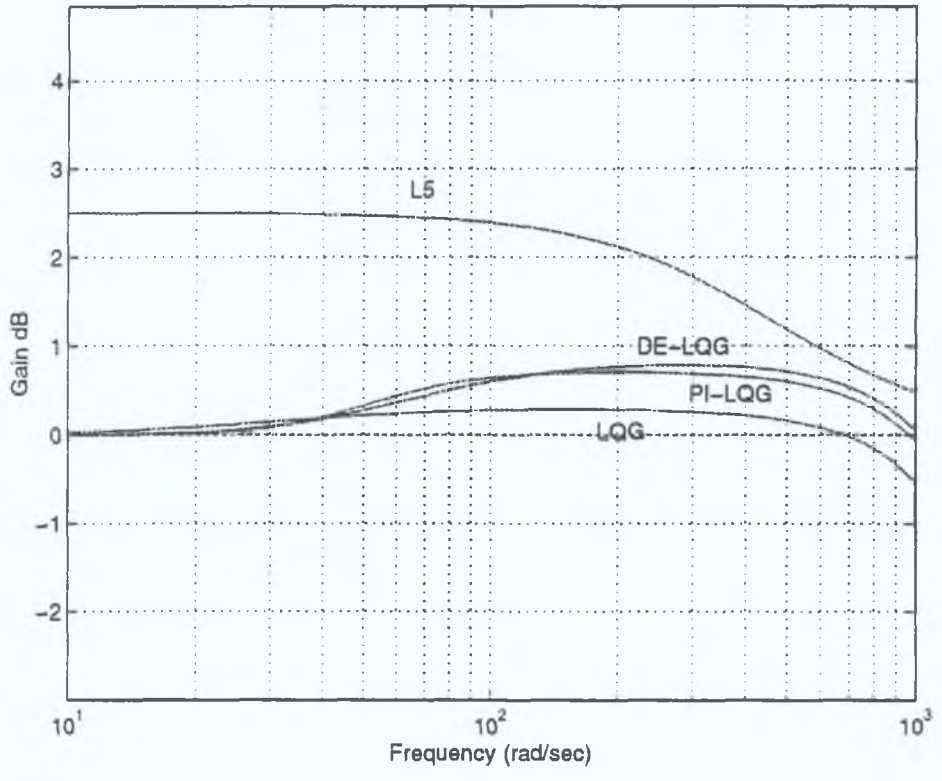

Fig. [4-19] Stability bounds 20kHz.

As stated previously the PI-LQG and DE-LQG designs can provide the same disturbance suppression and noise attenuation properties, given a suitable choice of design parameters. The DE-LQG design, however, offers superior command response properties. This can be seen by a comparison of impulse responses. Figure **[4-20]** shows the impulse response for each compensator design. The overshoot associated with the PI-LQG design puts a greater demand on the actuator. The DE-LQG design is favoured because of the superior command response properties.

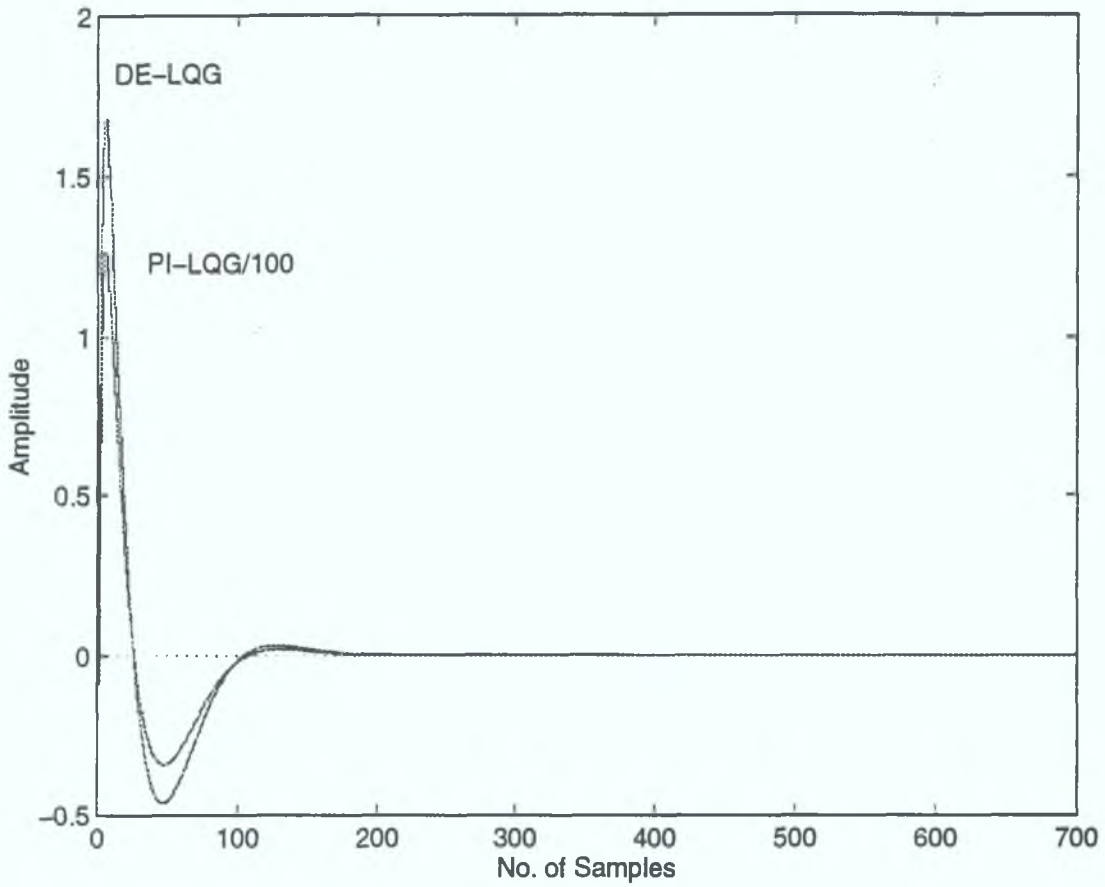

Fig. [4-20] Impulse response.

In most applications there is a limit on the availability of processing resources so the option of increasing the sample frequency may be restricted by the choice of development platforms. In such a situation the Kalman Smoother implementation can be used. Figure **[4-18]** shows the robustness improvements available from the Kalman smoother implementation. These robustness improvements again manifest themselves with a reduced overshoot in the complementary sensitivity function. This in turn allows the above disturbance suppression and noise attenuation trade-offs to be made. The use of the Kalman smoother implementation however introduces additional computational overhead in the compensator design. Indeed the steady state Kalman smoother requires approximately twice the computational resources of the Kalman predictor-corrector estimator.

Where computation resources are a fundamental consideration in the choice of a design, the converse of the results established in section 3.2.1.1 can be applied, namely the use of the gamma value to establish a suitable bandwidth for a given sample frequency. This approach will further improve the noise attenuation properties of the design, as the bandwidth of the corresponding estimator can be further reduced with a reduction in controller bandwidth. Indeed, where the measurement noise is

high, the noise attenuation properties of the estimator can dictate the bandwidth of the controller design.

In this particular implementation a 5kHz DE-LQG design uses most of the available computational resources. Thus the option of increasing sample frequency is not available. Furthermore, in the case of the resolver transducer the signal to noise ratio is low, this is a consequence of the development environment. Indeed, only 12 bits of information is available from each resolver channel. The use of an over sampling technique on the resolver channels will increase the signal to noise ratio, but would also increase the computational overhead of the design. Thus for the purpose of this implementation the gamma value is used to set the bandwidth of the controller for a sample frequency of 5kHz. The stability bounds are then used to halt the LTR procedure at the lowest permissible bandwidth for the estimator design. This approach optimises the robustness and maximises the noise attenuation properties of the design.

By reducing the bandwidth of the LQ controller it follows that the response time of the design will be reduced. However, as the bandwidth is reduced the complementary sensitivity function migrates down in frequency. This migration increases the bound between stability and instability. This increased bound can be used to relax the damped constraint in the cost-weights of the LQ design. By relaxing this constraint the degradation in response time can be offset to some extent. Alternatively this increased bound can be used to reduce the bandwidth of the estimator design, thus improving the noise attenuation properties.

Table **[4-16]** summarises the design parameters for a DE-LQG design where the bandwidth of the LQ design is reduced. The increased stability margin is used to both offset the degradation in the response of the design and reduce the bandwidth of the estimator, thereby improving the noise attenuation properties of the LQG design. Table **[4-17]** contains the resulting performance properties of the design. From the table it is apparent that there is a marked improvement in the noise attenuation properties of the design. This however is at the expense of the other performance properties.

Figure **[4-21]** depicts the theoretical and physical step responses of the latter design. From the figure it is apparent that the physical response adheres to the theoretical design. It is also apparent that the design realises a settling time of approximately 120ms. The disturbance response of the real system is shown in Figure **[4-22]**, this

response is produced by a square wave disturbance torque applied through the load. Figure **[4-23]** depicts the estimate of this disturbance torque as seen by the plant. From these figures it is apparent that a disturbance torque of 7 Nm is rejected in approximately 200ms.

Parameter	Description	Value
1/T	Sample frequency	5000 Hz
γ	Gamma	0.9606
ρ_c	Controller design param.	30
ρ_e	Estimator design param.	5000
Q_1	State cost weights matrix.	$\begin{Bmatrix} 1/150^2 & 0 \\ 0 & 1/\pi^2 \end{Bmatrix}$
Q_2	Input cost weight matrix	1
Q_e	State noise covariance matrix.	$\begin{Bmatrix} 0.000011 & 0 & 0 \\ 0 & 1 & 0 \\ 0 & 0 & 0 \end{Bmatrix}$
R_e	Measurement noise cov.	1

Table [4-16] Design parameters for improved noise attenuation (DE-LQG).

Property	DE-LQG
Gain Margin	12.56 dB
Phase Margin	49.2°
Distur. Atten. @ P1	47.9 dB
Noise Suppr. @ P2	43.5 dB
Command response Time	≈ 150ms
Disturbance response Time	≈ 230ms

Table [4-17] Performance results corresponding for Table [4-16].

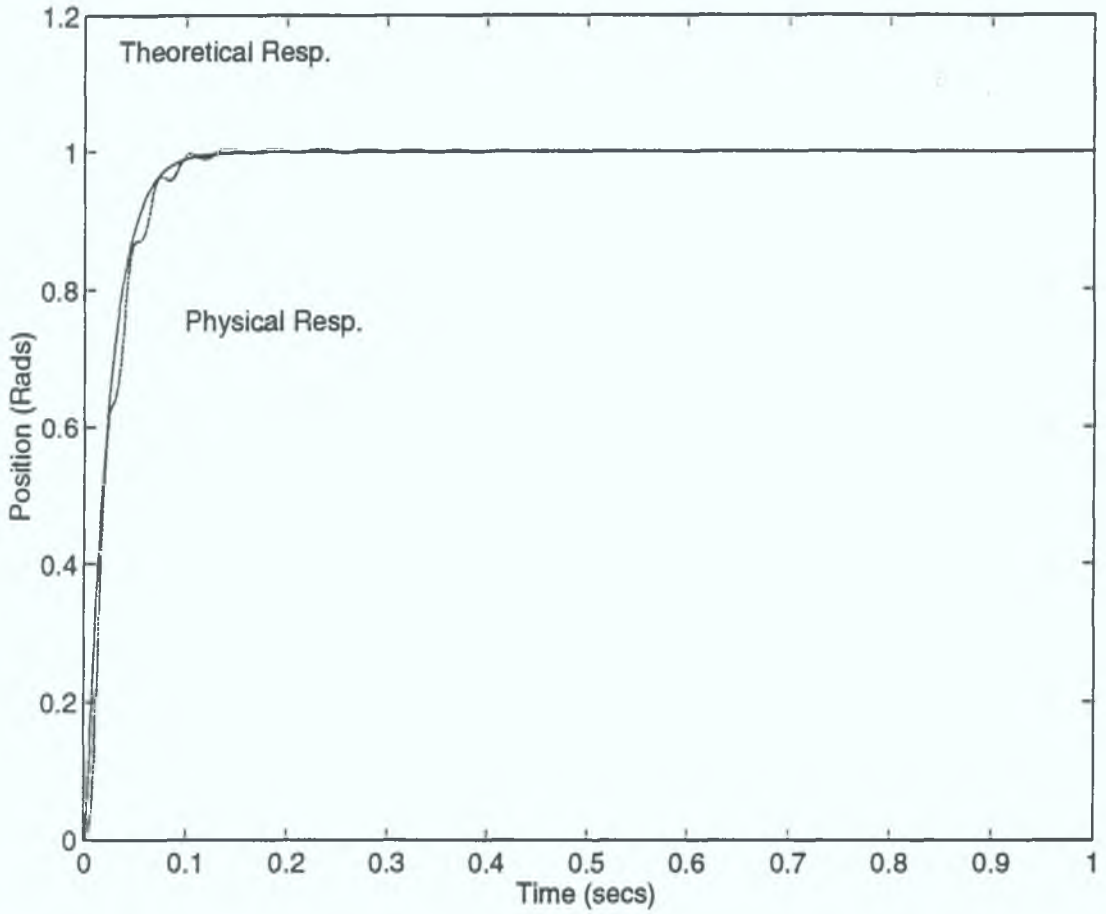

Fig. [4-21] Position step response.

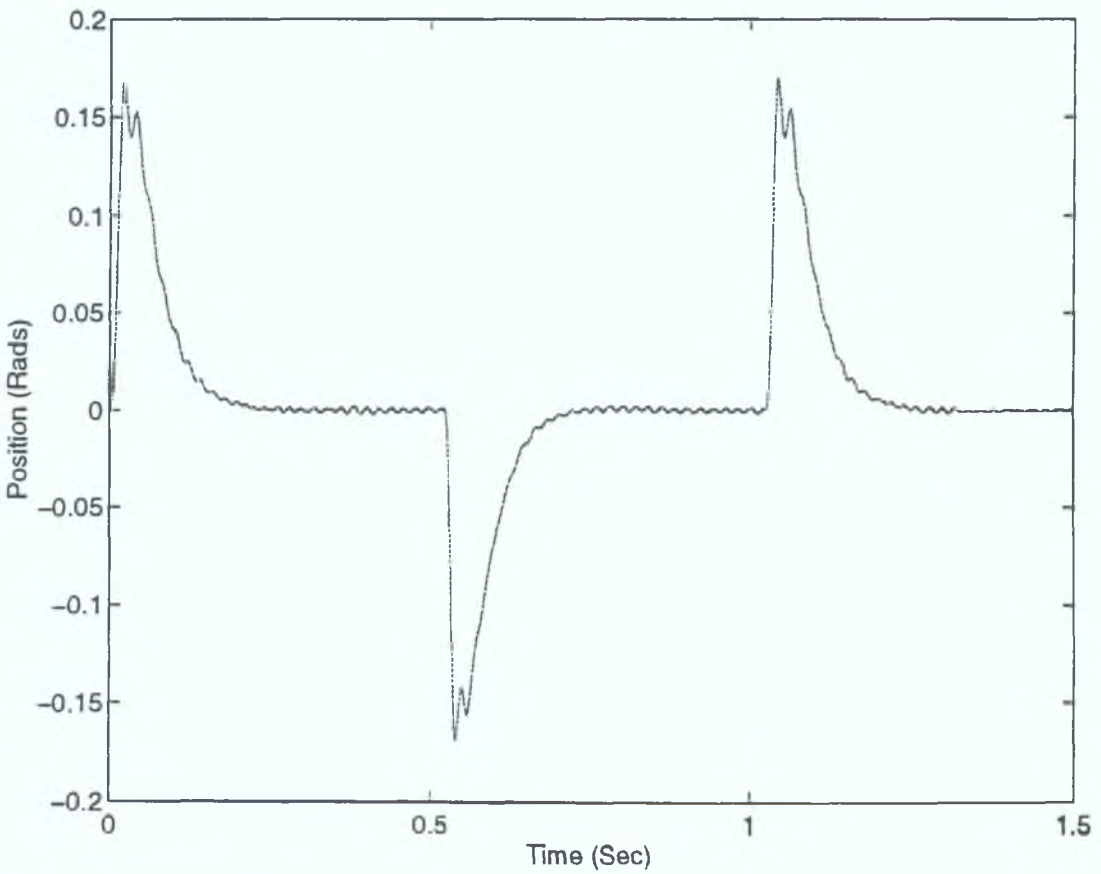

Fig. [4-22] Disturbance response.

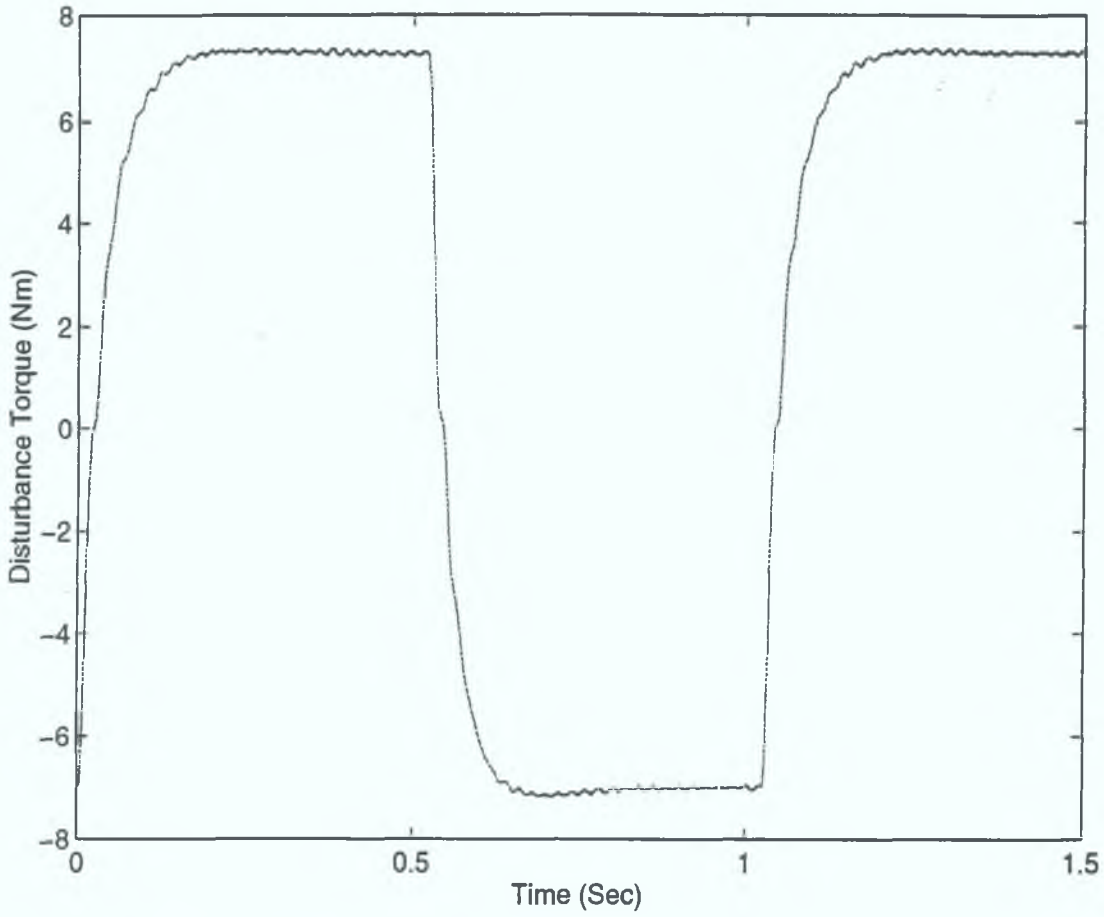

Fig. [4-23] Disturbance estimate.

In conclusion, the realisation of a robust design is at the expense of the response time for the closed loop system. A damped LQ design is required to meet the robustness specifications, furthermore the maximum bandwidth of the compensator is set by these specifications. As the bandwidth of the controller is increased the stability bounds necessitate increasing the damping used in the controller design. Hence there exists a limit on the response time of the design. With the realisation of such a limit the bandwidth of the controller design needs to be minimised, thereby allowing the estimator bandwidth to be minimised. This in turn maximises the noise attenuation properties of the design.

4.4 Motor Current Information.

It is apparent from the two previous examples that the compensator's performance is bounded by the unmodelled dynamics of the current amplifier. In this section these dynamics will be included in the compensator design. From the section on the identification of the current amplifier (Section 4.1.1) a second order approximation of the current loop dynamics is available. Equation **[4-18]** describes a discrete time approximation of the current loop for a sample frequency of 5kHz.

$$\frac{I_a}{I_c} = \frac{1.2335z^{-1} - 0.1659z^{-2}}{z^0 - 0.8975z^{-1} + 4.348e^{-9}z^{-2}} \qquad \textbf{[4-18]}$$

The compensator in this section is designed using the original motor model augmented with this current loop model. Two variations on this design will be considered, one with the availability of current measurement information and the other without. For a full digital controller implementation the armature current is available, this information is necessary for the implementation of a digital current loop. The armature current can thus be used in the servo compensator design without additional hardware costs or complexity. This current information is treated as a measurement in the Kalman estimator design. The benefits of making use of this current information is highlighted during the design process.

The augmented plant comprises four states, namely position, velocity and two canonical states attributed to the current loop dynamics. Figure **[4-24]** depicts a LQG servo for a design with current and position measurements. This servo is an input reference servo design. Such a design introduces additional implementation complexity, for now a reference model is required for the canonical current states. In reality only position and velocity servos are required. Figure **[4-25]** depicts a more favourable design which eliminates the need for a canonical current reference model. The output from the position and velocity servo u_e is used as a current reference for the cascaded current stage. This design can still regulate the armature current. Indeed the armature current can be limited by introducing a saturator on the current reference input.

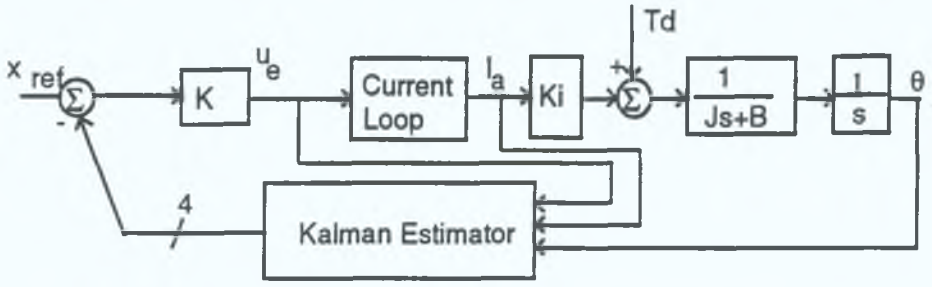

Fig. [4-24] LQG servo with current loop model.

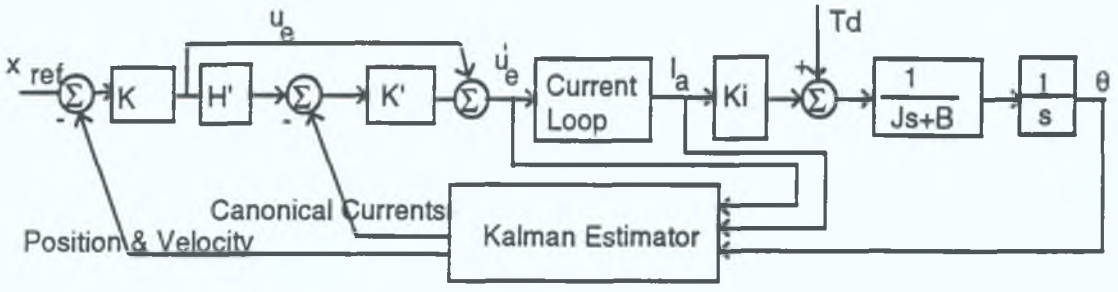

Fig. [4-25] LQG with position and velocity references.

In the previous design example a disturbance feedforward technique is used to overcome the effects of disturbance torque entering the plant. In this example a similar strategy can be developed, Figure **[4-26]** depicts the situation. However, with this design the disturbance estimate, which is modelled as a bias entering the motor, must be scaled by the gain of the current amplifier before feeding it forward. As seen in section 4.1.1.1 on the identification of the current loop, the gain of the current amplifier is not constant. Thus the asymptotic rejection of a disturbance is not possible during amplifier saturation. Hence a better strategy is to model the disturbance as a bias entering the plant at the input to the current amplifier, thus eliminating the need for scaling and inherently overcoming the side effects associated with the saturation of the current amplifier. Figure **[4-27]** depicts this latter situation.

The latter configuration is however only valid for a design which does not include a current feedback measurement, in which case a bias estimator at the input to the motor model is reflected through the current amplifier and is thus described as a bias at the input to the current amplifier. In the design which includes a current measurement the current feedback prevents the reflection of the disturbance torque through the current amplifier, without treating the measurement as the sum of the armature current and the effective disturbed current.

The disturbance torque estimate configuration (Figure **[4-26]**) is more applicable for a design which includes a current measurement. The problems associated with the saturation of the current amplifier are inherently overcome. The current measurement

information will reflect the saturation of the current amplifier. Thus asymptotic rejection of a disturbance is still available in the presence of a saturating amplifier.

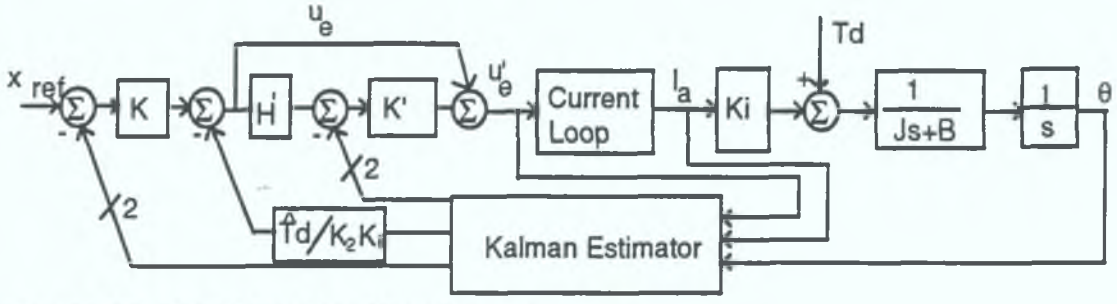

Fig. [4-26] DE-LQG with disturbance torque.

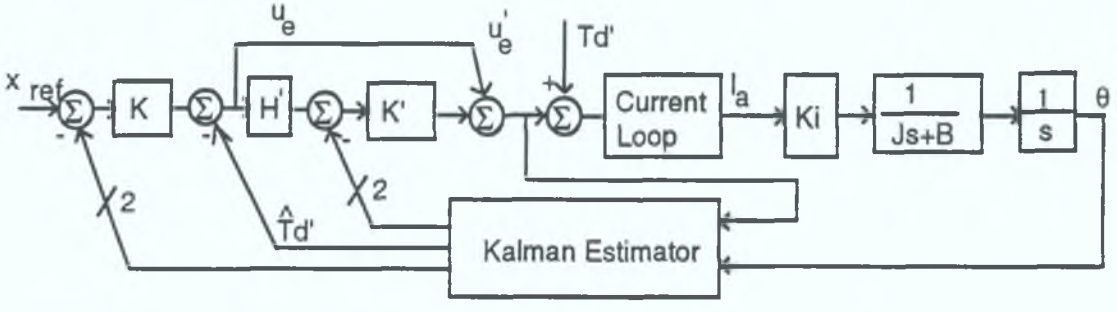

Fig. [4-27] DE-LQG with disturbance current.

4.4.1 Current Loop Model with No Current Measurement.

The first design to be considered in this section is a DE-LQG compensator for the plant model augmented with the current loop dynamics. For this example armature current information is not available. Disturbance torque entering the system is modelled as a bias entering the system at the input to the current loop. Figure **[4-27]** describes this situation. The H' matrix maps the reference current to the steady state reference canonical current states. For this design the Kalman predictor-corrector compensator is used (equation **[3-83]**).

Figure **[4-28]** shows the complementary sensitivity function and the relevant multiplicative uncertainty bounds for this design. With the introduction of the current loop dynamics into the controller design the associated multiplicative uncertainty bounds for the current loop dynamics are removed from the robustness analysis. The removal of the current loop multiplicative uncertainty bounds however, permits the previously shadowed multiplicative uncertainty associated with the Tachogenerator filters (L6) to be considered. In addition there are similar bounds associated with the anti-aliasing filters and post-sampling filters which are shadowed by the Tachogenerator filter uncertainty. To simplify the design these are not included at this

stage. However the designer must be aware of the accumulative effect of all these bounds which results in a tighter stability bound. Thus where such approximations take place the designer must allow for the fact that these are conservative approximations of the stability bounds. The worst case multiplicative uncertainty which comprises the accumulative effects of all the uncertainties is labelled L5.

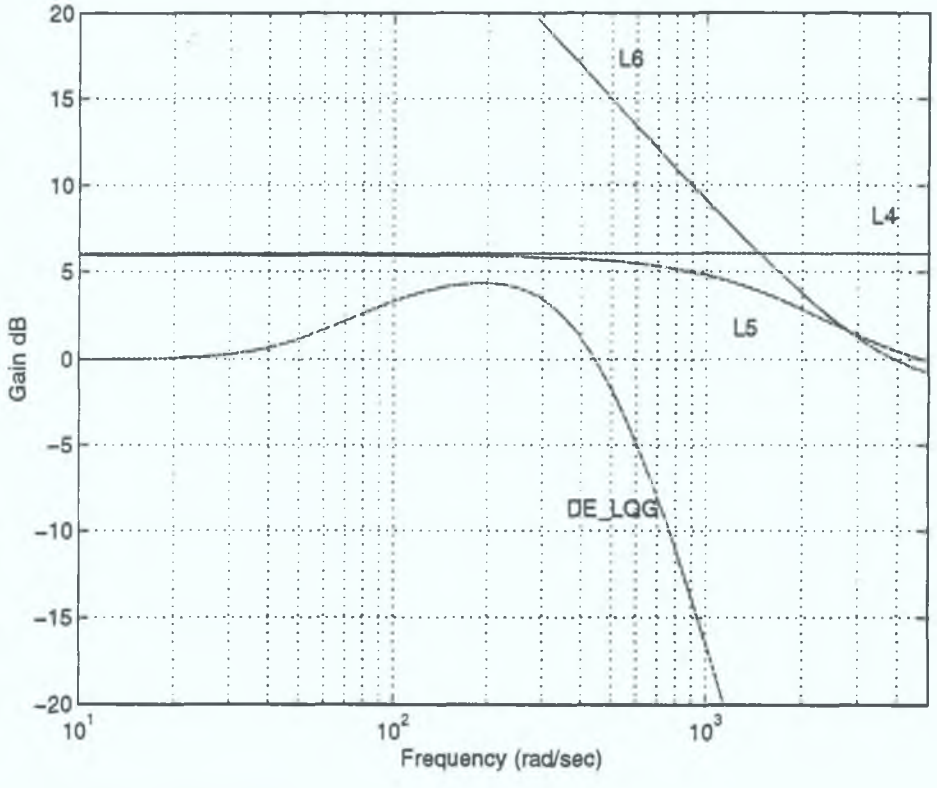

Fig. [4-28] DE-LQG with current loop model.

On comparing Figure **[4-28]** with Figure **[4-16]** the benefits of including the current loop dynamics in the controller design can be readily seen. The worst case multiplicative uncertainty (L5) has lifted up and expanded the stability bound. Furthermore the cut-off point for the worst case stability bound occurs at a higher frequency. The complementary sensitivity function can now be advanced forward in frequency since it is no longer bounded by the current loop multiplicative uncertainty. In this particular case the designer chooses not to increase the bandwidth of the complementary sensitivity function, but instead to relax the damped constraints of the LQ design which were necessary to meet the robustness specifications. In doing so the designer can realise faster response times, while maintaining the noise suppression properties of the design. Recall that as the damping constraints of the design are relaxed the peak amplitude of the complementary sensitivity function increases.

Alternatively the designer may decide to halt the LTR procedure at an earlier iteration, which will result in a compensator with improved noise suppression properties. Recall that as the bandwidth of the estimator is reduced the robustness of the design disimproves. This disimprovement manifests itself in an increased overshoot in the complementary sensitivity function. The designer also has the option to improve the disturbance response time of the design.

In this particular design the improved stability bounds are used to speed up both response to command and disturbances. Figure **[4-29]** shows the step response of the physical system for this design. In this particular example the controller is implemented as a regulator. From the figure it is evident that the response time of the design has improved. This improvement is achieved while still maintaining the bandwidth of the original design and corresponding noise attenuation properties.

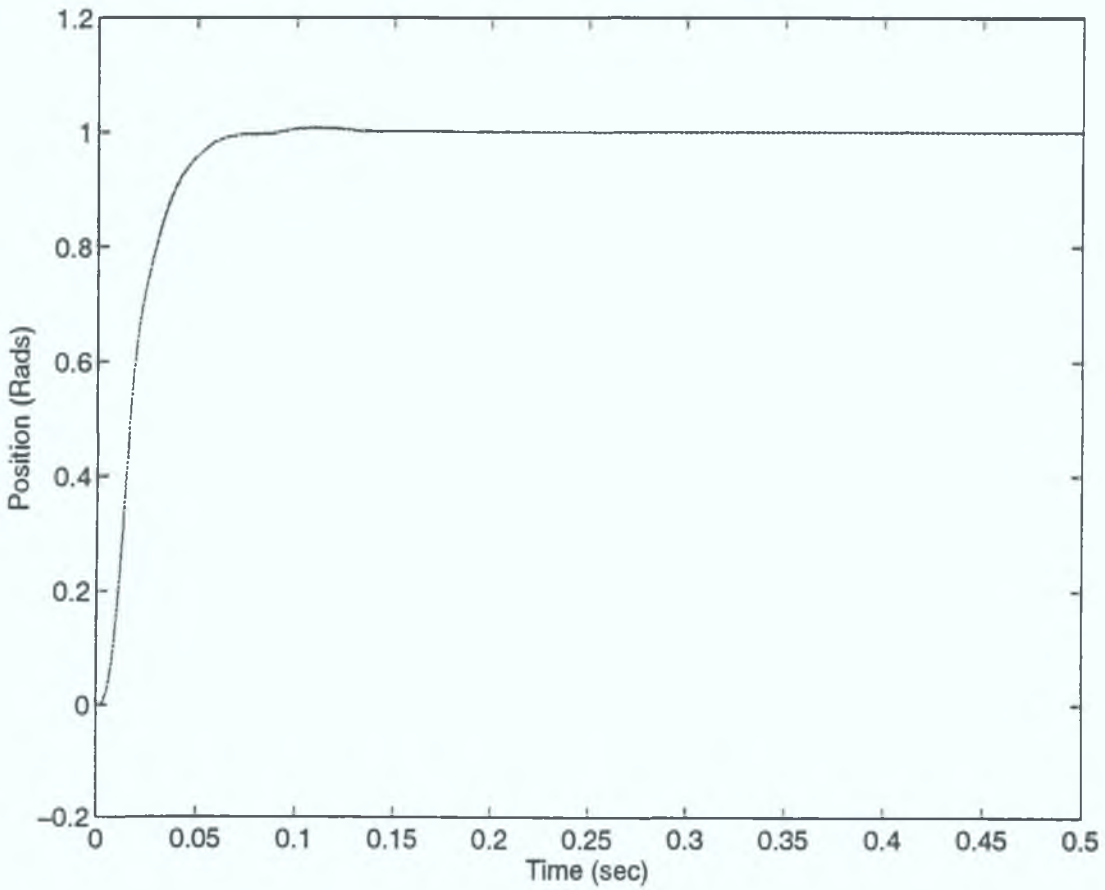

Fig. [4-29] Step response.

Figure **[4-30]** shows the position response for a step disturbance torque applied to the system through the load, again the improved response time is evident. The figure shows asymptotic rejection of the disturbance torque within approximately 150ms. Figure **[4-31]** shows the corresponding velocity response for this step disturbance. On

comparison with the previous design it is apparent that the inclusion of the current loop dynamics has reduced the velocity ripple.

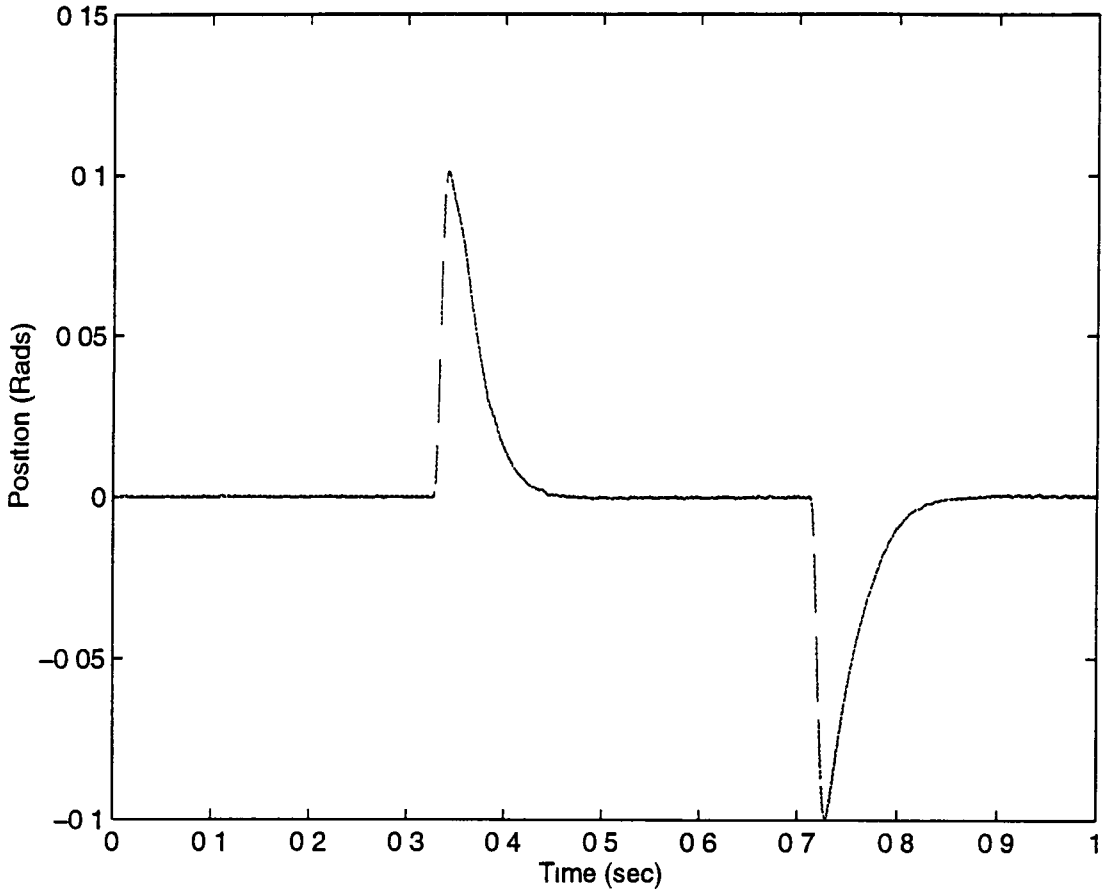

Fig. [4-30] Perturbed position response.

The reader must be cautioned over the interpretation of figure **[4-30]** and **[4-31]**. These results are the estimated position and velocity responses, which may contain transience internal to the estimator which are not present in the physical response.

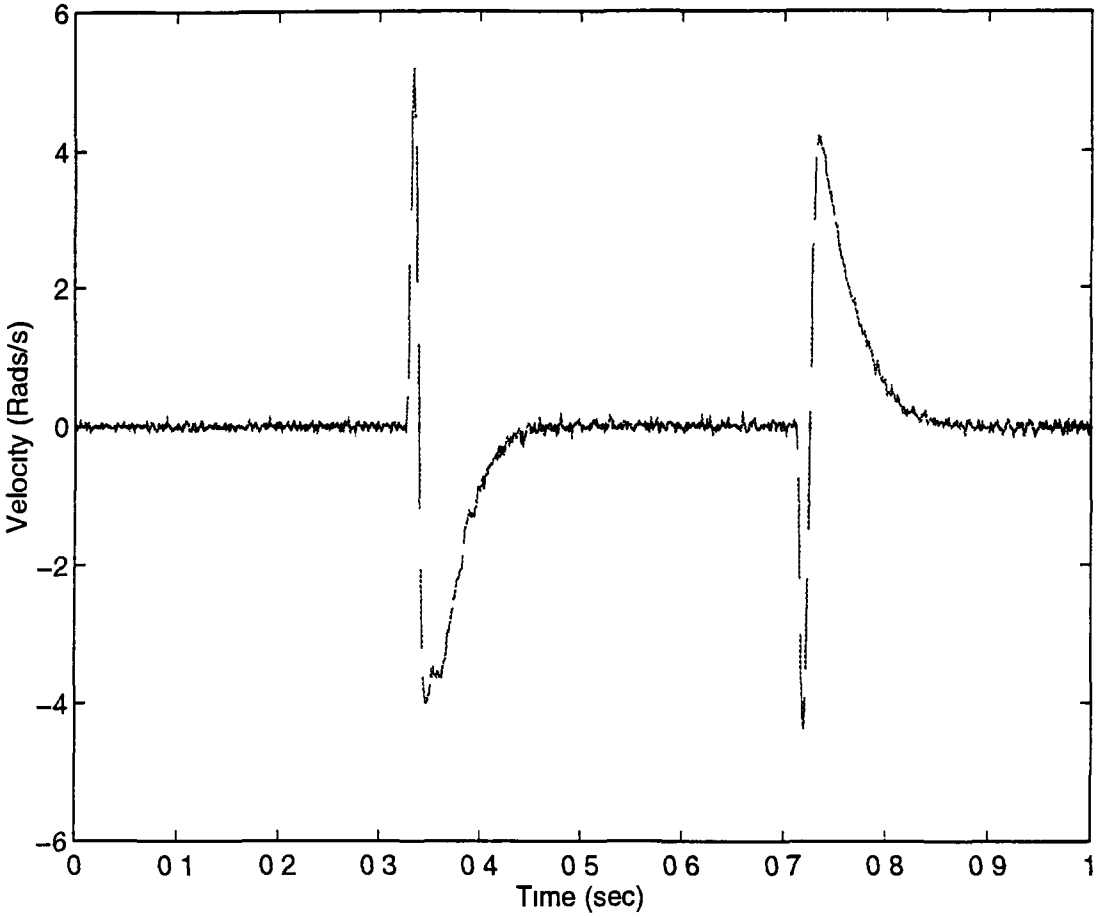

Fig. [4-31] Perturbed velocity response.

Figure **[4-32]** shows an estimate of the disturbance as seen at the input of the current loop This figure also contains the resulting output from the DE-LQG compensator From the figure the amplitude of the disturbance estimate seen at the input to the current loop is approximately 0 25, the equivalent disturbance torque seen at the input to the motor is given by equation **[4-19]** Thus the system asymptotically rejects a disturbance of 12 Nm in approximately 150 ms The compensator output shows that a peak current of approximately 45 Amps and a continuous current of 25 Amps is required to reject a disturbance of this magnitude

$$T_d = 0\ 25 * K_2 * K_t = 12\ 27 Nm \qquad \textbf{[4-19]}$$

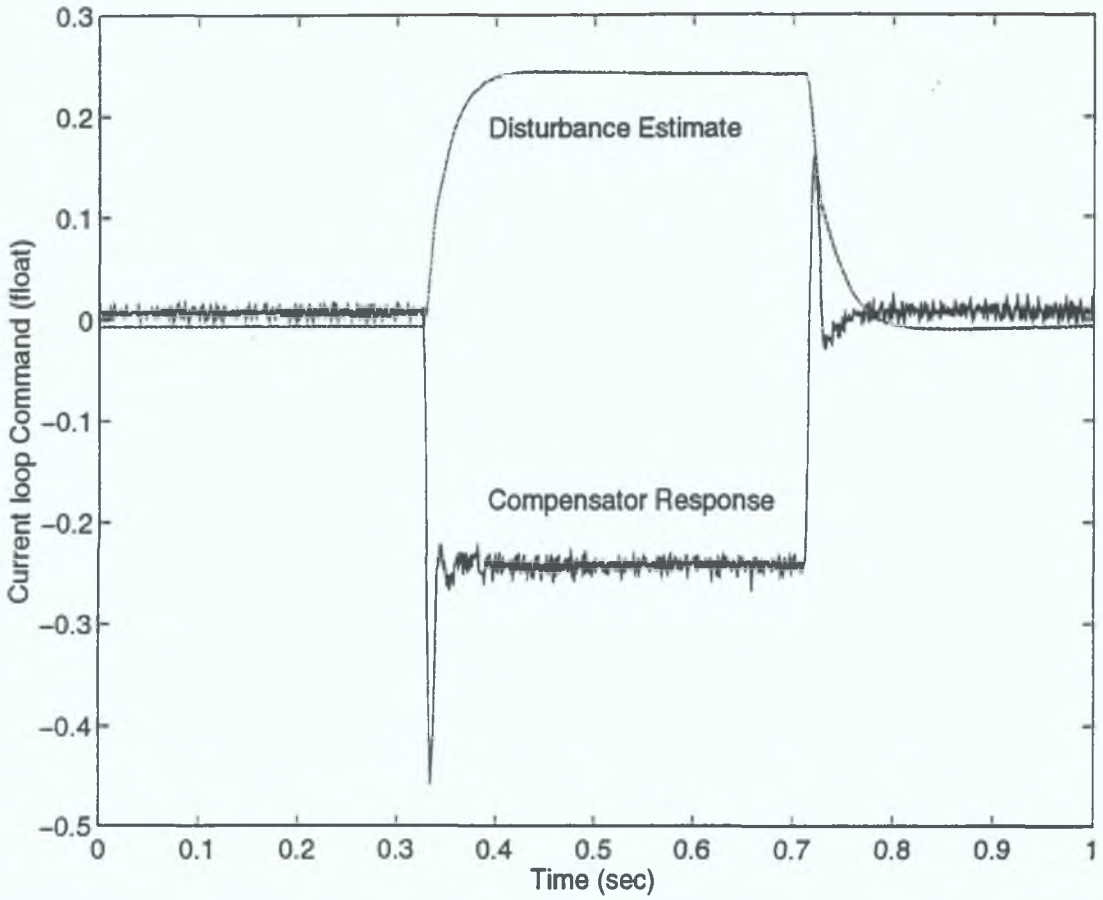

Fig. [4-32] Disturbance estimate and compensator response.

The LQ cost weight matrix used in this design is given in Table **[4-18]**. Bryson's inverse square method is used to assign weights to the canonical current states. The maximum rated current for the design is 50 Amps. During this design it is found that the control costs for the current states dominates the overall cost. This results in a controller which penalises the current and as a consequence exhibits a damped response. Indeed by using Bryson's inverse square method the costs attributed to maximum armature current is weighted the same as the cost associated with a maximum position deflection. Thus by this design maximum current is delivered by the controller to overcome a disturbed position deflection of π Rads. In reality a controller which delivers maximum current for a fraction of the maximum position deflection is required. By relaxing the cost weights associated with these current states, the current amplifier is driven harder. This makes better use of the amplifier's duty cycle. To facilitate this, an additional design parameter ρ_{cc} is introduced into the cost weight matrix Q_1. The H' matrix maps the canonical current states to physical states.

Param.	Description	Value
1/T	Sample frequency	5000 Hz
γ	Gamma	0.8826
ρ_c	1st Controller design par.	800
ρ_{cc}	2nd Controller design par	1
ρ_e	Estimator design param.	3,000
Q_1	State cost weights matrix.	$\begin{Bmatrix} \rho_{cc}/(50H_1')^2 & 0 & 0 & 0 \\ 0 & \rho_{cc}/(50H_2')^2 & 0 & 0 \\ 0 & 0 & \rho_c/286^2 & 0 \\ 0 & 0 & 0 & \rho_c/\pi^2 \end{Bmatrix}$
Q_2	Input cost weight matrix	1
Q_e	State noise covariance matrix. [24]	$\begin{Bmatrix} 0.0003 & 0 & 0 & 0 & 0 \\ 0 & +0 & 0 & 0 & 0 \\ 0 & 0 & +0 & 0 & 0 \\ 0 & 0 & 0 & 1 & 0 \\ 0 & 0 & 0 & 0 & 0 \end{Bmatrix} \rho_e$
R_e	Measurement noise cov.	1

Table [4-18] Design parameters with armature current model (DE-LQG).

From the design parameters specified in Table **[4-18]** it is apparent that the gamma value for this design is significantly less than one. This suggests the possibility for further improvement in the design. The following options are available to the designer:

- Increase the sample frequency
- Reduce the controller bandwidth
- Choose an alternative Kalman estimator implementation

[24] The +0 stands for a small non-negative number for example 0.00001. This is necessary to ensure that the solution of the Hamiltonian matrix is full rank.

For this particular example the design will be considered to be complete. Table **[4-19]** contains some of the performance results for this implementation

Property	DE-LQG
Gain Margin	7 67 dB
Down Side GM	≈ 0
Phase Margin	36 00°
Distur. Atten @ P1	-54 78 dB
Noise Suppr. @ P2	-49 38 dB
Command Resp Time	≈ 60ms
Distur. Resp. Time	≈ 150ms

Table [4-19] Performance results corresponding to Table [4-18].

4.4.2 Current Loop Model with Current Measurement.

The next implementation to be considered is a design which includes armature current information as a measurement in the Kalman estimator. Figure **[4-27]** depicts the compensator configuration for this implementation. The use of current measurement information in this controller design in effect puts a current loop around the existing current loop. This design is not intended to replace the existing current loop, but instead makes better use of all the available information about the current loop. The design objective is to use this information to speed up the disturbance response without having to widen the bandwidth of the estimator This will ensure a faster disturbance response while still maintaining the noise attenuation properties Indeed for a current measurement with a good signal to noise ratio the bandwidth of the estimator can often be reduced, further improving the noise attenuation properties of the design. Table **[4-20]** contains the design parameters used for this design.

As in the previous design example the LTR design is carried out implicitly The LTR procedure is halted when the complementary sensitivity function satisfies the condition **[3-41]** for the worst case stability bound (L5) Full robustness recovery would be at the expense of the noise attenuation properties of the design Hence the bandwidth of the estimator is kept at the minimum permissible bandwidth necessary to satisfy the robustness constraints of the design specification

Param.	Description	Value
1/T	Sample frequency	5000 Hz
γ	Gamma	0.8394
ρ_c	1st Controller design par.	800
ρ_{cc}	2nd Controller design par	1
ρ_e	Estimator design param.	45
Q_1	State cost weights matrix.	$\begin{Bmatrix} \rho_{cc}/(50H_1')^2 & 0 & 0 & 0 \\ 0 & \rho_{cc}/(50H_2')^2 & 0 & 0 \\ 0 & 0 & \rho_c/286^2 & 0 \\ 0 & 0 & 0 & \rho_c/\pi^2 \end{Bmatrix}$
Q_2	Input cost weight matrix	1
Q_e	State noise covariance matrix.	$\begin{Bmatrix} 10 & 0 & 0 & 0 & 0 \\ 0 & +0 & 0 & 0 & 0 \\ 0 & 0 & +0 & 0 & 0 \\ 0 & 0 & 0 & 0 & 0 \\ 0 & 0 & 0 & 0 & 0 \end{Bmatrix} \rho_e$
R_e	Measurement noise cov.	$\begin{Bmatrix} 1 & 0 \\ 0 & 1 \end{Bmatrix}$

Table [4-20] Design parameters for system with armature current model and armature current measurements (DE-LQG).

Figure **[4-33]** contains a plot of the complementary sensitivity function and the relevant stability bounds. Note that the margin necessary to satisfy the stability condition is a conservative margin to allow for approximations made during the choice of the worst case stability bound (L5).

Figure **[4-34]** shows the corresponding Nyquist plot for the final stage of the LTR procedure. From the plot several important observations can be made, firstly the Nyquist plot is almost excluded from the Gamma circle, which implies that the design is almost optimal in a LQ sense. The plot also shows the Nyquist contour crossing the real axis for a second time. Recall from section 3.2.1 the discussion regarding the downside gain margin. In previous designs the downside gain margin was zero

whereas for this design the margin is finite. The interpretation of this finite gain margin is that the design could become unstable if the feedback sensors were to fail. This is indeed the case when sensor failure is simulated in the physical plant. This potential instability is one of the disadvantages of this latter design.

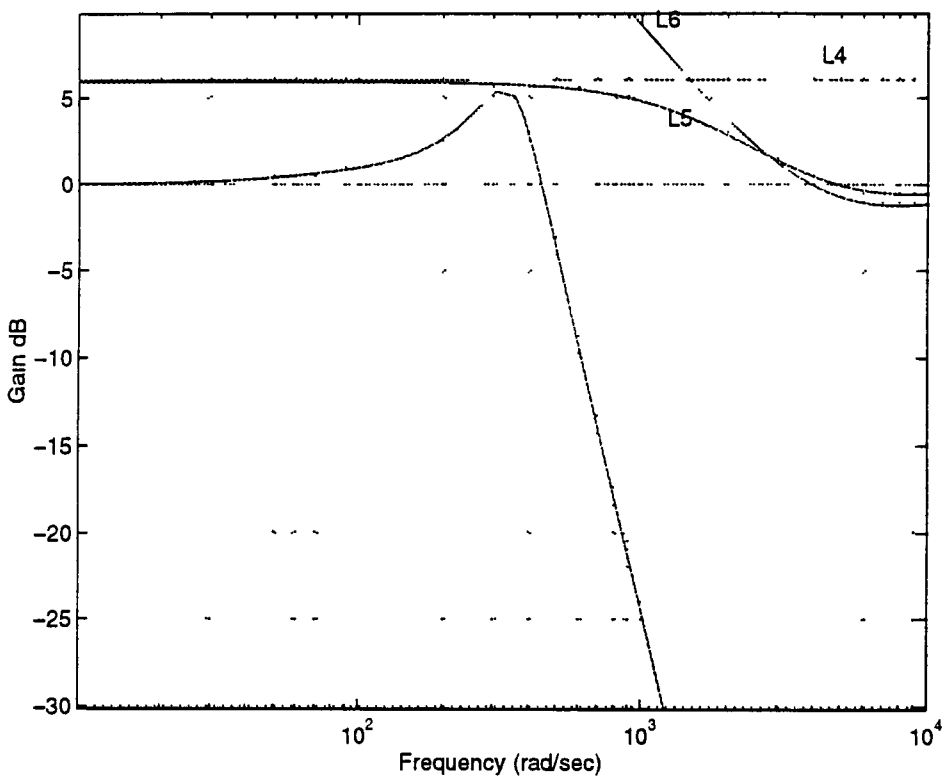

Fig. [4-33] Complementary sensitivity plot for design with current measurement information.

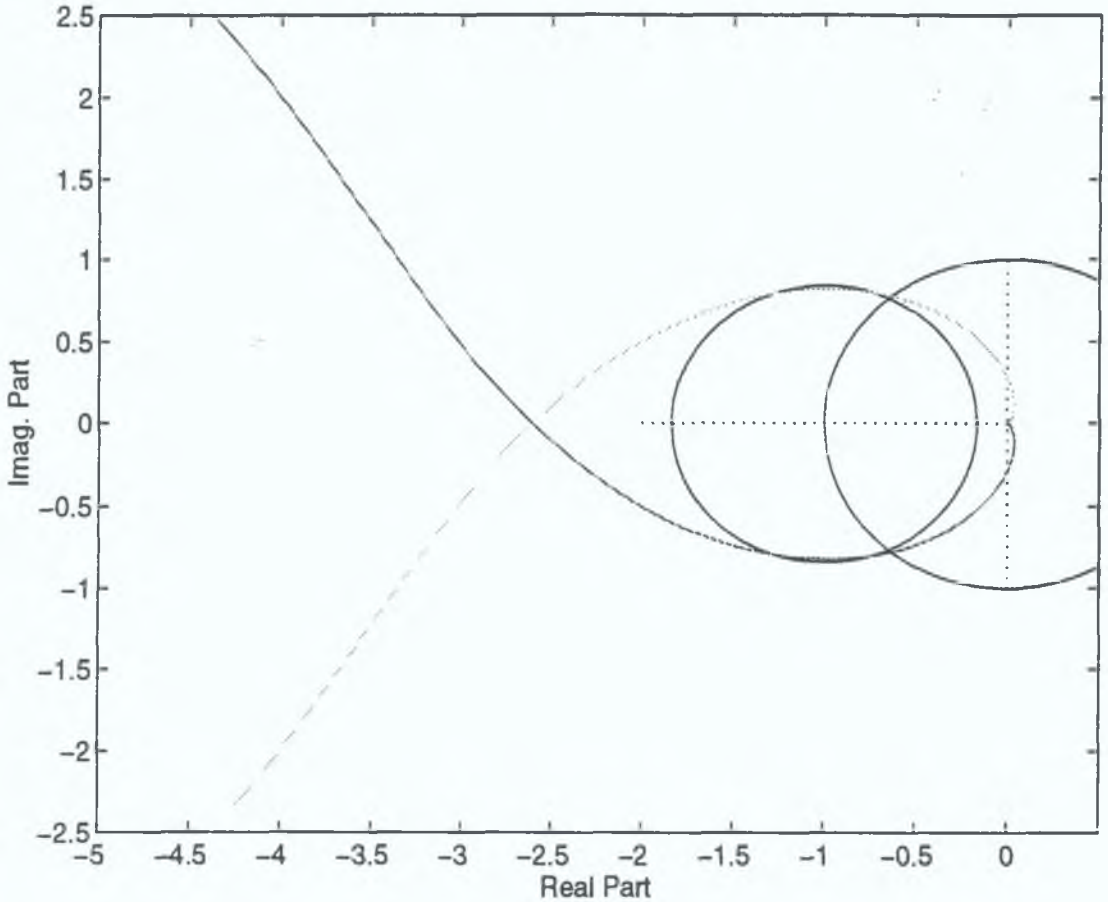

Fig. [4-34] Nyquist plot for design with current measurement information.

Figure **[4-36]** and Figure **[4-37]** show the position and velocity response to a step command in both position and velocity. A settling time of approximately 60ms can be realised for both these commands. Note that the LQ portion of this design is the same controller used in the previous design. Thus no improvement in command response is sought for this design.

Figure **[4-35]** shows the linear and non-linear regions of the current amplifier. A settling time of 60ms is only available while the current amplifier is in its linear region. A step change in command position of greater than 0.1 Rads will command from the current amplifier a current greater than the peak current rating of the amplifier, thus bringing the amplifier into a non-linear region resulting in a degradation in response time. Likewise a step change in command velocity of greater than 5 Rad/s will also bring the amplifier into its non-linear region. Figure **[4-37]** shows this degraded response for step changes in velocity greater than 5 Rads/s. For a step change of 20 Rads/s a settling time of approximately 80ms is realised. Note that by increasing the weighting for the current states in the controller design the range of the step commands for which saturation occurs can be increased. Increasing the current

weighting will however degrade the overall response time of the design. In this work the controller is designed to maximise the response time to small signal commands.

From a practical implementation point of view, care must be taken to prevent integral windup in the presence of actuator saturation. This is accomplished by constraining the errors between the feedback and the reference positions and velocities before applying the control law

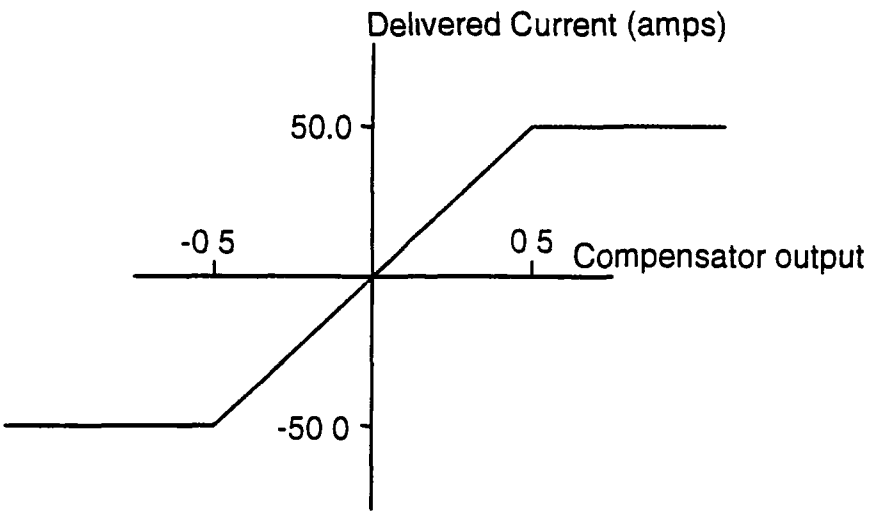

Fig. [4-35] Saturation limits of the current amplifier.

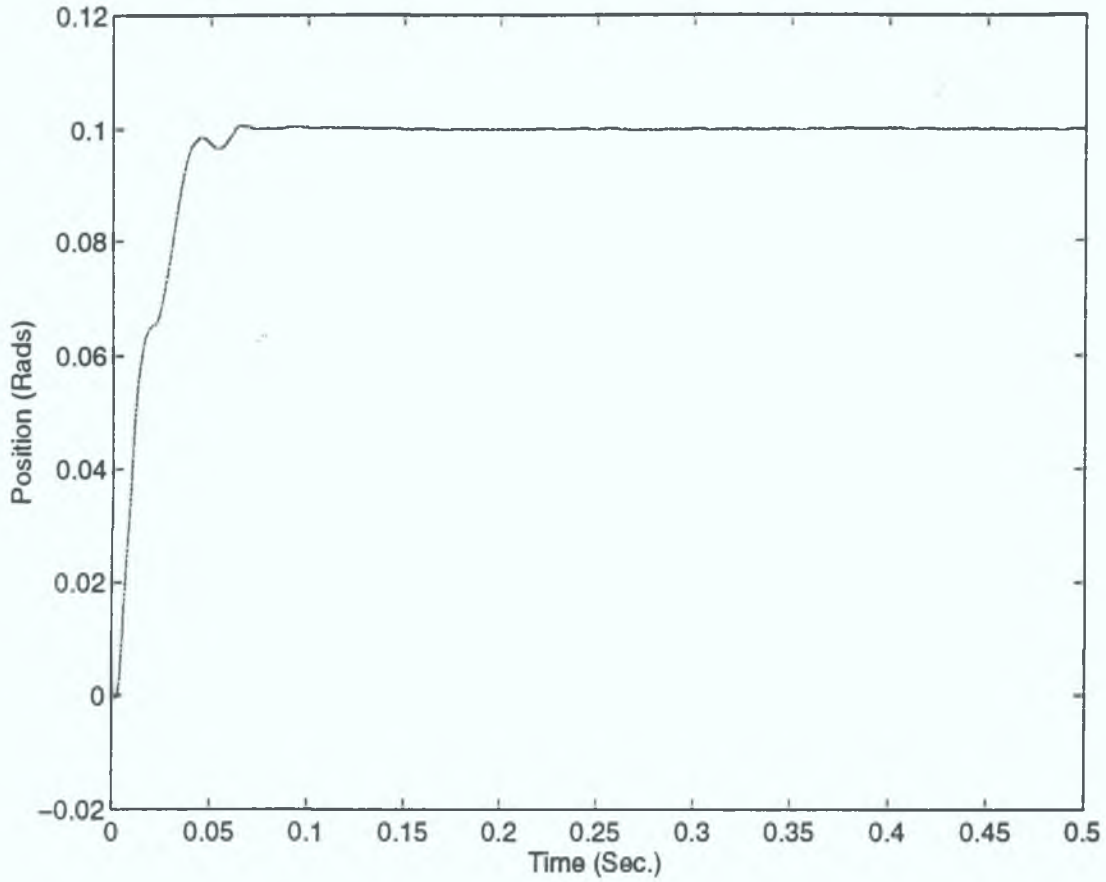

Fig. [4-36] Step response to command position.

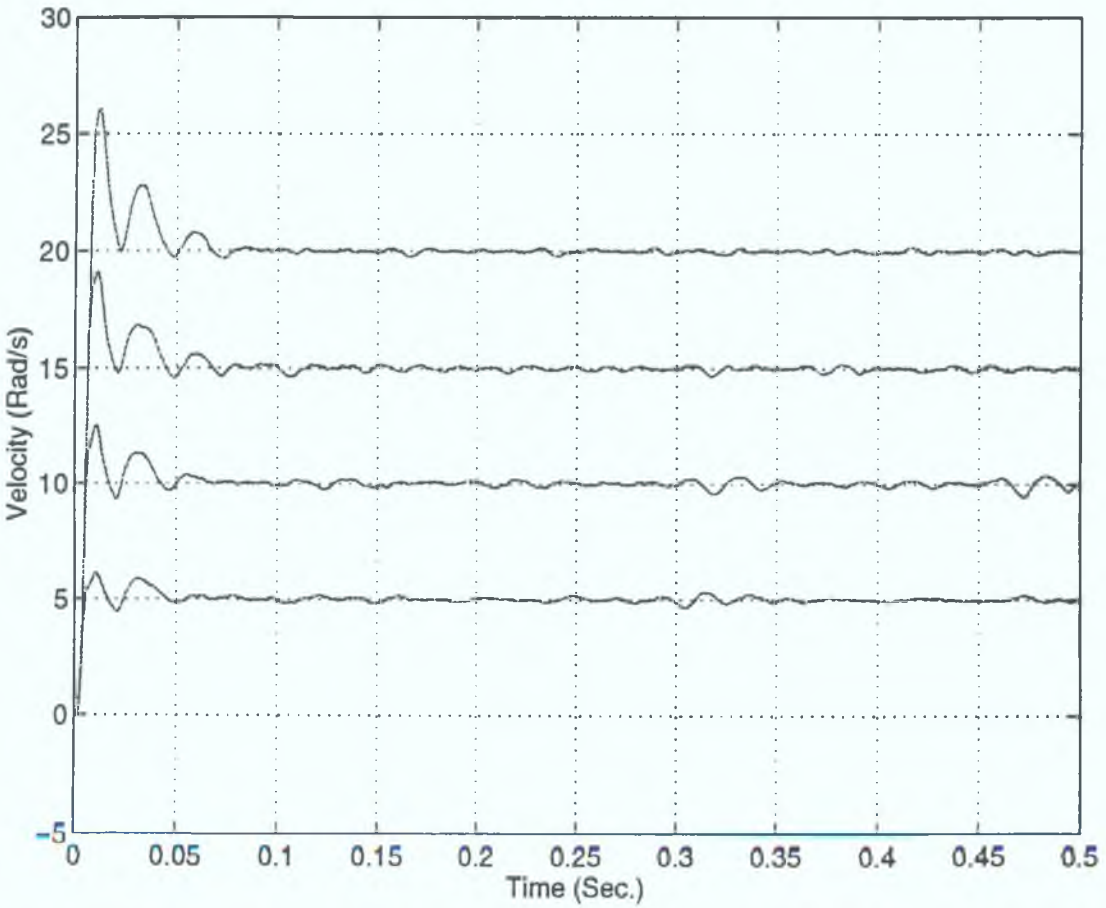

Fig. [4-37] Step response to command velocity for 5, 10, 15 and 20 rads/s.

The benefits of using armature current feedback information in this design are found through the improved disturbance response times of the design. Figure **[4-38]** shows the position response for a step disturbance of approximately 12 Nm. Figure **[4-39]** shows the corresponding velocity response and Figure **[4-40]** shows the resulting disturbance estimate. From these figures it is apparent that a disturbance response of approximately 80ms can be realised.

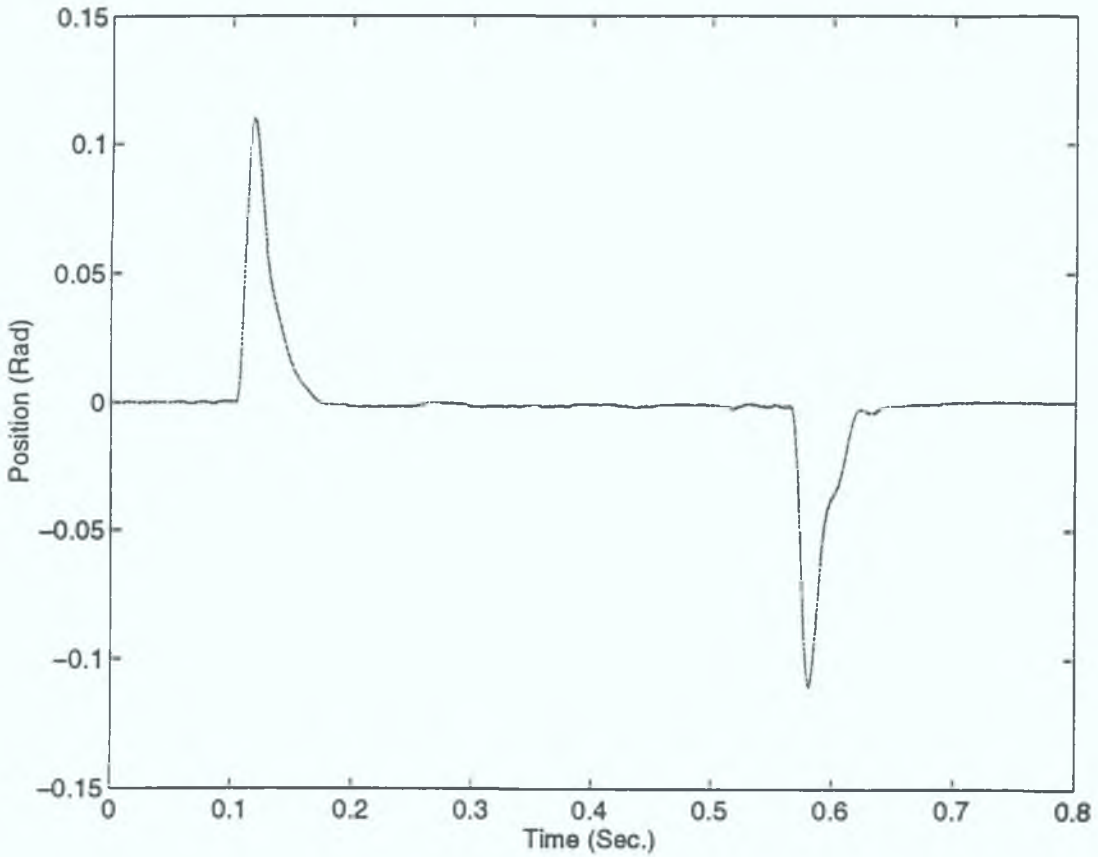

Fig. [4-38] Position response to a disturbance of 12Nm.

The reader must be cautioned over the interpretation of figure **[4-38]** and **[4-39]**. These results are the estimated position and velocity responses, which may contain transience internal to the estimator which are not present in the physical response.

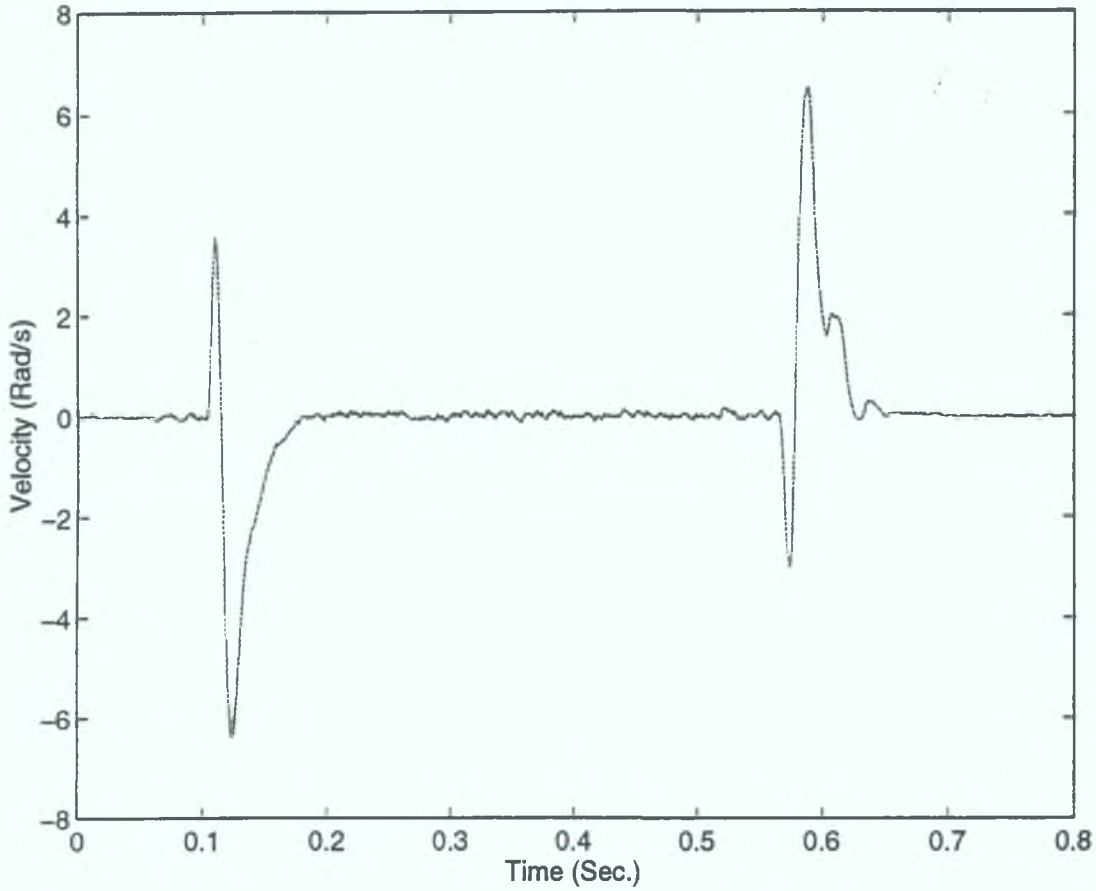

Fig. [4-39] Velocity response to a disturbance of 12Nm.

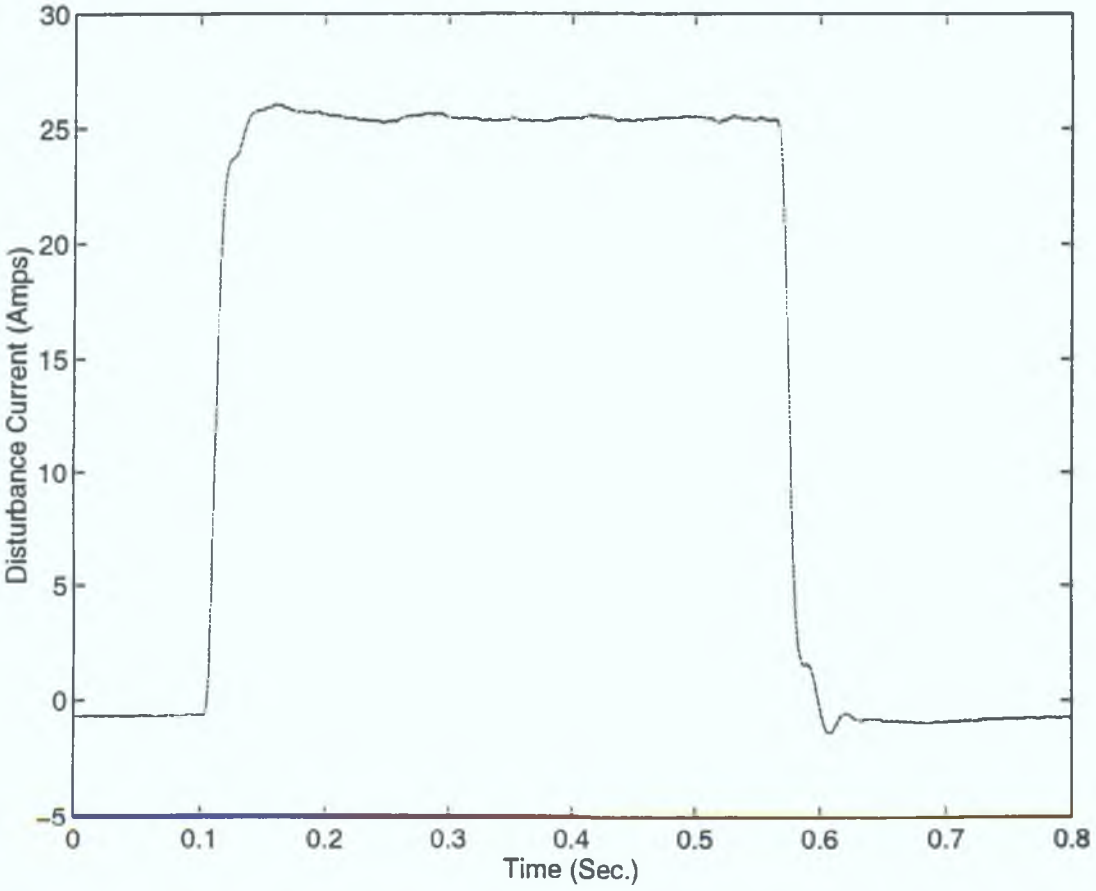

Fig. [4-40] Armature current estimate for a disturbance of 12Nm.

Property	DE-LQG
Gain Margin	58.80 dB
Downside GM	0.3704
Phase Margin	56.63°
Distur. Atten. @ P1	-52.588 dB
Noise Suppr. @ P2	-57.941 dB
Command Resp. Time	≈ 60ms
Distur. Resp. Time	≈ 80ms

Table [4-21] Performance results corresponding to Table [4-20].

In conclusion it is apparent from the performance results given in Table **[4-21]** that the latter design outperforms the previous designs. The noise attenuation properties of the design can be further improved by employing the FS-LTR technique described in section 3.3.3.3. Recall that this technique can increase the roll-off rate of the sensitivity function and hence improve the attenuation properties of the design. However the current amplifier model is in effect a frequency shaping filter in the recovery procedure. By increasing the order of the current amplifier model improved roll-off rates could be realised. The current roll-off rate for this design is of the order of 60dB/decade. Such a roll-off rate is sufficient for normal servo applications.

The Gamma value for this design suggests that robustness improvements can be made to the design by increasing the sample frequency and/or using an alternative Kalman implementation such as a Kalman smoother estimator, such considerations depend on the application.

5. Concluding Issues.

5.1 Concluding Summary.

With the reducing costs of fast digital signal processors the choice of suitable control algorithms for the commercial sector has expanded. In this work a LQG/LTR controller is presented as one such control algorithm, conventionally this algorithm because of its numerical complexity and computational overhead is not often used for commercial applications. Very few published papers deal with either the method itself or with the applications orientated studies that have exploited the LQG/LTR methodology. As a consequence, this powerful method is not readily accessible to the practising engineer. In this work a systematic design methodology is presented which eases the design process by making it transparent, conducive to educated trial and error design iterations, and minimises the number of design parameters. This work is an application orientated study of the LQG/LTR design methodology

Conventionally LQG/LTR synthesis is performed in continuous time, the resulting design is then mapped into discrete time prior to implementation. In previous literature very little consideration has been given to the robustness implication of such an approach. For this reason the LQG/LTR design synthesis in this work is performed in discrete time where these robustness considerations can be observed.

Within the servo control industry two position feedback sensors are commonly used, namely the optical encoder and the resolver. The resolver is attractive because of its robust construction which is particularly suited for industrial environments. In this work an estimator structure is developed which eliminates the need for a resolver to digital converter. Conventionally in control applications this component occupies a significant portion of the cost of the resolver interface. The elimination of this component partly justifies the additional costs of the digital signal processor.

An Extended Kalman estimator is used to convert the rectangular coordinate position information into polar position information. A steady state solution for the estimator provides a numerically robust and efficient solution. The outputs from the estimator are then subsequently used in a control feedback loop. The optical encoder has several advantages over the resolver, the optical encoder doesn't require calibration during installation as does the resolver, the encoder is not sensitive to electromagnetic interference and other noises as is the resolver. However the incremental form of the optical encoder which is price comparable to the resolver doesn't provide absolute

position information which is a requirement for AC Servo application. In this work the two disadvantages of the resolver described are overcome using a parameter estimation algorithm and the filter functionality of the Kalman estimator.

The resolver signals because of their analogue origin are often distorted, these distortions introduce amplitude, bias and phase discrepancies onto the resolver signal which result in a position error. Conventionally the effects of these distortions are minimised by matching the gain and phase on the resolver channels using matched filters. This calibration of the sensor is performed during installation. It is necessary to ensure that these parameters will not drift with changes in temperature or over the lifespan of the product, the net effect of which is an additional cost and complexity in the interface design. In this work a parameter estimation scheme is presented which eliminates the need for high tolerance matched filter components on the resolver channels. This scheme also eliminates the need for calibration of the resolver interface and compensates for temperature drift among others. The scheme also compensates for mismatches in the resolver design which is a consequence of a finite manufacturing process. Thus this parameters estimator scheme improves the resolver signal to noise ratio while at the same time reducing costs and complexity of the resolver interface, the net effect of which is to make the resolver a competitive option when choosing a position feedback sensor.

Both state and parameter estimation can be combined to form a joint estimation scheme. This scheme provides an integrated strategy for estimating plant states in the presence of resolver imbalances. The scheme however lacks the numerical efficiency which comes from a steady state solution of the estimator problem. Somewhat suboptimal performance is available given the realistic assumption that the dynamics of the parameters are slow in comparison with the dynamics of the plant. With this assumption the joint state and parameter estimation scheme can be decoupled into two separate estimation schemes. The resolver's imbalances detected with the parameter estimation scheme are used to correct the measurement information prior to state estimation. The sample frequency used for the parameter estimation scheme is chosen to reflect the rate at which the parameters are varying. However only linear imbalances can be corrected in this manner, hence the suboptimality.

The numerical efficiency of the Kalman implementation is a function of the Kalman form used for the estimator design and on the availability of a time invariant solution or steady state solution to the estimator problem. In this work it is shown that such a steady state solution exists for the non-linear resolver problem. Indeed it is shown that

the resolver problem is a superset of the optical Encoded estimator problem. The two estimator designs are equivalent except for the manner in which the innovation sequence is evaluated. Thus the subsequent robust controller designs for the resolver problem is applicable to the encoder problem with the modified innovation sequence.

For a given servo controller design it is necessary to establish bounds on the permissible load variations and the effects of disturbances on the stability of the closed loop system. Conventionally this stability verification is performed after the controller design. In this work these bounds on load variations are used as parameters in the controller design. This results in a well integrated controller design strategy. The design automates the conventional design and verification stages. The controller design is specified in terms of permissible variations on the load dynamics. The conventional time domain specifications are maximised subject to these load variation constraints.

The design strategy used in this work is to first and foremost satisfy the stability constraints subject to the load variation specification and then to satisfy the time domain design specifications. Often these design specifications may be conflicting, the robustness specifications are satisfied but the time domain specifications are not. Such conflicts can be used to size a particular actuator for a given application.

The particular controller used in this design is a linear quadratic gaussian controller with loop transfer recovery LQG/LTR. The LQ controller offers attractive robustness properties. The controller has an infinite gain margin a phase margin of 60° and a down side gain margin of 0.5. The LQG controller in an integration of the LQ design and a Kalman estimator used for state feedback. The loop transfer recovery procedure is used to recover the robustness properties of the LQ design.

The separation principle allows separate design of the LQ controller and the Kalman estimator, these combine to form the LQG controller. The robustness of a LQG controller is a function of the relative bandwidth of the LQ controller and the Kalman estimator. The LTR procedure formalises a mechanism for choosing the bandwidth of the estimator for a given controller design. In general the bandwidth of the estimator is faster than that of the controller. As the bandwidth of the estimator is increased the robustness of the LQG design improves. However as the bandwidth of the estimator is increased the noise attenuation properties of the estimator disimprove. Thus the robustness of a design is at the expense of the noise attenuation properties of the design.

The LTR procedure will recover the robustness of the LQG controller, however this is a blind recovery procedure, robustness is recovered for robustness sake without regard for the consequences of that recovery. Indeed as recovery unfolds the bandwidth of the estimator is increased, this increase is at the expense of the noise attenuation properties of the design, hence further recovery will potentially degrade performance. In this work the LQG/LTR synthesis procedure is augmented with a loop shaping procedure, robustness recovery is halted when robustness is within the established bounds.

In this work a relationship between sample frequency and optimality / robustness is established. This relationship provided a means of establishing the sample frequency for a particular robustness specification or vice versa. It also provides a technique for selecting a particular Kalman implementation. Indeed in an application where the computational resources are limited, as is the general case for most commercial application, there exists a trade-off between sample frequency, robustness, Kalman form and computational overhead. The relationships established in this work provides a mechanism for managing these trade-offs.

To overcome the degradation in noise attenuation or improve the noise attenuation in general a variation on the LTR design in presented, namely frequency shaped loop transfer recovery. Frequency shaping allows recovery to be focused on frequencies where the robustness improvements are required and not across the whole spectrum as in the case with conventional LTR. The net effect reduces the bandwidth of the estimator thus providing superior noise attenuation properties. The FS-LTR design augments the estimator and hence the resulting compensator with a minimum phase filter, the increased order of the compensator increases roll-off rate in the stopband further improving the noise attenuation properties within this band. In the case of this design the current amplifier model is used as a frequency shaping filter. The current amplifier focuses recovery at the crossover frequency for the closed loop system. The current amplifier model performs a dual function.

The disturbance rejection properties of the design are enhanced using a frequency shaped LQG design. In this case an estimate of the disturbance at the input to the plant is fed forward in the compensator. The disturbance estimator introduces an additional design parameter into the estimator design. Indeed there exists a trade-off between robustness and the disturbance suppression time of the system. This disturbance suppression technique provides asymptotic rejection of a disturbance even

in the presence of a saturated current amplifier. This feedforward technique performs the same role as an integrator in the controller without a degradation in command response performance.

By introducing an armature current measurement as an input to the estimator design improved noise attenuation and disturbance suppression properties are available. The robustness of the design is also improved, indeed the final design is almost optimal in a linear quadratic sense.

This work presents a design for a robust optimal servo motor controller with particular attention given to a resolver position sensor. The design is first and foremost robust, this robustness is at the expense of noise attenuation properties of the design. For robust applications it is necessary to have a good signal to noise ratio on the sensor interface.

LQG/LTR augmented with loop shaping is a very powerful design synthesis procedure. The procedure is conducive to educated trial and error design iterations, and offers a well defined trade-off management perspective on controller synthesis. Roughly 80% of the design effort is expended in specifying reasonable performance trade-off, stability-robustness constraints, and in establishing reasonable weighting parameters for the control and output variables. The details of the LQG/LTR and loop shaping design account for 20% of the effort.

5.2 Contribution of this Research.

The body of research presented in this dissertation is an extension of the linear quadratic controller with loop transfer recovery design methodology developed by Doyle in [Doyle 79]. This research augments the LTR procedure with a loop shaping halting criterion which places bounds on the robustness requirements of the design. This loop shaping criterion establishes physical significance to the interpretation of the robustness requirements of the design. This augmented procedure enables the designer to perform educated trade-off management between the robustness and the noise attenuation properties of the design. There are few published works which confront the practical design issues of a LQG/LTR controller, this research is presented as one such practical implementation of the LQG/LTR design methodology.

Discrete time LQG/LTR design issues have been studied by Maciejowski, Shaked and Ishihara in [Maciejowski 86], [Shaked 86] and [Ishihara 86]. These authors consider

the robustness recovery issues for the three common discrete implementations of the Kalman estimator. In this work the robustness recovery properties of a particular discrete Kalman implementation are used as a selection criterion for choosing the controller bandwidth, implementation sample frequency and discrete Kalman structure.

A unique steady state solution to the extended Kalman estimator problem particular to resolver sensor is developed in this work This steady state design aids in the practical implementation of the Kalman estimator

5.3 Further Areas for Research.

In this research a position and velocity servo is developed using a LQG/LTR design methodology The design assumes the availability of an existing current loop A suggested further area of research is to implement a digital current loop, this loop can be incorporated into the LQG/LTR design or can be implemented as a separate cascaded current loop A digital current loop should incorporate the protection and duty cycle functionality of the existing analogue current loop

The joint state and parameter estimation algorithm presented in this work can be extended to deal with further imperfections in the resolver sensor In particular, a non-sinusoidal resolver can be constructed cheaper than the existing sinusoidal design. The parameter estimator can accommodate a Taylor series expansion of this alternative resolver sensor The steady state solution developed here for the estimator problem is however unique to the sinusoidal resolver sensor.

With the availability of ample processing resources improvements to the signal to noise ratio of the resolver interface can be established by employing an oversampling / downsampling technique on the resolver channels.

References.

[Anderson 71] *Linear Optimal Control.* Brian D.O. Anderson and John B. Moore, Prentice-Hill 1971.

[Anderson 79] *Optimal Filtering.* Brian D.O. Anderson and John B. Moore, Prentice-Hill 1979.

[Anderson 89] *Optimal Control.* Brian D.O. Anderson and John B. Moore, Prentice-Hill 1989.

[Athans 86] *Tutorial on the LQG/LTR Method.* Michael Athans, Proc. American Control Conference, Seattle, WA, June 1986.

[Bierman 77] *Factorization Methods for Discrete Sequential Estimation.* Gerald J. Bierman. Academic Press Inc. 1977.

[Boyes 80] *Synchro and Resolver Conversion.* Edited by Geoffrey S. Boyes, Memory Devices Ltd. 1980. ISBN 0-916550-06-0.

[Bryson 75] *Applied Optimal Control.* Arthur E. Bryson, Jr. and Yu-Chi Ho 1975, Hemisphere Publishing Corporation, New York.

[Doyle 78] *Guaranteed Margins for LQG Regulators.* John C. Doyle, IEEE Transactions on Automatic Control, Vol. AC-23, no. 4, August 1978, pp. 756-757.

[Doyle 79] *Robustness With Observers.* John C. Doyle and G. Stein, IEEE Transactions on Automatic Control, Vol. AC-24, no. 4, August 1979, pp 607-611.

[Doyle 81] *Multivariable Feedback Design: Concepts for a Classical / Modern Synthesis.* John C. Doyle and Gunter Stein. IEEE Transactions Automatic Control, vol. AC-26, no 1, 1981, pp 4-16.

[Doyle 82] *Analysis of Feedback Systems with Structured Uncertainties.* John C. Doyle. IEE Proceedings vol. 129, Pt.D. no. 6 Nov 1982. pp 242-250.

[Franklin 80] *Digital Control of Dynamic Systems.* Gene F. Franklin, J. David Powell and Michael L. Workman. Addison-Wesley Publishing Company 1980.

[Gelb 74] *Applied Optimal Estimation.* Edited by Arthur Gelb. Massachusetts Institute of Technology. 1974.

[Graham 53] *The Synthesis of "Optimum" Transient Response: Crireria and Standard Forms.* Dunstan Graham and R.C. Lathrop, Trans. AIEE 1953 Vol. 72 Part 2. pp. 273-288.

[Grimble 88a] *Optimal Control and Stochastic Estimation Volume 1.* Michael J. Grimble and Michael A. Johnson. John Wiley & Son 1988.

[Grimble 88b] *Optimal Control and Stochastic Estimation Volume 2.* Michael J. Grimble and Michael A. Johnson. John Wiley & Son 1988.

[Hanselman 90] *Resolver Signal Requirements for High Accuracy Resolver-to-Digital Conversion.* Duane C. Hanselman. IEEE Transactions on Industrial Electronics. Vol. 37, No. 6, December 1990, pp 556-561

[Hanselmann 87] *Implementation of Digital Controllers- A Survey.* H. Hanselmann. Automatica, Vol. 23. No. 1. 1987. pp 7-32

[Haykin 89] *Modern Filters.* Simon Haykin. Macmillan Publishing Company NY. 1989. ISBN 0-02-352750-1

[Hori 88] *Disturbance Suppression on an Acceleration Control Type DC Servo System.* Yoichi Hori. IEEE Proc. PESC 1988. pp 222-229.

[Hori 89] *Position and Mechanical Impedance Control Method for Robot Actuators Based on the Acceleration Control.* Yoichi Hori. IEEE Proc. PESC 1989. pp 423-430.

[Ishihara 86] *Loop Transfer Recovery Techniques for Discrete-Time Optimal Regulators Using Prediction Estimators.* T. Ishihara, H. Trakeda. IEEE Transactions on Automatic Control, Vol. AC-31, No. 12, Dec 1986, pp 1149-1151.

[Jazwinski 70] *Stochastic Processes and Filtering Theory.* Andrew H. Jazwinski. Academic Press 1970.

[Kalman 60] *A New Approach to Linear Filtering and Prediction Problems.* R.E. Kalman Trans. ASME. Journal of Basic Eng., Mar 1960, Vol . 82, pp 34-45.

[Kalman 64] *When is a linear control system optimal.* R.E Kalman. Transactions of the ASME Journal of Basic Engineering. March 1964 pp 51-60.

[Kettle 93] *Disturbance Rejection and DC Motor Control.* P.J. Kettle and A. Murray. Proc. Irish Colloquium on DSP & Control, June 1993 pp. 43- 50.

[Kwakernaak 72] *Linear Optimal Control Systems.* Huibert Kwakernaak and Raphael Sivan, Wiley Intersciences 1972.

[Lewis 86] *Optimal Control.* Frank L. Lewis 1986. John Wiley & Son, Inc.

[Little 92] *Control System Toolbox for use with Matlab®*, John N. Little, July 1992.

[Ljung 79] *Asymptotic Behavior of the Extended Kalman Filter as a Parameter Estimator for Linear Systems.* Lennart Ljung. IEEE Transactions on Automatic Control, Vol. AC-24, No. 1, February 1979. pp 36-50.

[Lorenz 88] *High Resolution Velocity Estimation for All Digital, AC Servo Drives.* Robert D. Lorenz and Keith Van Patten. IEEE IAS Conf. Pittsburgh USA Oct. 1988. pp 363-368.

[Maciejowski 85] *Asymptotic Recovery for Discrete-Time System.* J. M. Maciejowski, IEEE Transactions on Automatic Control, Vol. AC-30, No. 6, Jun 1985, pp 602-605.

[Maciejowski 89] *Multivarable Feedback Design.* J.M Maciejowski. Addison-Wesley Publishers Ltd.. 1989.

[Mendel 71] *Computational Requirements for a Discrete Kalman Filter.* Jerry M. Mendel. IEEE Transactions On Automatic Control, Vol. AC-16, No. 6 December 1971. pp 748-758.

[Mendel 87] *Lessons in Digital Estimation Theory.* Jerry M. Mendel. Prentice-Hall 1987.

[Moore 81] *Performance and Robustness Trades in LQG Regulator Design.* John B. Moore, Dagfinn Gangsaas and James D. Blight. 20th IEEE Conf. Decision and Control, San Diego 1981, pp 1191-1200.

[Murray 91] *Digital Tracking Resolver to Digital Conversion.* A. Murray,W.D. Li, M.F. McMullin. European Power Electronics Conference. Florence, September 1991.

[Nakao 87] *A Robust Decentralized Joint Control Based On Interference Estimation.* Masato Nakao, Kouhei Ohnishi and Kunio Miyachi. IEEE International Conf. on Robotics and Automation, Vol. 1, 1987. pp 326-331.

[Ohishi 87] *Microprocessor-Controlled DC Motor for Load-Insensitive Position Servo System.* Kiyoshi Ohishi, Masato Nakao, Kouhei Ohnishi and Kunio Miyachi. IEEE Transactions on Industrial Electronics. Vol. IE-34, No.1, February 1987, pp 44-49.

[Ohishi 89a] *High Performance Motion Control Based on Model Following Acceleration Joint Control Method.* Kiyoshi Ohishi, Yasumasa Ogino and Masaaki Hotta. Proc. IEEE Int. Conf. on Robotics and Automation, Vol. 3, 1989. pp 1792-1798

[Ohishi 89b] *DSP-Based DC Servo Acceleration Control Without Speed Sensor.* Kiyoshi Ohishi, Satoshi Matsuda and Kouhei Ohnishi. IEEE Proc. IAS San Diego California 1989, pp 480-485.

[Rognon 88] *A Simple Speed Observer for Digitally Controlled Motor Drives at Low Speeds.* J.P. Rognon, D. Roye, D.E. Sheng Zhu. IEEE Proc. IAS Conf. Pittsburgh, USA Oct. 1988. pp 369-375.

[Rosenbrock 71] *Good, Bad, or Optimal ?,* Howard H. Rosenbrock and Peter D. McMorran. IEEE Transactions on Automatic Control, Vol. AC-16, No. 6, Dec 1971, pp 552-554.

[Safonov 77] *Gain and Phase Margins for Multiloop LOG Regulators.* M. G. Safonov and M. Athans. IEEE Transactions on Automatic Control, Vol. AC-22, No. 2, April 1977, pp173-179.

[Safonov 81] *Feedback Properties of Multivariable Systems: The Role and Use of the Return Difference Matrix.* Michael G. Safonov, Alan J. Laub and Gary L. Hartmann. IEEE Transactions. Automatic Control., Vol AC-26, no. 1, Feb 1981, pp 47-65.

[Schmidt 92] *Design Principles and Implementation of Acceleration Feedback to Improve Performance of DC Drives.* Peter B. Schmidt and Robert D Lorenz. IEEE Transactions on Industry Applications, Vol 28, No. 3. May/June 1992 pp 594-599.

[Schuchman 64] *Dither Signals and Their Effect on Quantization Noise.* Leonard Schuchman. IEEE Transactions on Communications Technology Vol. 12, December 1964. pp 162-165.

[Shaked 86] *Guaranteed Stability Margins for the Discrete-Time Linear Quadratic Optimal Regulator.* U. Shaked, IEEE Transactions on Automatic Control. Vol. AC-31, No. 2. Feb. 1986, pp 162-165.

[Sripad 77] *A Necessary and Sufficient Condition for Quantization Error to be Uniform and White.* Anekal B Sripad and Donald L Snyder. IEEE Transactions on Acoustics, Speech and signal Processing Vol. ASSP-25, No. 5 October 1977, pp 442-448

[Swaszek 85] *Quantization* Peter F Swaszek. Benchmark Papers in Electrical Engineering and Computer Science, Van Nostrand Reinhold Company NY 1985.

[Vaughan 70] *A Nonrecursive Algebraic Solution for the Discrete Riccati Equation.* David R Vaughan. IEEE Transactions on Automatic Control, Oct 1970, Vol AC-15 pp. 597-599

[Verhaegen 86] *Numerical Aspects of Different Kalman Filter Implementations.* Michel Verhaegen and Paul Van Dooren. IEEE Transactions on Automatic Control Vol. AC-31, No 10, October 1986

[Willems 78] *The Return Difference for Discrete-Time Optimal Feedback Systems.* Jacques L. Willems and Hermam Van De Voorde. Automatica Vol. 14 , 1978, pp 511-513

[Zames 81] *Feedback and Optimal Sensitivity Model Reference Transformations, Multiplicative Seminorms, and Approximate Inverses.* George Zames. IEEE Transactions on Automatic Control Vol AC-26, no.2 Apr 1981 pp 301-320

[Zames 83] *Feedback, Minimax Sensitivity, and Optimal Robustness* George Zames and Bruce A Francis IEEE Transactions Automatic Control Vol AC-28, no 5, May 1983, pp 585-601.

Appendix A.

A.1 Resolver Envelope Detection Circuit.

Each resolver channel must be demodulated so that the sine and cosine information can be extracted. A classical envelope detection described by Figure [A-1] will perform the task. However the turnon voltage of the diode will cause non-linearities at or about the origin of the resulting wave. For this reason a more elaborate technique is required. With the availability of the carried signal it is possible to use this signal to change the sign of the modulated signal, the resulting waveform is then filtered through a low pass filter. The output is the desired sine and cosine information. Figure [A-3] describes the circuit and Figure [A-3] described the wave form at different stages of the circuit. Note that the carried signal must undergo phase correction to allow for the characteristic phase shift of the resolver.

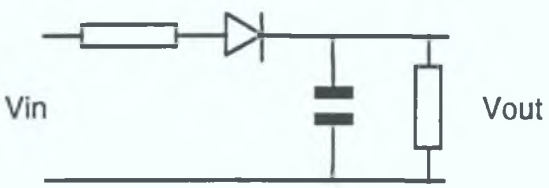

Fig. [A-1] Envelope Detector (passive).

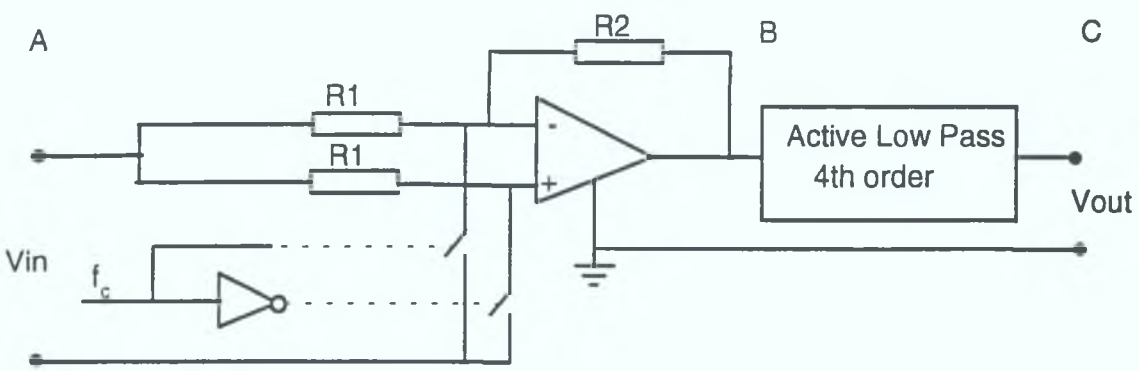

Fig. [A-2] Envelope Detector (Active).

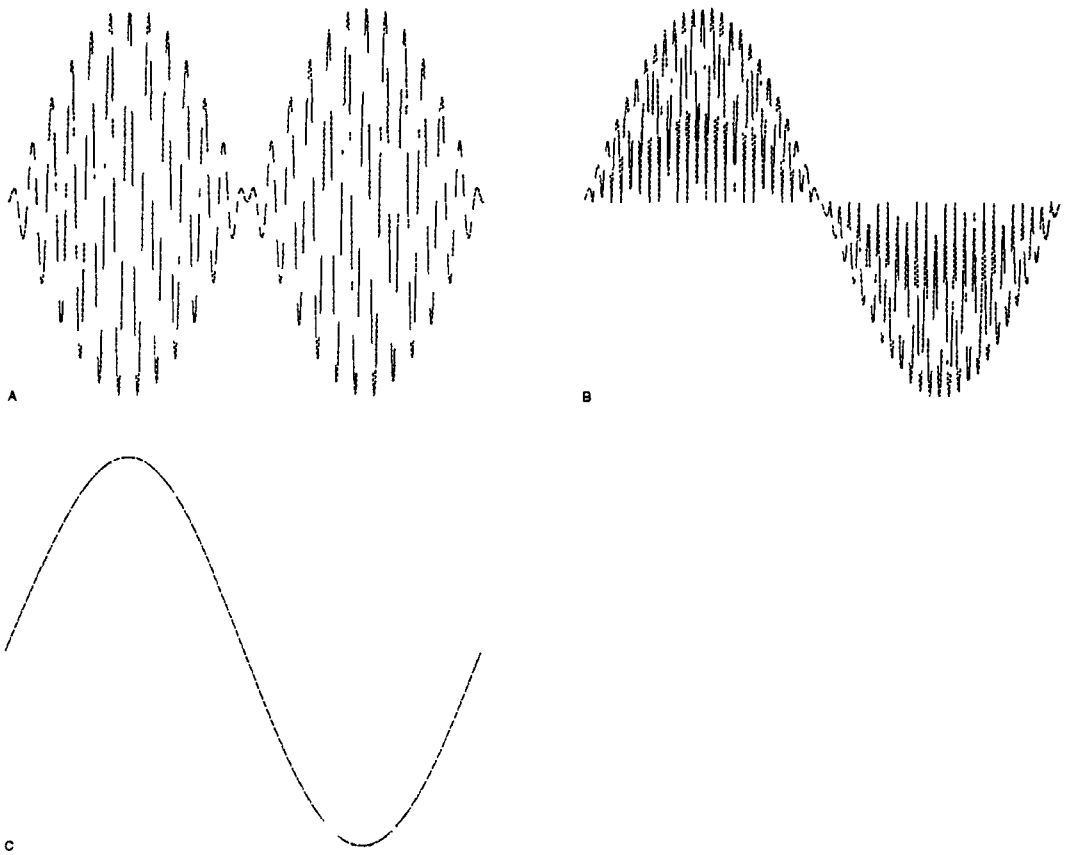

Fig. [A-3] Envelope Detector at stages A, B and C.

A.2 The Inverter.

This section deals with the analytical modelling of the AEG PWM/K Inverter. This modelling is carried out to provide validation for the empirical work in the plant model identification. Figure [A-3] represents the Inverter broken down into its essential components. Subsequent sections will take a closer look at these components.

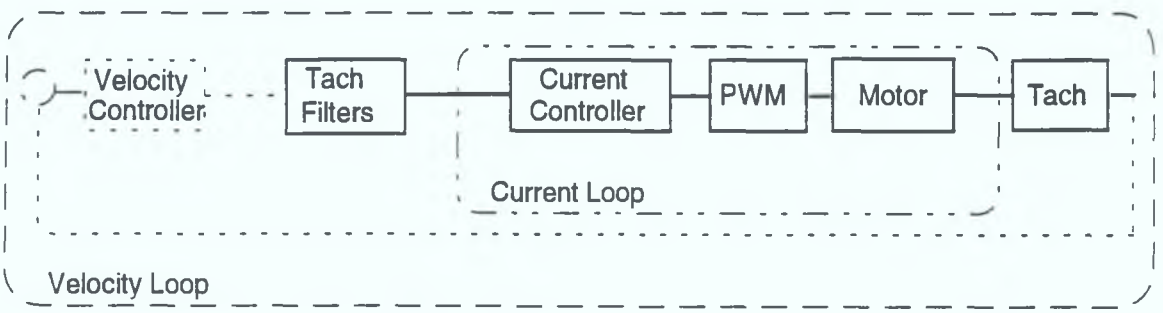

Fig. [A-4] AEG Inverter.

A.2.1 Current Loop

Figure [A-4] represents a model of the AEG current loop. The current controller used in the AEG PWM/K Inverter is a PI controller with phase lead-lag correction. The circuit and transfer function for this controller are given in Figure [A-5] and equation [A-1]. The output of the current controller is filtered through a low pass filter and in turn drives the PWM generator.

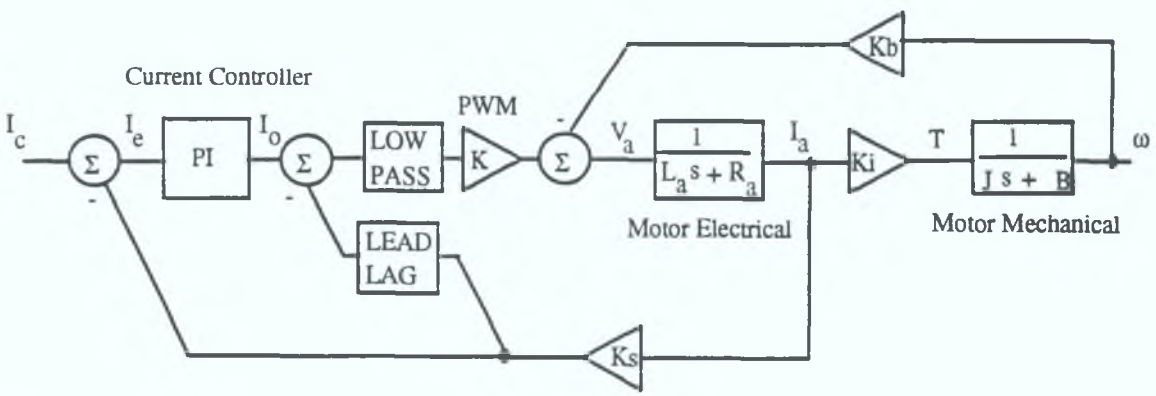

Fig. [A-5] Current Loop.

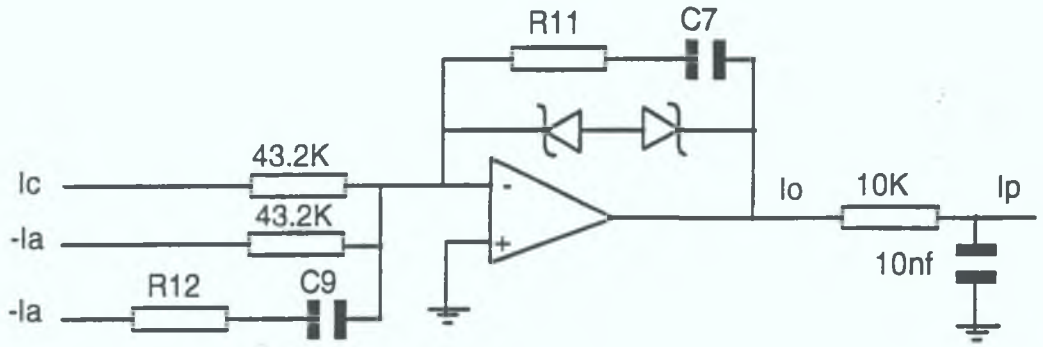

Fig. [A-6] Current controller.

$$I_o = \frac{R_{11}s + 1/C_7}{43.2e^3 s}(I_c - I_a) - \frac{R_{11}s + 1/C_7}{R_{12}s + 1/C_9} I_a \qquad \text{[A-1]}$$

The remaining parameters for the model depicted in Figure [A-5] can be obtained from the date sheets or via direct measurement of the component values, Table [A-1] shows these values and indicates their sources. A transfer function for the closed loop system is given by equation [A-2][25]. It is evident from the transfer function that the current amplifier has fifth order dynamics. By performing pole zero cancellation on this model, the closed loop system can be approximated by a second order system given by equation [A-3]. The roots of the closed loop system and its reduced order model are given in tables [A-2] and [A-3]. Figure [A-6] represents a Bode plot for full current loop and Figure [A-7] represents the step response of the current loop.

Parameter	**Value**	*Description*	*Source*
K_b	0.506	Back EMF const.	Data Sheets
K_i	0.506	Torque Constant	Data Sheets
K_s	1/10 Amp/Volt	Current Sensor FB	Measured
K_{PWM}	14	PWM Gain	Measured
La	3.2 mH	Inductance @1kHz	Date Sheets
J	0.0014	Inertia	Date Sheets
K_{Pc}	2.3	Proportional Gain	Component Values
K_{Ic}	476.2	Integral Gain	Component Values
La (drive)	2.83 mH	Drive Inductance	Measured
Ra (drive)	1.226 Ω	Armature Resistance	Measured

[25] This tranfer function was obtained using block manipulation functions within matlab.

La (load)	3.06 mH	Load Inductance	Measured
Ra (load)	1.130 Ω	Armature Resistance	Measured
C7	20 nf	Lag Cap.	Measured
R11	100K Ω	Lag Res.	Measured
C9	22 nf	Lead Cap.	Measured
R12	100K Ω	Lead Cap.	Measured
C1	9 nf	Tach Filter A	Measured
C3	9 nf	Tach Filter C	Measured

Table [A-1] Current loop parameter values

$$\frac{I_a}{I_c} = \frac{-3.638e-12s^4 + 1.013e8s^3 + 9.603e10s^2 + 2.27e13s + 5.674e12}{s^5 + 1.076e4s^4 + 2.23e4s^3 + 1.347e10s^2 + 2.4e10s + 5.674e11} \qquad \text{[A-2]}$$

Poles	Zeros
s = -8255	s = 2.783e19
s = -1642.7	s = -494.969
s = -534	s = -453.244
s = -331	s = 0
s = -0.2	

Table [A-2] Root locations of the full closed loop systems

$$\frac{I_a}{I_c} = \frac{1.2e4s + 5.44e6}{s^2 + 1.97e3s + 5.44e5} \qquad \text{[A-3]}$$

$$\left.\frac{I_a}{I_c}\right|_{s=0} = 10 \qquad \text{[A-4]}$$

Poles	Zeros
s = -1642.7	s = -453.244
s = -331	

Table [A-3] Root locations of the reduced order closed loop systems

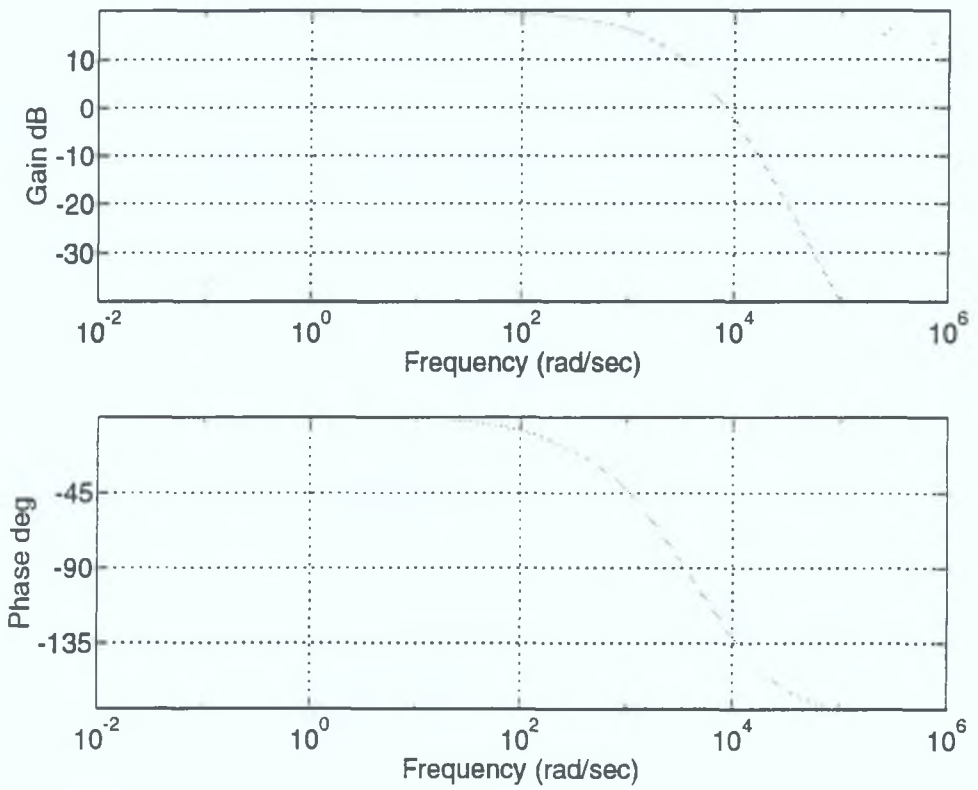

Fig. [A-6] Bode plot of AEG current loop .

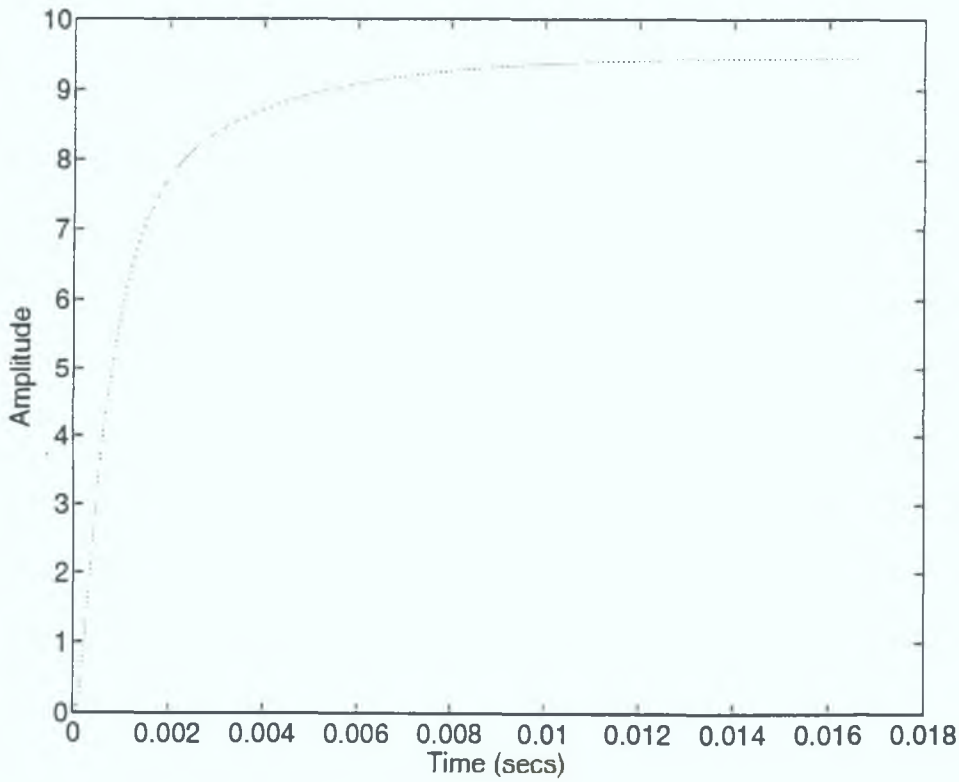

Fig. [A-7] Step response of AEG current loop .

A.2.2 The Tachogenerator Filter.

Commands from the DSP are fed into the AGE Inverter at the input to the Tachogenerator filter A. Bypassing this filter will remove the current protection from the Inverter. The output from the Tachogenerator filter C feeds directly into the current command of the current controller The Tachogenerator filters are thus in the forward path of a potential closed loop system. The transfer function for this filter configuration depicted in Figure **[A-8]**, is given in equation **[A-5]** and the corresponding Bode plot is given in Figure **[A-9]** As is evident from the Bode plot the Tachogenerator filter's cut-off frequency is much faster than that of the current controller. Thus the presence of this filter is often neglected while modelling the open loop system. The Tachogenerator filters do however contribute to a faster gain roll-off, for the cascaded open loop system The phase roll-off of the Tachogenerator filters is also inside the bandwidth of the current controller, and bears consideration in the context of phase margins for the closed loop system

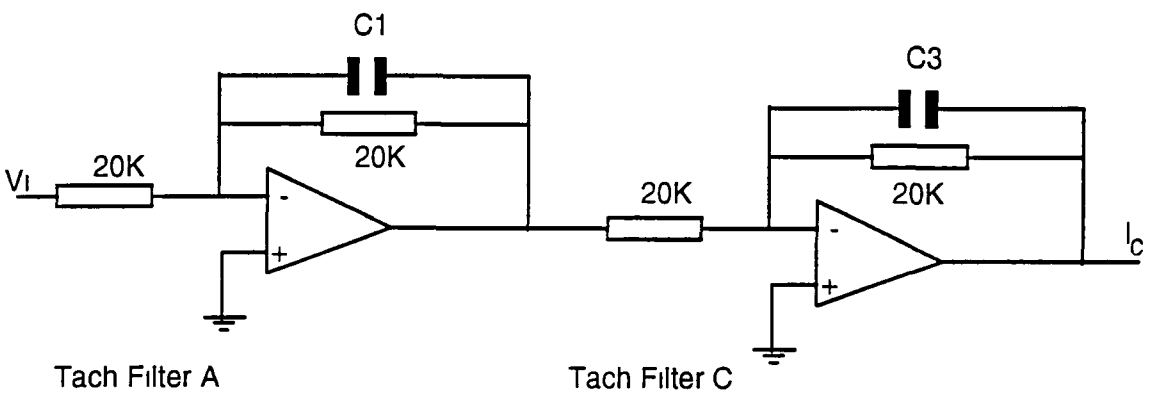

Fig. [A-8] AEG Tachogenerator filter A&C.

$$\frac{I_c}{V_I} = \frac{1}{(RCs+1)^2} = \frac{1}{(1\ 8e-4+1)^2} \qquad \text{[A-5]}$$

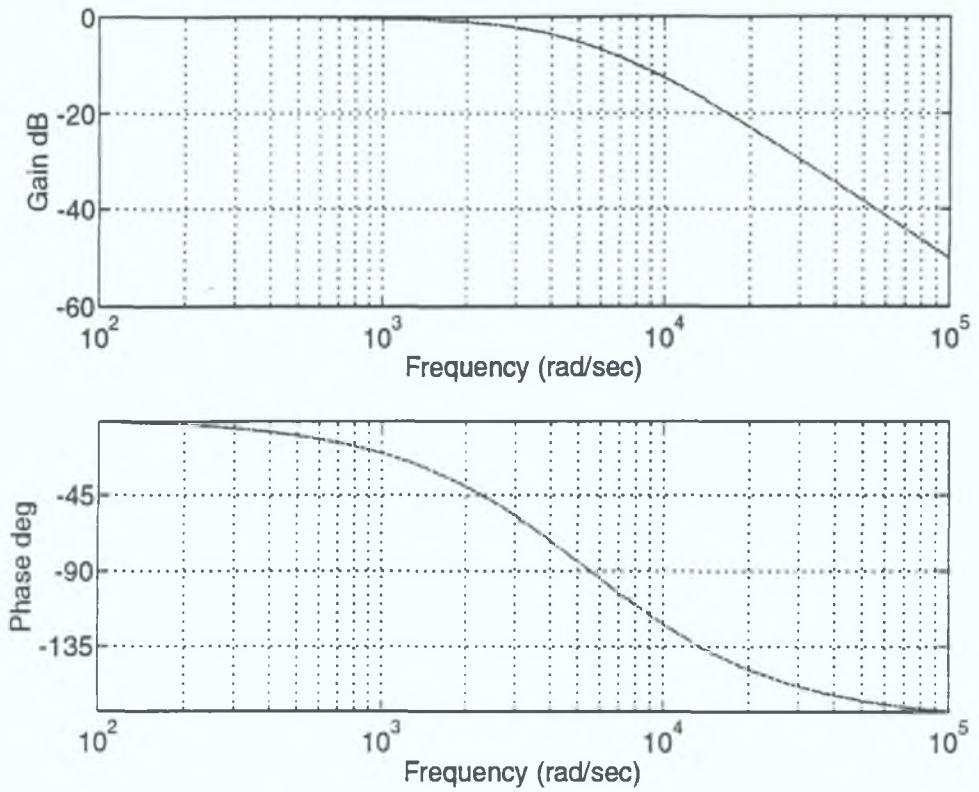

Fig. [A-9] Bode plot of AEG Tachogenerator filters A&C cascaded.

A.2.3 Velocity Loop.

The AEG velocity controller is a PI controller. The circuit and transfer function for this controller are given in Figure [A-11] and equation [A-8].

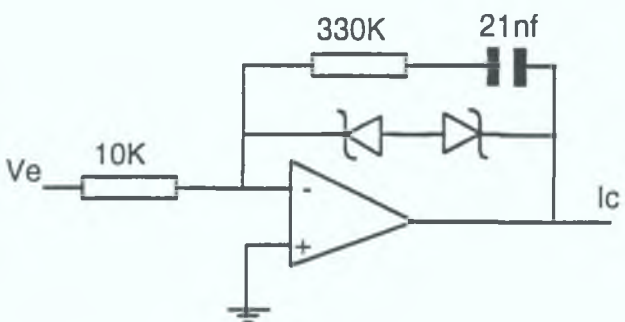

Fig. [A-11] PI velocity controller.

$$\frac{Ic}{Ve} \approx K_{Pv}(1 + K_{Iv}/s) = 33(1 + 144/s) \qquad \textbf{[A-8]}$$

The AEG velocity loop is the cascaded combination of the velocity controller, Tachogenerator filters, current loop and the motor.

Appendix B.

B.1 comp_model.m

```
function [al,bl,cl,dl]=comp_model(A,B,H,af,bf,cf,df,type);
%COMP_MODEL.  This function augments plant and compensator
%            [al,bl,cl,dl]=comp_model(A,B,H,af,bf,cf,df);
%            where ABC described the plant and
%            where af..df described a SS dicscrption of the
%            compensator. The first n states correspond to the
%            compensator states.
%            The output corresponds to the compensator
%            output and the controller input u(k)..
%            Use type 'default'
%            The output corresponds to the disturbed output
%            Use time 'disturbance'
%            Paul Kettle 16/4/1994
%
%       Related Functions models.m fs_model.m

if findstr(type,'def')

%augmented model discription (default)
%output following
al=[af bf*H;-B*cf A-B*df*H];bl=[bf ;-B*df];
dl=df; cl=[df*H -cf];
%becouse the system is output following, the estimator states drive to zero
%consequently the u will converg to zero. To over come u=Kx and
%cl=[-cf df*H];
end

%distrubance model
if findstr(type,'dis')
al=[af bf*H;-B*cf A-B*df*H];
bl=[zeros(size(af)*[1; 0],1) ;B];
cl=[zeros(size(H)*[1;0],size(af)*[0;1]) H];
dl=df;
```

```
end

% reference input followning
if findstr(type,'input')
al=[af bf*H;-B*cf A-B*df*H];
%bl=[zeros(size(af)*[1; 0],size(B*cf)*[0;1]) ;B*cf];
bl=[[0 ;B]*cf+bf*H*B*cf;[0 B]*cf];
%bl=[bf;B*cf];
cl=[zeros(1,size(af)*[0;1]) H];
dl=df;
end

% closed loop system command to output
if type(1)=='c'
[al,bl,cl,dl]=series(af,bf,cf,df,A,B,H,[0]);
[al,bl,cl,dl]=cloop(al,bl,cl,dl);
end

% closed loop system controller output
if type(1)=='u'
[al,bl,cl,dl]=series(af,bf,cf,df,A,B,H,[0]);
[al,bl,cl,dl]=cloop(al,bl,cl,dl);
[al,bl,cl,dl]=series(al,bl,cl,dl,af,bf,cf,df);
end
```

B.2 models.m

```
function [af,bf,cf,df,bfi]=models(A,B,C,D,K,L,method)
%
%MODELS Returns a state space model for the compensator defined by method
%       [af,bf,cf,df]=models(A,B,C,D,K,L,method)
%       method= 'predictive' |'current' |'smoother' |'fsfb'
%       Paul Kettle 11/3/1994
Kc=K;
Kf=L;
H=C;
%Current comp.. default


if method(1)=='c'
af = A - L*H*A -B*Kc +L*H*B*K ;
bf = L; cf = K; df = zeros(size(Kc)*[1;0],size(Kf)*[0;1]);
bfi=[B*K+L*H*B*K];
end

% Full state feedback for LQ case
if method(1)=='f'
af=zeros(size(A));
bf=zeros(size(B))
cf=K;
df=zeros(size(D));
end

%predictive compensator
if method(1) =='p'
disp('Predictive model')
Kc=K;
Kp=A*L;
af=A-B*K-Kp*C;
bf=Kp;
cf=K;
df=zeros(size(Kc)*[1;0],size(Kf)*[0;1]);
% account for 1 sample delay !
```

```
af=[0 zeros(1,size(af)*[0;1]); bf af];
bf=[1;zeros(size(bf)*[1;0],1)];
cf=[0 cf];
end

%Smoother compensator
if method(1) =='s'
disp('Smoother model')
af=(A-B*Kc)*(eye(size(L*C))-L*C);
bf=(A-B*Kc)*L;
cf=Kc*(eye(size(L*H))-L*H);
df=Kc*L;
end
```

B.3 costs.m

```
function [J,x,u,xn,un]=costs(A,B,H,D,K,L,Q1,Q2,method)
%
%COSTS evaluates the LQG cost normalised against the LQ cost
%       [J,x,u,xn,un]=costs(A,B,C,D,K,L,Q1,Q2,method)
%       where K is the controller gain
%       L is the estimator gain
%       method= 'predictive' |'current' |'smoother'
%

Kc=K;
Kf=L;
C=H;
D=[0];

[af,bf,cf,df]=models(A,B,H,D,K,L,method) ;

%augment plant and compensator
al=[af bf*H;-B*cf A-B*df*H];bl=[bf ;-B*df];
dl=df; cl=[df*H -cf];
[u,x]=dstep(al,bl,cl,dl,1,500);

x=x(:,(size(af)*[1;0]+1):,max(size(x)))';
if method(1)=='p'
x=x(2:3,:); % remove delay state
end
range=1:200;

x=x(:,range);
u=u(range,:);

Ja=sum(diag(x'*Q1*x))+sum(diag(u'*Q2*u))

[un,xn]=dstep(A-B*K, -B*K*H',-K,D,1,500);
xn=xn';
xn=xn(:,range);
```

```
un=un(range,:),

Jn=sum(diag(xn'*Q1*xn))+sum(diag(un'*Q2*un))
J=Ja/Jn
```

B.4 perbou.m

```
function [num,den]=perbou(num1,den1,num2,den2)
%       This function construct a preturbation bound function for the
%       multiplacitive uncertanity Pm=num1/den1
%       and numinal plant P=(num2/den2)
%       The function returns [num,den]=(Pm(s)-P(s))/P(s)
%       Author Paul Kettle 7/5/1994

%       This function is used in establishing the performance bounds of
%       a given controller using the sensitivity function


n1=conv(num1,den2),
n2=conv(den1,num2),
if length(n1) > length(n2)
num=n1-[zeros(1,length(n1)-length(n2)) n2],
else
num=[zeros(1,-length(n1)+length(n2)) n1]- n2,
end
den=conv(den1,num2),
```

B.5 designc.m

```
% This script executes a full design cycle for the different controller implementations
% The models used in this design are those for the system with current loop
% dynamics and armature current measurement information
% The controller design in specified using a single parameter "design"
% This parameter is a string containing the following keywords
%LQG design Keywords: {current , smoother ,predictive, LQG , PI_LQG, DE_LQG
%                      qe,qc,Input_ref}
%
% qe and qc represent the free design parameter for the LQ controller
% and Kalman estimator
% If qe or qc are not specified in the design string then there default values
% will be used.

K1= 10.38;
K2= 9.4123;
Ki= 0.506;
Jmm=0.00505;
Bmm=0.001445;

if ~size(findstr(design,'qc'))*[1;0]
qc=350;
end

if ~size(findstr(design,'qe'))*[1;0]
qe=1;
end

if findstr(design,'current')
method='current';
elseif findstr(design,'predictive')
method='pre';
elseif findstr(design,'smoother')
method='smoother';
end
```

```
disp(sprintf('LQ design parameter is set to %f',qc));
disp(sprintf('Estimator design parameter is set to %f',qe));
disp(sprintf('Nominal controller design'));

%current amplifier
denc=[1 -0.941 -0.0404];
numc=-[0 -0.3752 0.1815]*K2;
[numcc,dencc]=d2ctf(numc,denc,1/30000);
[numcd,dencd]=c2dtf(numcc,dencc,1/5000);
[ac,bc,cc,dc]=tf2ss(numcd,dencd);
%
T=1/5000;
disp(sprintf('Sample frequency set to %fKhz',1/T));
%Plant model
Am=[-Bmm/Jmm 0;1 0];
Bm=[Ki/Jmm;0];
cm=[0 1];
dm=[0];
[am,bm]=c2d(Am,Bm,T);
[numm,denm]=ss2tf(am,bm,cm,dm);

%Augmented plant motor and current loop
[numa,dena]=series(numcd,dencd,numm,denm);
[aa,ba,ca,da]=series(ac,bc,cc,dc,am,bm,cm,dm)
am=aa;
bm=ba;
cm=ca;
dm=da;

[amc,bmc]=d2c(am,bm,T);
[numm,denm]=ss2tf(amc,bmc,cm,dm);

Q1=[(1/268)^2 0; 0 (1/(pi))^2];
Q1=[1/(50/cc(1))^2 0 0 0;0 1/(50/cc(2))^2 0 0;[zeros(2,2) Q1]*qc2/qc]*qc3
Q1=Q1+bm*bm'*qc4

Qc=Q1;
Qcd=Q1;
```

```
Q2=1;

if findstr(design,'LQG')
disp('Nominal Controller design for LQG')
[K,S,E]=dlqr(am,bm,Q1*qc,Q2);
gama=(bm'*S*bm+1)^(-0.5);
disp(sprintf('Andersons Gamma %f',gama))
disp('Nominal Estimator design for LQG')
ae=am;be=bm;ce=cm;de=dm;
H=[cm];
R=1;
G=bm;
Qe=G*G';
[L,Se,Ee]=dlqr(am',H',Qe*qe,R);
end

if findstr(design,'PI_LQG')
disp('PI-LQG controller design')
[aam]=[am zeros(max(size(am)),1);H*T 1];
[bam]=[bm;0];
Qa=[Q1 [0;0];0 0 150];
R=1;
[K,S,E]=dlqr(aam,bam,Qa*qc,R);
end

if findstr(design,'DE_LQG')
disp('Kalman disturbance estimator')
Ae=[1 zeros(1,size(am)*[1;0]) ;bm am];
Be=[0 ;bm];
ce=[0 cm];
de=[0];
H=[0 H;K1*K2 cc 0 0 ];
R=[1 0; 0 500];
ae=Ae;
be=Be;
Qe=[0.0000003 0 0 0 0; 0 0 0 0 0 ; 0 0 0 0 0; 0 0 0 1 0; 0 0 0 0 0];
[L,S,Ee]=dlqr(ae',H',Qe*qe,R);
end
```

```
if findstr(design,'PI_LQG')

disp('Building compensator model PI_LQG')
A=[am zeros(max(size(am)),1);H*T 1];
B=[bm;0];
C=[cm 0];
L=[L 0];
[af,bf,cf,df]=models(A,B,C,dm,K,L',method);
[al,bl,cl,dl]=comp_model(am,bm,cm,af,bf,cf,df,'def');
[bli]=compb_model(am,bm,cm,A,B,C,[0],K,L','PI_LQG');
[ald,bld,cld,dld]=comp_model(am,bm,cm,af,bf,cf,df,'dis');
[y,x]=dstep(al,bli*[0 0 1]',cld,dl,1,5000);

elseif findstr(design,'DE_LQG')
 if findstr(design,'Input_ref')
 disp('Building compensator model I-DE_LQG')
 [af,bf,cf,df]=models(ae,be,ce,de,[1 K],L',[method]);
 [al,bl,cl,dl]=comp_model(am,bm,cm,af,bf,cf,df,'def');
 [bli]=compb_model(am,bm,cm,ae,be,ce,de,K,L','DE_LQG');
 [ald,bld,cld,dld]=comp_model(am,bm,cm,af,bf,cf,df,'dis');
 [y,x]=dstep(al,bli*[0 0 1]',cld,dl,1,5000);
 [yv,xv]=dstep(al,bli*[0 1 0]',[0 0 0 1 0],dl,1,5000);
return
else
disp('Building compensator model DE_LQG')
[af,bf,cf,df,bfi]=models(ae,be,H,de,[1 K],L',method);
[al,bl,cl,dl]=comp_model(am,bm,[cm;cc 0 0],af,bf,cf,df,'def');
[ald,bld,cld,dld]=comp_model(am,bm,[cm;cc 0 0],af,bf,cf,df,'dis');
 end
elseif findstr(design,'LQG')
disp('Building compensator model LQG')
[af,bf,cf,df]=models(am,bm,cm,dm,K,L',method);
[al,bl,cl,dl]=comp_model(am,bm,cm,af,bf,cf,df,'def');
[ald,bld,cld,dld]=comp_model(am,bm,cm,af,bf,cf,df,'dis');
end
```

B.6 bou.m

```
%This script plots perturbation bounds for Inertia variations, viscosity variations,
%current amplifier variations saturation and variations and a worst case variation. The
%system is specified using the designc.m script.

numm=Ki;
denm=[Jmm Bmm];
denc=[1 -0.941 -0.0404];
numc=-[0 -0.3752 0.1815]*K2;
[numcc,dencc]=d2ctf(numc,denc,1/30000);
[numm,denm]=series(numcc,dencc,numm,denm);

%a1=am(1:3,1:3);
%b1=bm(1:3);
%c1=[0 0 1];
%[a1,b1]=d2c(a1,b1,T);
%[numm,denm]=ss2tf(a1,b1,c1,dm);
delta=2

%Inertia increases a Factor of 4 (delta=2) times the nominal

[n1,d1]=series(numcc,dencc,Ki,[delta*Jmm Bmm]);
[n,d]=perbou(n1,d1,numm,denm)
bodem(d,n,w);

%Viscusity of load increased by a fact of delta times the nominal

[n1,d1]=series(numcc,dencc,Ki,[Jmm Bmm*delta]);
[n,d]=perbou(n1,d1,numm,denm)
bodem(d,n,w);

%Current amplifier saturating

[n,d]=series(n1,d1,1,2);
[n,d]=perbou(n,d,numm,denm);
bodem(d,n,w);
```

```
%id current loop

%denc=[1 -0.941 -0.0404]
%numc=[0 -0.3752 0.1815]
%[numcc,dencc]=d2ctf(numc,denc,1/30000);
%[n2,d2]=series(numcc,dencc,numm,denm);
%[n2,d2]=series(1,dcgain(numcc,dencc),n2,d2);
%[n,d]=perbou(n2,d2,numm,denm);
%bodem(d,n,w);

% Tachogenerator filters

[numtc,dentc]=series([1],[1.8e-4 1],[1],[1.8e-4 1]);
%[numt,dent]=c2dtf(numtc,dentc,1/5000);
[n2,d2]=series(numtc,dentc,numm,denm);
[n,d]=perbou(n2,d2,numm,denm);
bodem(d,n,w);

%Theoritical current loop

%n1=[1.2e4 5.44e6];
%d1=[1 1.97e3 5.44e5];
%n1=[-3.638e-12 1.013e8 9.603e10 2.27e13 5.674e12];
%d1=[1 1.076e4 2.23e7 1.347e10 2.4e12 5.674e11];
%[n2,d2]=series(n1,d1,numm,denm);
%[n2,d2]=series(1,dcgain(n1,d1),n2,d2);
%[n,d]=perbou(n2,d2,numm,denm);
%bodem(d,n,w);

% Everything at once

[numc,denc]=series([1],[1.8e-4 1],[1],[1.8e-4 1]);
[n2,d2]=series(numc,denc,numcc,dencc);
[n2,d2]=series(n2,d2,0.5,[delta*Jmm delta*Bmm]);
[n,d]=perbou(n2,d2,numm,denm);
bodem(d,n,w);
```

B.7 nyq2.m

```
function [resp,est_resp]=nyq2(A,B,H,af,bf,cf,df,K,L,Ts,w,gama)
% This function draws a Nyquist plot local to a unit circle centered about
% the point (-1,0)

count=0;
axis([-2,0,-1,1]),

limits = axis,
plot([limits(1 2),0,0]',[0,0,limits(3 4)]','w '),

count=0,

Kc=K,
Kf=L,
C=H,
D=[0],
hold on
circle(gama,200,[-1 0])
circle(1,200,[0 0]),

[al,bl,cl,dl] = series(af,bf,cf,df,A,B,C,D),
[re,im] = dnyquist(al,bl,cl,dl,Ts,1,w),

plot(re,im,re,-im),
return
if method(2)=='b'
        figure(2)
        dbode(al,bl,cl,dl,Ts),
        figure(1)
endfunction [num,den]=sensit(al,bl,cl,dl,as,bs,cs,ds)
```

B.8 sensit.m

```
% SENSIT determines the a sensitivity function for a plant and estimator
%       in series
%       [num,den]=sensit(al,bl,cl,dl,as,bs,cs,ds)
%       al..dl represent the state space discription of estimator
%       as .ds represent the state space discription of the plant
%       S(z)=num/den
%       Paul kettle 11/3/1994
%

[A,B,C,D]=series(al,bl,cl,dl,as,bs,cs,ds),

[nums,dens]=ss2tf(A,B,C,D,1),

num=dens,
den=nums+dens,
```

B.9 csensit.m

```
function [num,den]=csensit(al,bl,cl,dl,as,bs,cs,ds)
% SENSIT determines the a complementary sensitivity function for a
%       plant and estimator inseries
%       [num,den]=csensit(al,bl,cl,dl,as,bs,cs,ds)
%       al..dl represent the state space discription of estimator
%       as  ds represent the state space discription of the plant
%       T(z)=num/den
%       Paul kettle 11/3/1994
%

[A,B,C,D]=series(al,bl,cl,dl,as,bs,cs,ds),

[nums,dens]=ss2tf(A,B,C,D,1),

num=dens,
den=nums+dens,
num=nums,
den=den;
```

B.10 sen.m

```
% This scripts plots the sensativity and complementary sensitivity
% functions for a controller designed using the design m script file
% Author Paul Kettle.

[num,den]=sensit(af,bf,cf,df,am,bm,cm,[0]) ,
dbodem(num,den,T,w),
ax=axis,
hold on
[num,den]=csensit(af,bf,cf,df,am,bm,cm,[0]) ,
dbodem(num,den,T,w),
axis(ax),
```